12 Past and Future Sea Level Change

Authors:
Trina Ng, Nidheesh Gangadharan, Aurel Florian Moise, Matthew Palmer

Meteorological Service Singapore
Centre for Climate Research Singapore

Summary

This chapter discusses observed and projected mean sea-level rise around Singapore and the wider Southeast Asian region. Various physical mechanisms and processes driving past and future mean sea-level rise around Singapore are discussed here. Our findings specifically highlight vertical land movement (VLM) as an important driving process of relative sea-level rise in many parts of Southeast Asia.

We found that the rate of observed and future mean sea-level rise around Singapore is comparable to the global-mean rate. Past sea-level change in Singapore is shown at ten tide-gauge locations whilst future sea-level change in Singapore is shown at six of these ten tide-gauge locations.

Relative mean sea level has been rising at a rate of 3.6 mm/yr off Singapore (average rate across four tide-gauges with rate varies between 3.27 - 3.77 mm/yr) for the 1993 - 2021 period, and is projected to continue rising at different rates depending on the future emission pathways. We show that the relative mean sea level is *likely* to reach up to 0.74 m under the low emissions scenario (SSP1-2.6) and up to 1.24 m under the high emissions scenario (SSP5-8.5) by 2100 (relative to 1995-2014) at a particular location in the southern coast of Singapore (Sultan Shoal). Projected relative sea-level rise at this location could *likely* increase to 1.15 m (SSP1-2.6) and 2.12 m (SSP5-8.5) by 2150.

We show that the contemporary mass redistribution (CMR) between the oceans and the land, which refers to freshwater from ice sheets, glaciers and other terrestrial water storages, is the main driver of observed sea-level rise around Singapore during the 1993 - 2021 period (70% of the total rise). On the other hand, manometric sea-level, or in other words the ocean internal mass distribution, drives a large part of the sterodynamic sea-level rise (~23% of the total rise) in Singapore with a very weak contribution from steric sea-level rise. Our findings indicate that nearly 90% of the observed sea-level rise off Singapore is “mass-driven” and highlights the importance of having a bottom pressure recorder in the shelf region of Singapore to assist future studies of mean sea-level changes around Singapore.

We present the contribution from six driving components to mean sea-level change in Singapore by 2100 and 2150 under the low and high emission scenarios: Antarctic and Greenland ice sheets, glaciers, land water storage, ocean sterodynamics. Our projections show that mass changes in the Antarctic ice sheet are projected to *likely* contribute the most significantly to the projected sea-level rise in Singapore (Sultan Shoal) by 2100 and 2150 regardless of emission scenarios.

Low confidence sea-level projections for Singapore and the global mean up to 2300 are also presented in this chapter. These projections follow single paths of low-likelihood high-impact scenarios consistent with unstable ice sheet feedback processes such as marine ice cliff instability (MICI) and marine ice shelf instability (MISI). Despite their low confidence, these projections offer a more comprehensive view of potential future climate scenarios, providing essential information for stakeholder planning. It is, however, important to use these projections cautiously, with awareness of their inherent uncertainties.

This chapter centers on mean sea level in Singapore and the surrounding region, excluding an analysis of extreme sea level. Coastal water level fluctuations are also contributed from tides, storm surges, and waves. For robust mitigation and adaptation and planning in response to sea-level rise, an understanding of extreme sea levels is as vital as comprehending mean sea-level change. The mean sea-level change projections outlined in this chapter hence provide a foundation for future studies on extreme sea levels, aiding in comprehensive coastal sea-level change studies.

The availability of coastal observational systems and data is very sparse in many parts of the Southeast Asian region, including Singapore. Sustaining the existing observing networks (e.g. tide gauges) and initiating coordinated ocean observational programmes (e.g., coastal hydrographic measurements) is fundamental in addressing sea-level rise in the Southeast Asian seas. The complexity of understanding the drivers behind mean sea-level rise also calls for

developing modeling frameworks for the Southeast Asian region encompassing high-resolution regional and coastal hydrodynamic models. This will aid sea-level-rise-induced coastal impact assessments (e.g., inundation, erosion and land/infrastructure loss).

12.1 Introduction

Global mean sea-level rise is one of the most significant consequences of climate change, with the potential to impact coastal communities worldwide. Over the past century, global-mean sea level rose by an average rate of 1.8 mm per year, and this rate is expected to increase in the coming decades due to increased mass loss of ice sheets and glaciers and the thermal expansion of ocean waters (Fox-Kemper et al. 2021). Countries in southeast Asia are particularly vulnerable to sea-level rise due to the large population living in low-lying coastal areas (Nicholls and Cazenave, 2010; Nicholls et al. 2021; Asian Development Bank, 2018) and making robust estimates of sea-level rise and its coastal impacts is challenging for this region mainly due to sparse observational data and complex oceanographic and climatic features of the region as illustrated in Figure 12.1. Situated at the southern tip of the Malay Peninsula, Singapore is particularly at risk from sea-level rise impacts such as inundation, erosion and coastal flooding (Ministry of Sustainability and the Environment, 2021; Figure 12.2). The coastal sea-level rise and associated impacts indeed pose significant challenges to Singapore's public safety, infrastructure, and economy (National Climate Change Secretariat, 2018).

Singapore Prime Minister Lee Hsien Loong, in his National Day Rally speech in 2019, emphasised the importance of addressing sea-level rise around Singapore, highlighting the government's commitment to tackling this critical issue over the coming years (Prime Minister’s Office Singapore, 2019). To address the challenges posed by sea-level rise, the Singapore government has implemented various measures that collectively enhance state resilience to climate change. For example, the Coastal and Flood Protection Fund was established in 2018 as part of the Climate Action Plan, with an initial budget of SGD 5 billion to support coastal adaptation measures (National Climate Change Secretariat, 2018). Additionally, to enhance research in understanding sea-level rise and its impacts around Southeast Asia, which includes seas around Singapore, the National Sea Level Programme (NSLP) was launched by the Singapore government in 2019 with an initial budget of SGD 10 million (Ministry of Sustainability and the Environment, 2020).

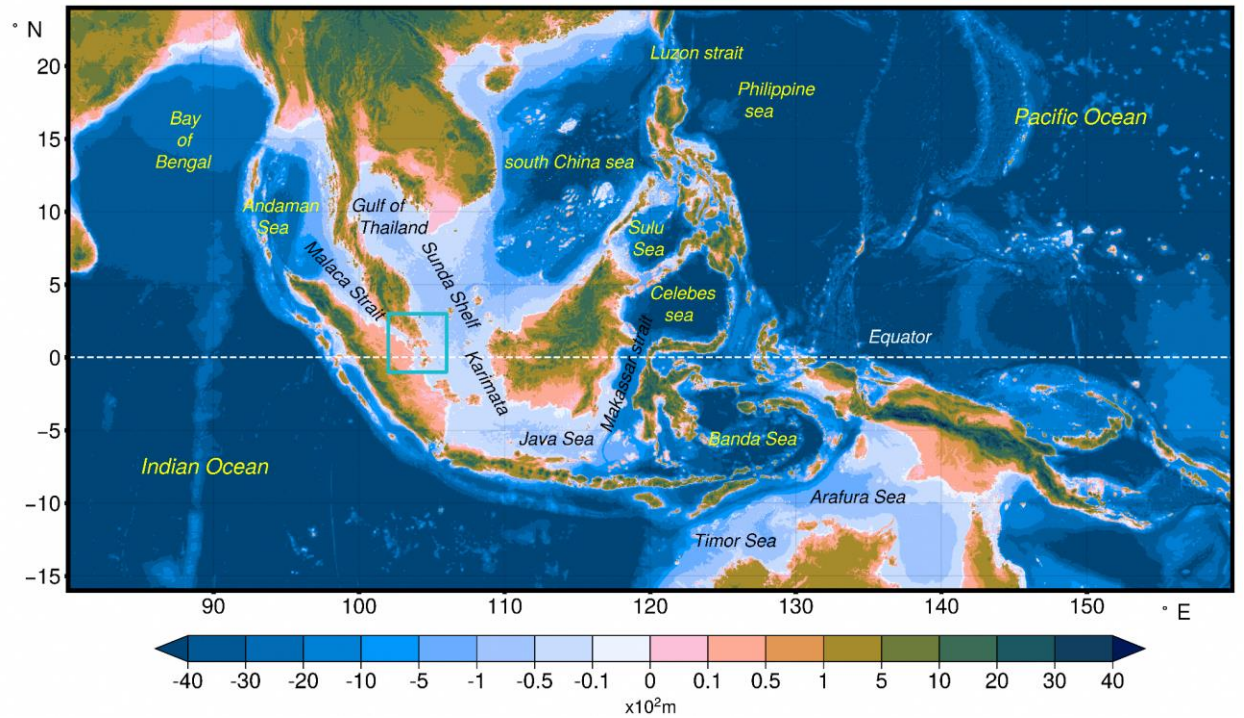

Figure 12.1: Land surface elevation and sea-floor depth relative to mean sea level of the Southeast Asian region. Major seas, shelves, and straits are shown and the geographic location of Singapore is marked by a rectangle. Units are 10^2 m, e.g., 0.1 = 10 m above sea level. Data source: General Bathymetric Chart of the Oceans (GEBCO_2022 Grid).

Changes in coastal water level can occur either through changes in regional relative mean sea-level or by means of changes caused by tides and extreme weather processes (waves, storm surges) or some combination of both.

Singapore's Second National Climate Change Study - by evaluating both time-mean sea level and sea-level extremes using different physical models - indicated that the projected coastal water levels around Singapore by the end of this century are predominantly driven by mean sea-level rise and changes in extreme sea levels are not so significant.

Hence, in this report, we focus mainly on how and why relative mean sea level rose around Singapore and the wider southeast Asian region over the historical period (Sections 12.3 and 12.4) and provide robust estimates of projected mean sea levels around Singapore for this century for different emission scenarios, using IPCC sea-level projection methodology.

In the following sections, we provide a general description for main drivers of coastal sea level following the historical sea-level change for Southeast Asia and Singapore using observational data, and subsequently discuss future sea-level change for these regions based on the Intergovernmental Panel on Climate Change (IPCC) Sixth Assessment Report of Working Group I (AR6).

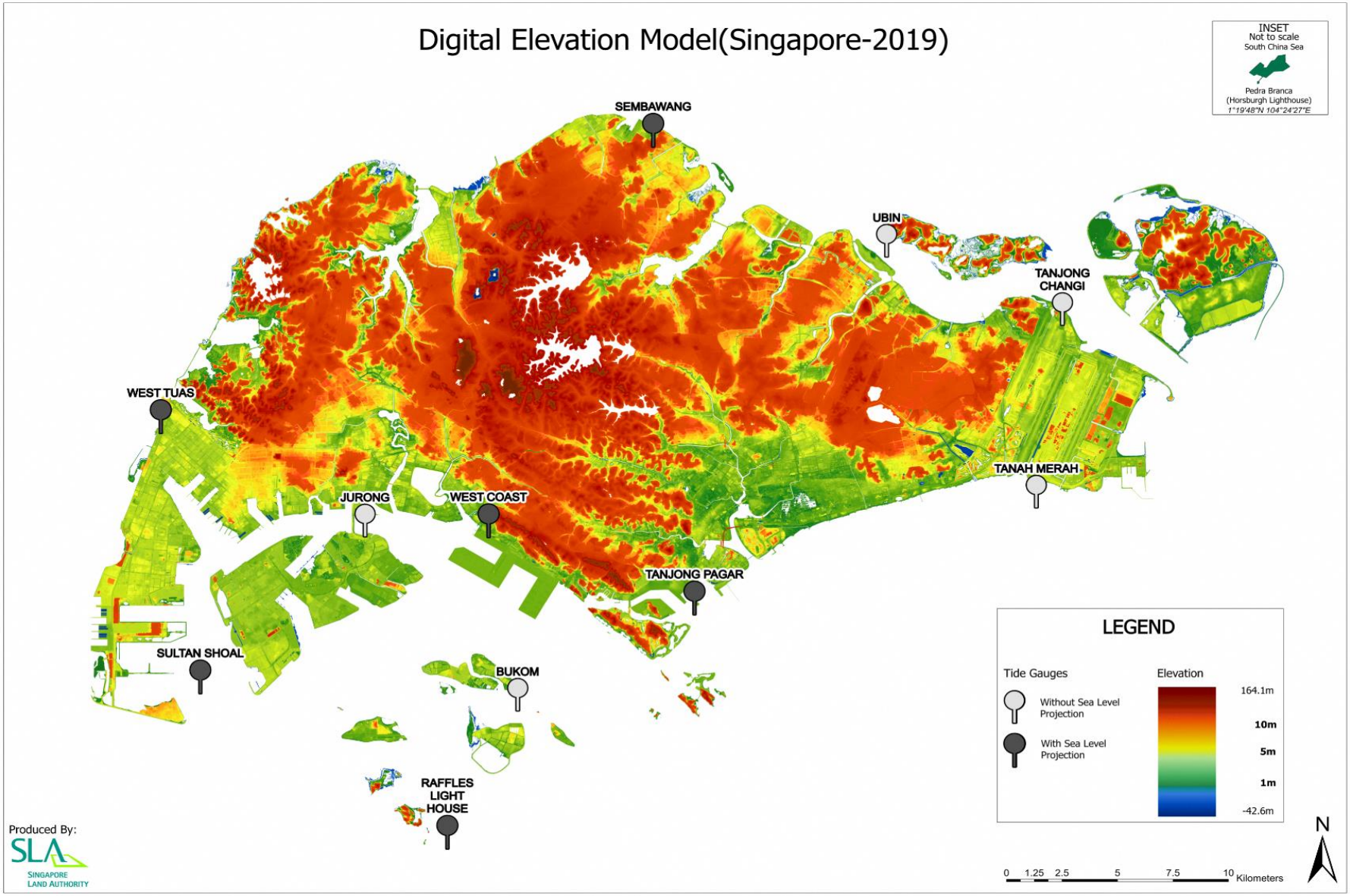

Figure 12.2: Map of elevation of Singapore (provided by Singapore Land Authority). Units are meters relative to mean sea level.

12.2 Drivers of sea-level change

Sea level varies over a wide range of spatial (from a point to global scale) and time (from seconds to millennia) scales. Sea level is an integrative ocean variable, meaning it integrates changes over the entire ocean depth and also reflects changes in other components of the climate system such as land, atmosphere and cryosphere. Therefore, sea level seldom settles down to a steady state (a condition in which no sea-level change occurs over time), but it constantly changes under the influence of several geophysical processes as shown in Figure 12.3.

Mean sea level at a given location is usually defined as the average of sea surface height over a certain period. It is the annual average water level at the coast upon which shorter-term variations from tides, surges and waves are superimposed. The averaging period could vary and hence, it is crucial to note that the rate of MSL could differ significantly if not compared over identical periods of time.

For a given location, subtracting the mean sea level from the original sea-level measurements would yield sea-level anomalies, which represent deviations of sea surface from a mean level due to several processes operating at different spatial and time scales, as illustrated in Figure 12.3.

Sea level can be measured with respect to a reference level, or also known as the datum, which is either fixed to the land (e.g., tide-gauge sea-level measurements) or based on Earth's center (e.g. satellite observations). Tide-gauge measured sea-level changes are hence affected by (or include information of) local vertical land movement (VLM) at the tide-gauge location, and hence called relative sea-level (RSL) changes.

Global-mean sea level[1] (GMSL) is the area-weighted average of sea surface height over the global oceans. Consequently, temporal changes in GMSL indicate a net change in the global ocean volume caused by ocean thermal expansion and/or exchange of water between other components of the Earth (e.g., mass balance changes in ice sheets, glaciers and terrestrial water storages). GMSL change due to the net mass change of the ocean is known as global-mean barystatic sea-level change, and that is caused by a net change in the global ocean heat content is called global-mean thermosteric sea-level change (Gregory et al., 2019).

[1] Mean sea level averaged over the global oceans. Refer to the Glossary for a complete list of sea level terminology definitions.

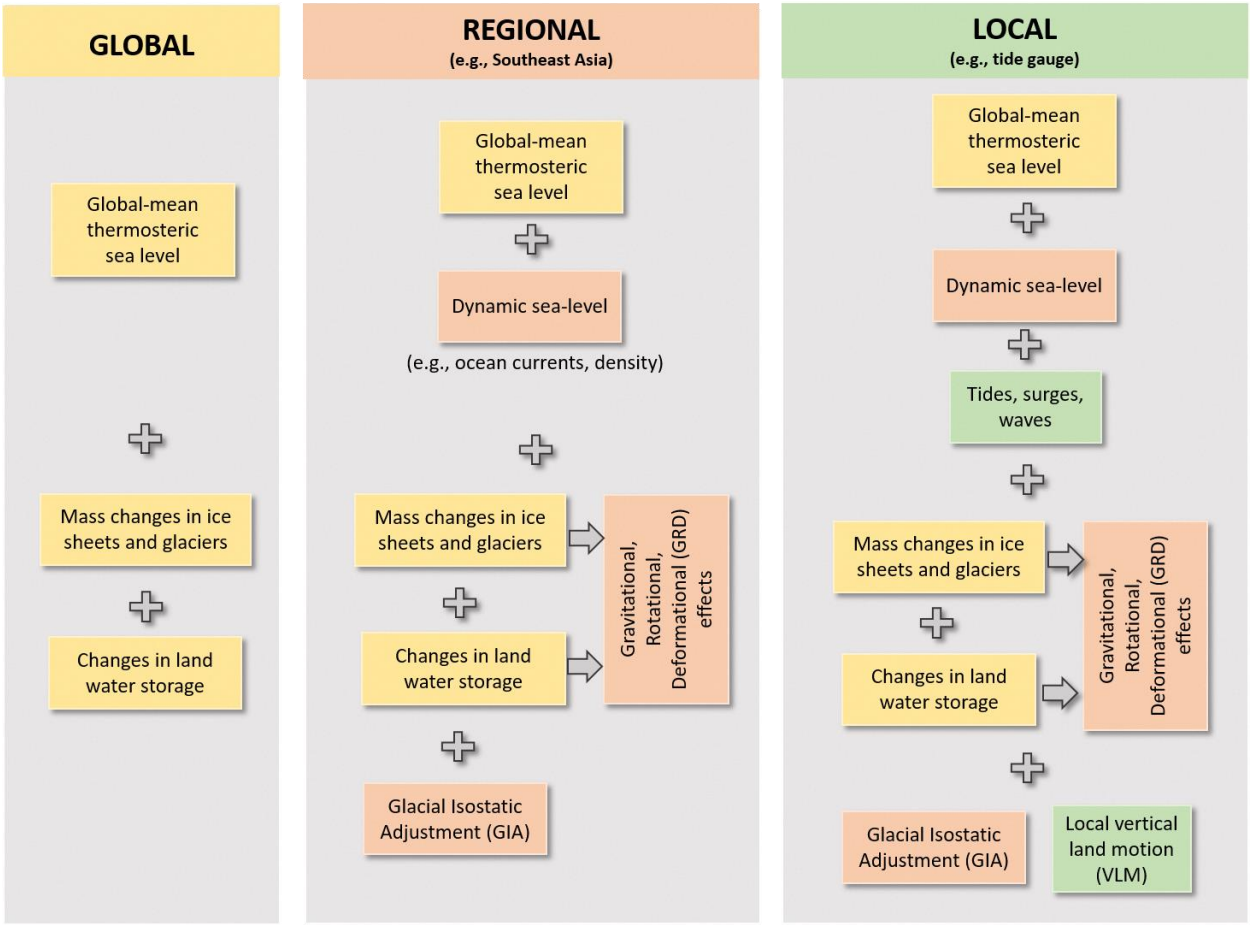

Figure 12.3: Schematic of different geophysical processes contributing to global, regional and local sea-level change. Note, the color-coding reflects the spatial scales on which the different processes operate, as per the column titles and that these are treated additively as we progress to smaller scales (left-to-right).

Regional and local sea-level changes can deviate from the global mean due to a number of processes (e.g. ocean circulation and tides) as summarised in Figure 12.3. By definition, these regional processes do not contribute to GMSL change since averaging their contributions over the entire ocean surface results in zero net change. The key processes that induce regional sea-level changes are ocean circulation (dynamic sea-level change) and the regional sea-level variations associated with freshwater exchange between the oceans and the land.

In the following sections, we focus on the drivers of mean sea level that occur on different temporal and spatial scales with a few contextual remarks for the sea-level changes around Singapore. We separate and discuss the drivers contributing to global, regional and local mean sea level.

12.2.1 Global drivers

GMSL rise is one of the major consequences of anthropogenic global warming. The earth system gained substantial energy during the last fifty from increased greenhouse gas emissions and associated positive radiative forcing. This surplus energy is closely linked to GMSL rise through the global ocean thermal expansion (Fox-Kemper et al., 2021). For instance, the GMSL rise (1.2 – 1.5 mm/yr ; Figure 12.4a) in the 20th century (e.g. Hay et al., 2015; Frederikse et al., 2020) is linked to the fact that nearly 90% of the excessive radiative heating of the climate system, due to greenhouse gas emission, has been stored in the

oceans (e.g. von Schuckmann et al., 2016, 2023; Church et al., 2013; Zanna et al., 2019; Meyssignac et al., 2019).

Global-mean thermosteric sea-level (GMTSL) rise accounts for nearly 90% of the observed energy increase since 1971 with much smaller amounts going into melting of ice (3%) and heating of the land (5%) and atmosphere (1%). Notably, majority of the ocean warming (~ 60%) is confined in the upper 700 meters of the oceans, causing about 4 - 5 cm of GMSL rise since 1971 and such rapid warming of the ocean (thermosteric sea-level rise) is shown to be indeed unprecedented over the last two thousand years (Fox-Kemper et al., 2021; Nidheesh et al., 2022). Nevertheless, it is important to note that the thermosteric sea-level rise is not spatially uniform across the oceans and in fact the thermal expansion is almost negligible over the shallow shelf regions like Singapore, leading to additional oceanic processes balancing the spatial variations as discussed in Section 12.3.

The remaining heat due to global warming (~10%), although small compared to what is being stored in the oceans, is in fact more efficient in changing the GMSL via changing the mass balance of land-based ice (i.e., polar ice sheets and glaciers) and the global hydrological cycle (Forster et al. 2021; WCRP Global sea Level Budget Group, 2018; von Schuckmann et al. 2020; Fox-Kemper et al. 2021). For instance, Figure 12.4a clearly shows that the GMSL change due to the redistribution of mass between the oceans and land is nearly twice the GMTSL change over the entire twentieth century, and the rates of global-mean barystatic and thermosteric sea-level rise are almost equal in magnitude during 1971 - 2018 (Fox-Kemper et al., 2021). More specifically, the GMSL rise over 1971 - 2018 (7.3 - 14.6 cm with a central estimate of 10.96 cm) can be closed with largest contribution comes from ocean thermal expansion (3.4 - 6.1 cm with a central estimate of 4.75 cm) and remaining contributions from glaciers (2.1 cm [1 - 3.2 cm]), Greenland ice sheet (1.2 cm [0.8 - 1.6 cm]), Antarctic ice sheet (0.67 cm [-0.4 - 1.7 cm]) and terrestrial water storage (0.73 cm [-0.2 - 1.7 cm]).

Additionally, a number of recent studies (e.g. Nerem et al., 2018; Dangendorf et al., 2019) pointed out that there is an apparent acceleration in the rate of GMSL rise, as evident in the higher rate of satellite-measured GMSL rise (~ 3.4 mm/yr since 1993), possibly related to accelerating levels of anthropogenic forcings in the climate system. Satellite-based observations and other in-situ measurements also suggest that mass loss from glaciers and the polar ice sheets has increased over recent decades, and can potentially become large sources of sea-level change in the current century (Fox-Kemper et al., 2021).

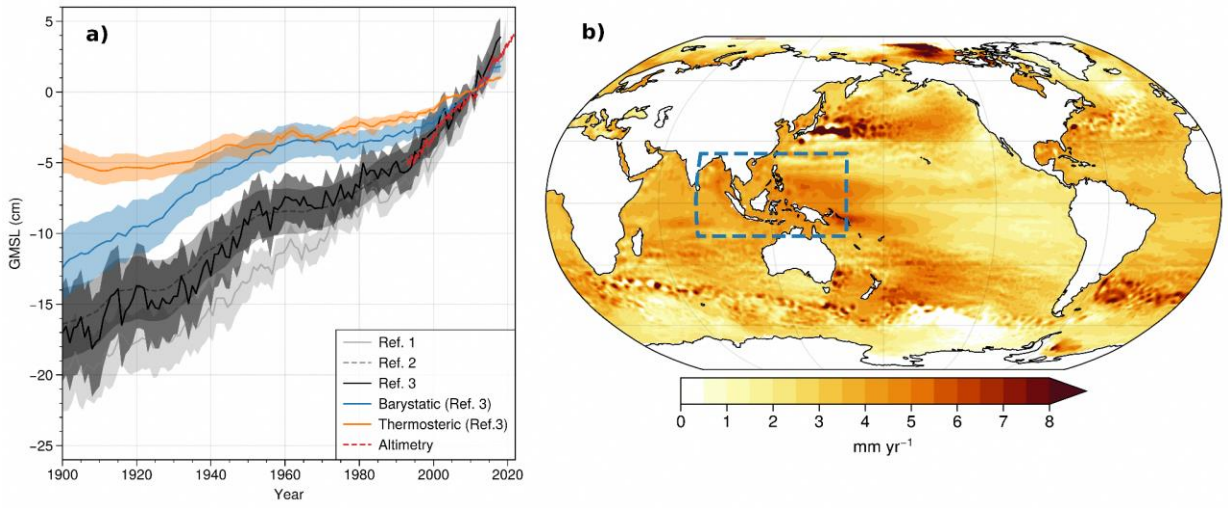

Figure 12.4: (a) Estimates of twentieth-century global-mean sea-level (GMSL) rise from different sources: Commonwealth Scientific and Industrial Research Organization (CSIRO; Ref. 1), Hay et al. 2015 (Ref. 2) and Frederikse et al. 2020 (Ref. 3). The two major components - thermosteric and barystatic contributions - of the GMSL are also shown from Frederikse et al. (2020). GMSL curve from satellite altimetry is also shown. (b) Spatial map of mean sea-level rise trend for the period 1993 -

2021 estimated from satellite altimetry. The southeast Asian region is highlighted by a rectangle [Note that satellite-observed sea-level rise does not include the effects of vertical land motion].

12.2.2 Regional drivers

Sea-level rise is not spatially uniform (Figure 12.4b). For instance, the rate of satellite-observed sea-level rise in the far western Pacific (about 5-6 mm yr−1 is clearly larger than the GMSL rate over the same period. Mean sea-level rise is generally higher (lower) than the global-mean in the Southern Ocean mid-latitudes (eastern tropical Pacific), as seen in Figure 12.4b. This spatially non-uniform sea-level rise, or also known as dynamic sea-level change, is primarily caused by ocean circulation, which redistributes water mass and heat within the ocean basins under the influence of winds and density differences.

For example, strengthened trade winds in the Pacific during the falling phase of Interdecadal Pacific Oscillation (IPO) since 1990s have resulted in increased ocean heat uptake by the equatorial Pacific and warm water accumulation in the west (e.g. England et al. 2014), causing a higher (lower) rate of mean sea-level rise in the western (eastern) tropical Pacific as seen in Figure 12.4b. Regional sea-level changes are often driven by surface winds and spatially varying atmospheric heat and freshwater fluxes, often associated with regional climate modes. For instance, the sea-level changes in the Atlantic ocean is primarily driven by wind and heat flux variations associated with the North Atlantic Oscillation (NAO) and changes in ocean heat transport associated with the Atlantic Meridional Overturning Circulation (AMOC; Oppenheimer et al. 2019). Similarly, the high rates of sea-level rise in the north Indian Ocean during the second half of the 20th century was linked to the weakening of Indian Monsoon circulation (Swapna et al. 2017).

Such natural variability in the climate system is very efficient in channelising non-uniform distribution of heat, salt and water masses within the ocean and to lead non-uniform sea-level changes at different oceanic regions. Ocean general circulation models are widely used to understand this ‘circulation-induced’ sea-level variations, known as ‘dynamic’ sea-level changes (Gregory et al. 2019). The global-mean density of the ocean can vary in time and contributes to regional as well as global-mean sea-level changes. The regional sea-level change due to the combined effects of dynamic sea-level change and global-mean thermosteric sea-level change is called ‘sterodynamic’ sea-level changes (Gregory et al. 2019).

Understanding the natural climate variability and ocean circulation is a key aspect in the understanding of climate-change-induced regional sea-level rise. For instance, several studies have examined the sea-level rise in the tropical Pacific and showed that accounting for natural climate variability (i.e., ENSO and/or IPO) could substantially modify the observed sea-level rise pattern. This is useful in detecting the trends originating from anthropogenic warming (e.g. Royston et al. 2018). Sea-level rise in the Southeast Asian seas could also be influenced by low-frequency natural climate variability rooted in both Indian and Pacific oceans. Understanding what drives regional variability in sea level is also key for deriving robust sea-level projections.

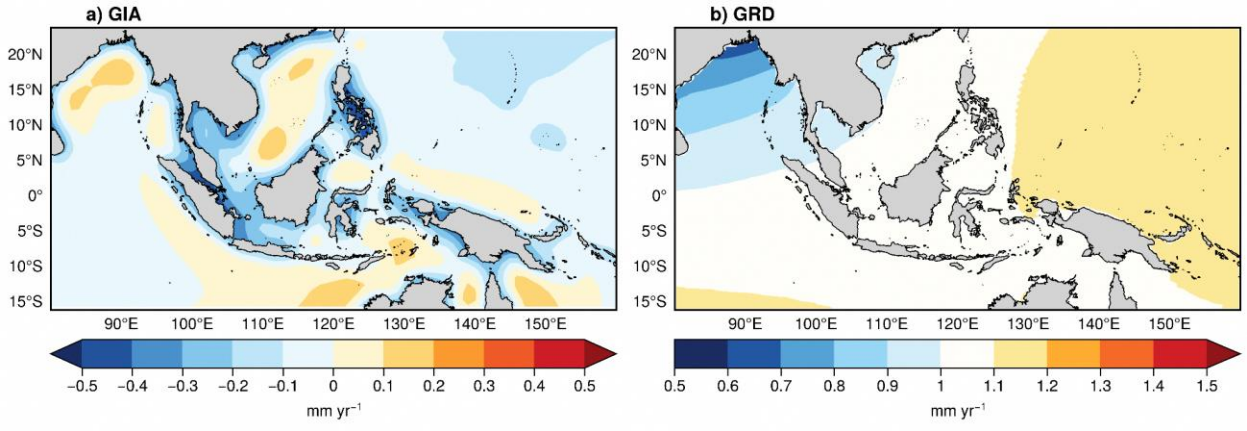

Figure 12.5: Relative sea-level rise in the southeast Asian region due to GIA (a) and GRD (b) effects. The rate of GIA-induced sea-level change is taken from the ICE-6G_C (VM5a) model (Peltier et al. 2015). The GRD fingerprint (b) represents the relative sea-level rise caused by mass redistribution between the oceans and ice sheets (Antarctic and Greenland), mountain glaciers and terrestrial water storages for the period 1900 - 2018, as described in Frederikse et al. (2020).

Sea-level change in response to land-ice melting and changes in land water storage is also not uniform across the oceans. The associated changes in Earth's **g**ravity, **r**otation and crustal **d**eformations impose characteristic patterns of regional sea-level change (Farrel and Clarke, 1976), collectively referred to as GRD fingerprints. GRD effects on sea level can be due to past changes (e.g. changes occur over glacial cycles) in land-ice storage, which is known as glacial isostatic adjustment or GIA. GRD effect could also be due to ongoing changes in the land-ice or land water storages, which is termed contemporary GRD effects. Observed RSL rise is affected by both GIA and GRD effects. For example, on average, the ocean basins are slightly subsiding (uplifting) due to the loading (unloading) of sea water since the Last Glacial Maximum that occurred about 20,000 years ago. On the other hand, mass loss from the Greenland ice sheet over the last few decades has caused a sea-level fall around Greenland by a few centimeters as a response to changes in the local gravitational field (e.g. Coulson et al. 2022) while sea level rose over most of the tropical oceans in response to that melting.

While the GRD sea-level fingerprints impose large spatial gradients in RSL near glaciated regions (e.g. the northeast US coasts or Greenland ice sheet), those effects are relatively small in the tropics (Wang et al. 2021). For example, Figure 12.5 illustrates the current rate of RSL rise due to GIA (Figure 12.5a) and GRD (Figure 12.5b) from Peltier et al. (2015; GIA rate) and Frederikse et al. (2020; GRD), respectively in the Southeast Asian region. The GIA-induced sea-level rise represents the sea-level response to deglaciation history over the last 25,000 years from an updated GIA model (ICE-6G_C (VM5a); Argus et al. 2014). Figure 12.5a suggests that RSL falls with rates ranging from -0.1 to -0.4 mm/yr at many of the coastal locations in the Southeast Asia due to GIA, including Singapore (Table 12.5 for GIA-induced RSL change at tide-gauge stations around Singapore).

Figure 12.5b indicates the RSL change due to the net mass balance changes in the ice sheets, glaciers and land water storage for the period 1900 - 2018 (Frederikse et al., 2020). The GRD-induced sea-level rise is mostly uniform around Singapore and the wider south China sea region (~1 mm/yr) for the 1900 - 2018 period (Figure 12.5b).

12.2.3 Local drivers

In addition to the factors discussed in the previous sections, sea-level rise at the coasts is further affected by various physical processes such as tides, storm surges and waves, changes in coastal morphology, and VLM. VLM is one of the most important yet often understudied issues in the detection of RSL rise at many coastal regions. As we will see in Section 12.3, many of the coastal

locations in the Southeast Asian region indeed experience significant local VLM that exacerbates the climate-change-driven sea-level rise.

For instance, Indonesia's capital city Jakarta, is subsiding at an alarming rate of a few centimeters per year (e.g., Bott et al. 2021), and the country is moving its capital to mitigate the associated risks. The Solomon Islands, a low-lying island nation in the western tropical Pacific, has lost at least five of its reef islands to the rising seas and intense wave action, and many of the small islands in the archipelago await a similar fate (Albert et al. 2016).

Factors such as tectonic activities and anthropogenic subsidence potentially cause significant RSL changes in the Southeast Asian seas. Monitoring and understanding those factors are critical to understanding RSL rise in the region.

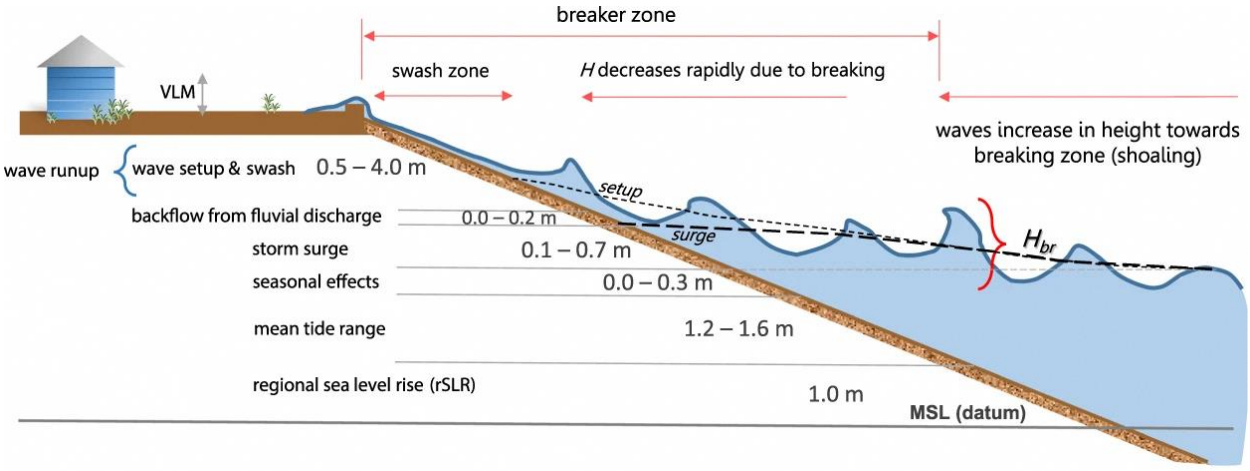

Figure 12.6: An illustration for California for 1 m of sea level rise of the significant water level components that comprise total water levels on a beach during a storm resulting in potential flooding. The range of values are based on observations and modeling conducted for California as described in Barnard et al. (2019). (H = wave height, H_{br} = breaking wave height). The total water level at the coast is a combined effect of regional sea-level rise and other coastal phenomena (e.g. tides, storm surges, seasonal effects and waves). Adapted from Barnard et al. 2019).

At the coasts, tides, storm surges and waves constitute the major processes, coupled with mean sea-level change, that contribute to significant water level oscillations at the coasts (Figure 12.6). Consequentially, this results in extreme sea level change.

Tides around Singapore are typically mixed diurnal and semidiurnal with a range around 2 – 3 m. Cyclonic storm activities around Singapore are weak due to its proximity to the equator. However, sea-level seasonal variations associated with monsoons are substantial (~ 20 cm amplitude; see appendix A1). The monsoon-driven wind-setup drives high (low) sea levels during the northeast (southwest) monsoon and the extreme sea-level anomalies around Singapore indeed tend to occur during the northeast monsoon (Tkalich et al. 2009). A key finding of Singapore's Second National Climate Change study was indeed that the projected changes in surges or waves are dominated by projected mean sea-level rise. Cannaby et al. (2016) pointed that the highest recorded surge level in the Singapore Strait (~ 84 cm) lies between the central and upper estimates of mean sea-level rise by 2100, highlighting the role of mean sea-level rise in driving the extreme water levels at the coasts and the vulnerability of the region.

For the southeast Asian region, the lack of long-term, spatially dense ocean and coastal observations is one of the main challenges in improving understanding of sea-level rise. Ideally, each tide-gauge installation should include a complementary Global Navigation Satellite System (GNSS) receiver to directly monitor VLM. Spatial monitoring of VLM with InSAR (Synthetic

Aperture Radar interferometry) techniques provides another means of estimating the VLM for coastal regions (e.g. Catalao et al. 2020, Tay et al., 2022). Temperature, salinity and current measurements are also fundamental in understanding coastal ocean dynamics and sea-level changes. By analysing observed and model-based sea-level data, this report indicates that the sea-level rise around Singapore is essentially "mass-driven" (Section 12.3). The deployment of a bottom pressure recorder in the shelf region around Singapore would significantly help to observe and interpret the sea-level changes here. However, the availability of such complementary observational systems and data is very sparse in many parts of the Southeast Asian region, including Singapore. Sustaining the existing observing networks (e.g. tide gauges, LIDAR) and initiating coordinated ocean observational programmes would hence be an important step forward in addressing sea-level rise in the SEA region.

The complexity of fully comprehending local sea-level change on varied timescales (Figure 12.3) also calls for developing modeling frameworks for the Southeast Asian region encompassing high-resolution regional ocean modeling and coastal hydrodynamic models, which are essential tools to translate the sea-level rise information into coastal impacts (e.g., inundation, erosion and land/infrastructure loss).

12.3. Observed sea-level rise in Southeast Asia

Tide-gauges have been the key observational records of coastal sea-level changes, and a large body of literature has discussed the mean sea-level changes using those records, at both global and regional scales (e.g. Peltier and Tushingham, 1991; Douglas, 2001; Jevrejeva et al. 2008; Church and White, 2011; Gregory et al. 2013; Hay et al. 2015; Wyrtki, 1987; Mitchum and Wyrtki, 1988; Unnikrishnan and Shankar, 2007; Feng et al. 2004; Woodworth et al. 2019; Nidheesh et al. 2013; Royston et al. 2022). Tide-gauge measures local sea-level changes relative to the land to which the gauge is fixed. A number of oceanic and land processes can thus affect tide-gauge readings as illustrated in Figure 12.3.

Although tide-gauges possess data over multi-decadal periods, a natural limitation of tide-gauges lies in their sparse and uneven geographical distribution. Extreme care has been given in most literature to minimise the biases originating from sparse spatial coverage while estimating global and regional sea-level-rise trends from those records (e.g. Hay et al. 2015; Unnikrishnan and Shankar, 2007). In addition, the record length of sea-level data varies across gauges. Many of the records across the world suffer from substantial data gaps, and this includes many coastal regions in Southeast Asia. Few studies have attempted to quantify the mean sea-level rise in the South China sea and the adjacent shallow shelves using tide gauges (e.g. Tkalich et al. 2013), although a large body of literature has addressed tide-gauge-based sea-level rise estimates in the western Pacific ocean (e.g. Merrifield, 2011; Feng and Meyers, 2004).

Ideally, the VLM-corrected mean sea-level change estimate from tide-gauges is expected to closely match the mean sea-level change measured by satellite altimetry at the same location (Section 12.2). As we will see in the following section, synergising the estimates of mean sea-level rise from tide-gauges and satellite altimetry could provide better insights on local mean sea-level change and potentially indicate the rates of VLM over their overlapping period. Satellite altimetry provides global-scale, gridded sea-level measurements and has greatly aided the understanding of open ocean variability since 1993. A few studies in the past have shown that employing satellite sea-level data in conjunction with tide-gauge records can provide meaningful information on regional and coastal sea-level rise (e.g. Vinogradov and Ponte, 2011; Unnikrishnan et al. 2015; Allison et al. 2022).

In the following section, we describe the observed sea-level rise in Southeast Asian seas (SEAS) by analysing sea-level data from selected tide-gauges and satellite altimetry for the 1993 - 2021 period.

12.3.1 Sea-level rise from satellite altimetry and tide gauges

Monthly sea-level data from tide-gauge records are obtained from the Permanent Service for Mean Sea Level (PSMSL) repository (Holgate et al., 2013; PSMSL, 2022). All the records used in this report are the 'revised local reference' records to assure that the sea-level heights at all stations are referenced to a common datum. More details can be seen in the PSMSL website (https://psmsl.org). Satellite-measured sea-level anomaly (with respect to mean sea-surface height for the period 1993 - 2012) data from the Copernicus Marine Environment Monitoring Service (CMEMS) are another key observational data used in this report, which is based on a merged product from multiple satellite missions (TOPEX/Poseidon, ERS-1/2, Jason-1, Jason-2, and Envisat). The monthly-mean sea-level data have global coverage and are available at a spatial resolution of 0.25° × 0.25°. We analyzed the data for the period 1993 - 2021, for this report. We considered 12 tide-gauge records in the SEAS (Figure 12.7 and Table 12.1), each of them having at least 90% of data coverage during the altimetry period (1993 - 2021). Note that all the twelve gauges, as shown in Figure 12.8, do not extend to the entire satellite period, but some of them do not have a couple of years of data at the end of the period (Malakal [1993 - 2019], Kota Kinabalu [1993 - 2019], Zhapo [1993 - 2020], Sultan Shoal [1993 - 2020], Tanjung Geylang [1993 - 2019], and Ko Taphao Noi [1993 - 2020]). As we focus on long-term trends, the sea-level seasonal cycle is removed for both tide-gauge and satellite monthly data. Hence, all the sea-level data analysed in this report, including the reanalysis data, are anomalies with respect to 1993 - 2012 time-mean sea level and seasonal climatology estimated over the period of analysis (1993 - 2021). The sea-level trends are estimated through a linear regression of the sea-level data in time, and the standard error of the trend is provided as a measure of trend uncertainty.

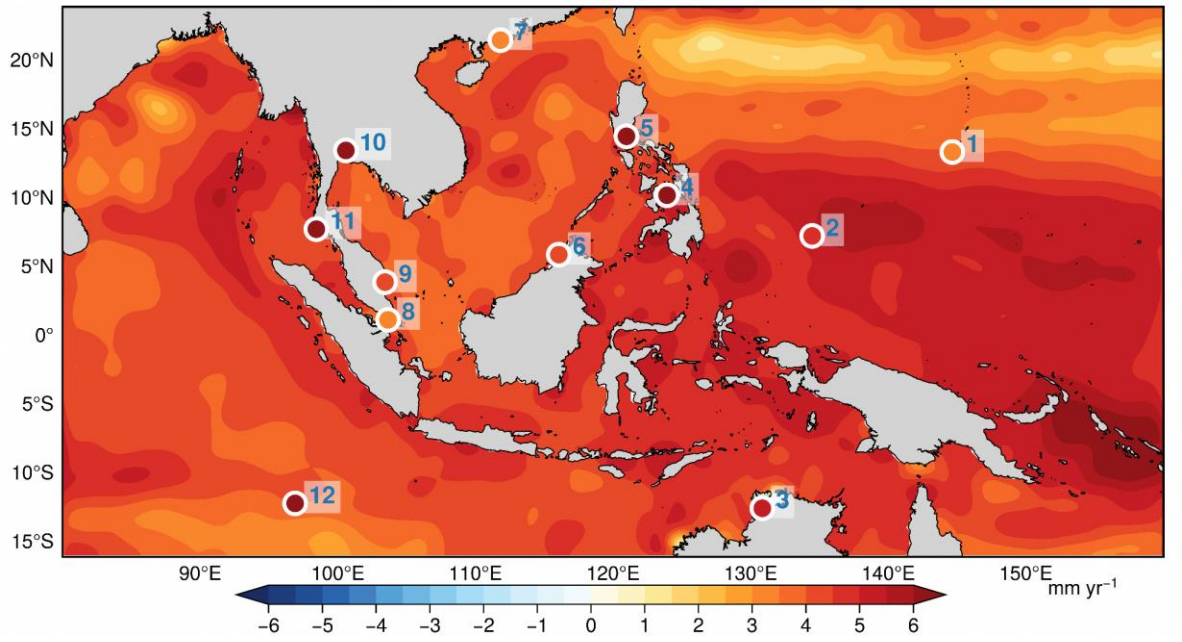

Figure 12.7: Observed sea-level trend from satellite altimetry (spatial map) and tide gauge records (circle) for the period 1993 - 2021. The selected tide gauges are, from east to west: 1. Pago Bay (Guam); 2. Malakal (Palau); 3. Darwin (Australia); 4. Cebu (Philippines); 5. Manila (Philippines); 6. Kota Kinabalu (Malaysia); 7. Zhapo (China); 8. Sultan Shoal (Singapore); 9. Tanjung Gelang (Malaysia); 10. Fort Phrachula Chomklao (Thailand); 11. Ko Taphao Noi (Thailand); 12. Home Island (Cocos Islands).

Satellite sea-level trend map for the period 1993 - 2021 shows that mean sea level is rising almost everywhere in the Southeast Asian region, with a regional-mean rate of ~ 4.4 mm/yr (Figure 12.7). The rate of sea-level rise is not the same everywhere in the region and exhibits deviations from the regional-mean and the global-mean rate (~3.4 mm/yr). For instance, the rates are higher in the western equatorial Pacific (4 - 6 mm/yr) and the eastern Indian Ocean (off the Andaman Islands) whereas relatively weak sea-level rise (0 - 2 mm/yr) is observed in the tropical northwest Pacific (Figure 12.7).

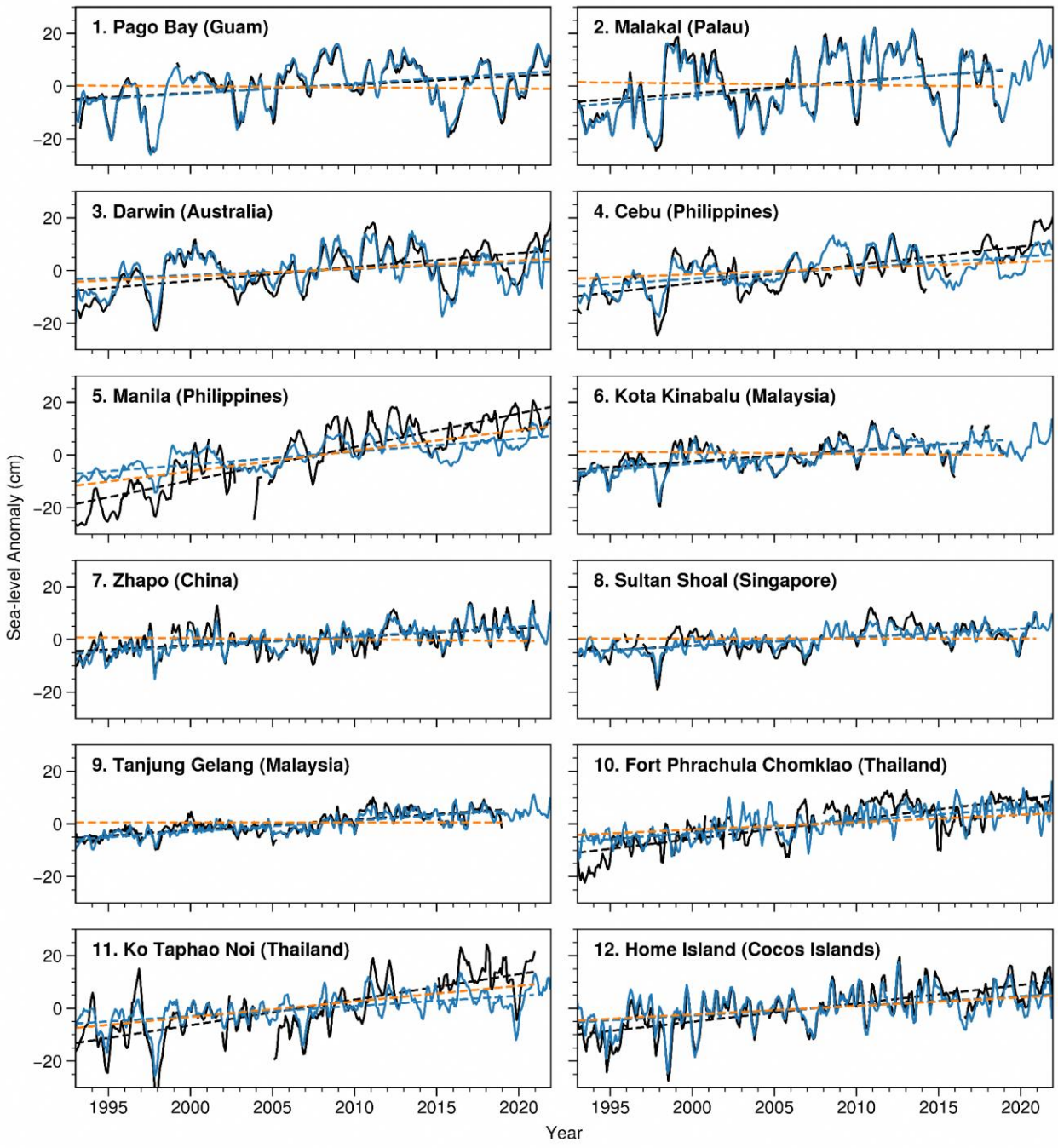

Figure 12.8: Time series of sea-level anomalies from tide gauges (black) and satellite altimetry (blue, averaged over 1 degree around each gauge location shown in Figure 12.5). The difference between the tide-gauge and satellite time series is also shown (orange). A linear trend based on the least-square method is also plotted as a dashed line over each time series with the same color. The trend and corresponding standard error for each tide-gauge is given in Table 12.1.

Note that the rate of mean sea-level rise in the South China sea (SCS) and off Singapore is close to the global-mean rate. Regional deviations in the rate of sea-level change can arise through various geophysical processes, such as the regional ocean circulation and GRD effects (c.f. Figure 12.3). We will come to these points in the following sections.

Rate of sea-level rise across selected tide-gauge records in the SEAS (locations of gauges are shown in Figure 12.7 with color indicating the sea-level trend) also show similar spatial variations. Notably, the tide-gauge trends differ significantly from satellite-based trend estimates (Figures 12.7 & 12.8, Table 12.1) at six locations, namely - Darwin (Australia), Cebu (Philippines), Manila (Philippines), Fort Phrachula Chomklao (Thailand), Ko Taphao Noi (Thailand), and Home Island (Cocos Islands). As explained in section 12.2, the difference in the rates of sea-level rise between altimetry and tide gauge at a given location provide an indication of the local VLM (Woppelmann and Marcos, 2016).

Table 12.1 also suggests that the Sultan Shoal (Singapore) does not have significant local VLM compared to other coastal locations in the SEA region (also refer to Sections 12.4 and 12.6). As detailed in Section 12.6, the GIA-induced VLM in Singapore drives a land uplift (RSL fall) which may counter any local land subsidence due to other factors. Two of the Malaysian gauges (Kota Kinabalu and Tanjung Gelang), as shown in Figure 12.8, stopped recording sea-level change around 2018. This accentuates the importance of sustaining tide-gauge for monitoring and improved understanding of long-term sea-level rise at coastal regions. Ideally, tide-gauge measurements should be supplemented with direct VLM estimates (e.g. using GNSS; Martinez-Asensio et al. 2019), which are absent at many of these tide gauge locations. We call for joint programs to monitor the VLM in Singapore and other vulnerable locations in the Southeast Asian region toward reliable future sea-level projections and coastal adaptation procedures.

Table 12.1: Sea-level trend and standard error for the selected tide-gauge records in the SEAS. Satellite sea-level is averaged at a 1-degree area surrounding each tide-gauge station and the trend of this satellite time series is also given. The trend estimates for the difference time series (i.e. tide-gauge - altimetry) is shown in the last column. Unit is in mm/yr.

	Tide Gauge	Lon (E)	Lat (N)	Tide gauge	Satellite	Difference
1	Pago Bay (Guam)	144.65	13.44	3.20 ± 0.55	3.84 ± 0.52	-0.42 ± 0.10
2	Malakal (Palau)	134.47	7.33	4.59 ± 0.87	5.35 ± 0.82	-0.63 ± 0.11
3	Darwin (Australia)	130.85	-12.47	5.26 ± 0.45	2.27 ± 0.45	2.99 ± 0.20
4	Cebu (Philippines)	123.92	10.3	6.96 ± 0.40	4.18 ± 0.33	2.33 ± 0.30
5	Manila (Philippines)	120.97	14.58	12.71 ± 0.41	4.92 ± 0.25	7.78 ± 0.30
6	Kota Kinabalu (Malaysia)	116.06	5.98	4.28 ± 0.41	4.74 ± 0.28	-0.6 ± 0.14
7	Zhapo (China)	111.82	21.58	3.23 ± 0.31	3.79 ± 0.23	-0.51 ± 0.16
8	Sultan Shoal (Singapore)	103.65	1.23	3.26 ± 0.29	3.34 ± 0.20	-0.01 ± 0.19

9	Tanjung Gelang (Malaysia)	103.43	3.97	4.11 ± 0.21	4.19 ± 0.17	-0.04 ± 0.13
10	Fort Phrachula Chomklao (Thailand)	100.58	13.55	7.49 ± 0.33	4.67 ± 0.25	2.8 ± 0.35
11	Ko Taphao Noi (Thailand)	98.43	7.83	9.69 ± 0.53	3.89 ± 0.33	5.93 ± 0.35
12	Home Island (Cocos Islands)	96.89	-12.12	6.96 ± 0.38	3.66 ± 0.36	3.26 ± 0.09

12.3.2 Decomposition of observed sea-level rise

The sea-level trend from satellite altimetry can be decomposed into two main sources. First, the sea-level trend which is caused by ongoing freshwater exchange between the ocean and land (this includes ice mass changes in grounded ice sheets and glaciers and changes in terrestrial water storages). Following Harvey et al. (2021), we call this source (component) “contemporary mass redistribution” (CMR). Note that, in our definition, the CMR sea-level trend includes both global-mean barystatic sea-level trend and the associated regional GRD fingerprints (Gregory et al. 2019). Second, the sea-level trend caused by ocean sterodynamic changes reflects the sea-level change caused by ocean circulation and seawater density variations (Section 12.2.2). Satellite sea level is also affected by GIA, and hence, we have corrected the satellite trend for GIA by subtracting GIA (GSL) solutions from ICE-5G (Peltier, 2004; Appendix A2) to focus on the remaining two contributions - sterodynamic and CMR. We can hence write the GIA-corrected sea-level rise (SLR) from altimetry as:

SLR (altimeter) = Sterodynamic + CMR + residual

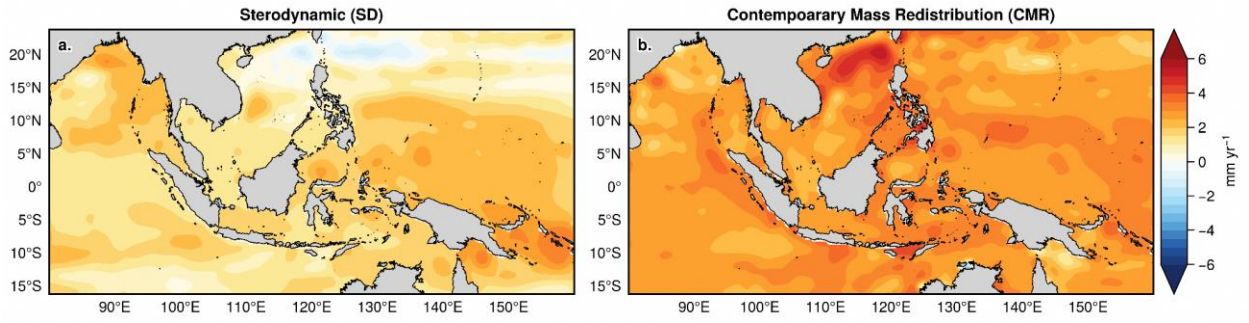

Figure 12.9: a) Sterodynamic sea-level rise (which includes the effects of ocean density variations and regional circulation) for the period 1993 - 2021. b) Sea-level rise trend estimated from the residual signal (i.e. satellite sea level - minus - sterodynamic sea level), considered here as an estimate of sea-level trend caused by contemporary mass redistribution (CMR) between the ocean and land (i.e. sea-level rise caused by ice-melting from ice sheets and glaciers, and terrestrial water storage changes).

The ocean sterodynamic sea-level trend is estimated from the European Centre for Medium-Range Weather Forecasts (ECMWF) Ocean Reanalysis System 5 (ORAS5; Zuo et al. 2019) sea surface height for the satellite period (1993 - 2021). Since ORAS5 is constrained to satellite sea-level trend, we have subtracted the global-mean sea level (estimated from the ORAS5 sea level) from each grid-point and then added back the global-mean thermosteric sea level (GMTSL; estimated from ORAS5 ocean temperature and salinity), to obtain the sterodynamic sea level. The

sterodynamic sea-level rise hence represents both dynamic sea-level rise (due to changes in regional ocean circulation) and the global-mean thermosteric sea-level rise. We subtracted the sterodynamic sea level from altimeter sea level to obtain the “residual signals'', which are approximated to be representative of the sea-level change due to CMR (assuming the uncertainties in the sterodynamic sea level is small as our period of analysis is well constrained by observational data). This exercise provides us a unique way to detect CMR-induced sea-level changes in the SEAS without independent estimates of the GRD fingerprints.

The sterodynamic sea-level rise in the SEAS is positive and rather uniform (with a regional-mean rate of ~ 1.5 mm/yr), except for a few regions (Figure 12.9a) showing deviation from the regional-mean rate. For instance, the sterodynamic sea-level rise in the western equatorial Pacific and the eastern Bay of Bengal (BoB) is slightly higher compared to other regions, and there is a narrow zonal belt of slightly negative (1 - 2 mm/yr in magnitude) rate in the northwest Pacific (~20°N). The higher values in the western equatorial Pacific could be linked to the enhanced trade winds associated with the negative phase of Interdecadal Pacific Oscillation (IPO, see England et al. 2014) during the first decade of the altimeter period. The higher rates along the eastern rim of BoB are also attributed to natural wind variations in the equatorial Indian Ocean (Nidheesh et al. 2013; Unnikrishnan et al. 2015), over recent decades. The sterodynamic sea-level rise in the SCS varies between 1 - 2 mm/yr, with a notable higher rate in the central SCS (Figure 12.9a).

The CMR-driven sea-level rise, in general, is spatially uniform and higher than the sterodynamic sea-level rise almost everywhere in the SEAS (Figure 12.9b). The regional-mean rate due to CMR is ~ 2.9 mm/yr which is nearly twice the regional-mean rate due to sterodynamic sea-level rise (~ 1.5 mm/yr). Note that the sterodynamic and CMR sea-level rise includes sea-level rise due to global-mean thermosteric sea-level rise (~1.2 mm/yr) and global-mean barystatic sea-level rise (~ 2.1 mm/yr) respectively, for the 1993 - 2021 period. Figure 12.9 hence suggests that about two-thirds of net sea-level rise in the SEAS is caused by CMR. The sterodynamic sea-level rise is mostly contributed by GMTSL rise, indicating that the dynamic sea-level rise is weak and confined to a few regions (western equatorial Pacific and eastern BoB) over the satellite period. In the following sections, we will further decompose the sterodynamic sea-level rise into contributions from local density (steric sea-level rise) and local mass changes (manometric sea-level rise, see Gregory et al. 2019), and will discuss how these different processes contribute differently in the SEAS.

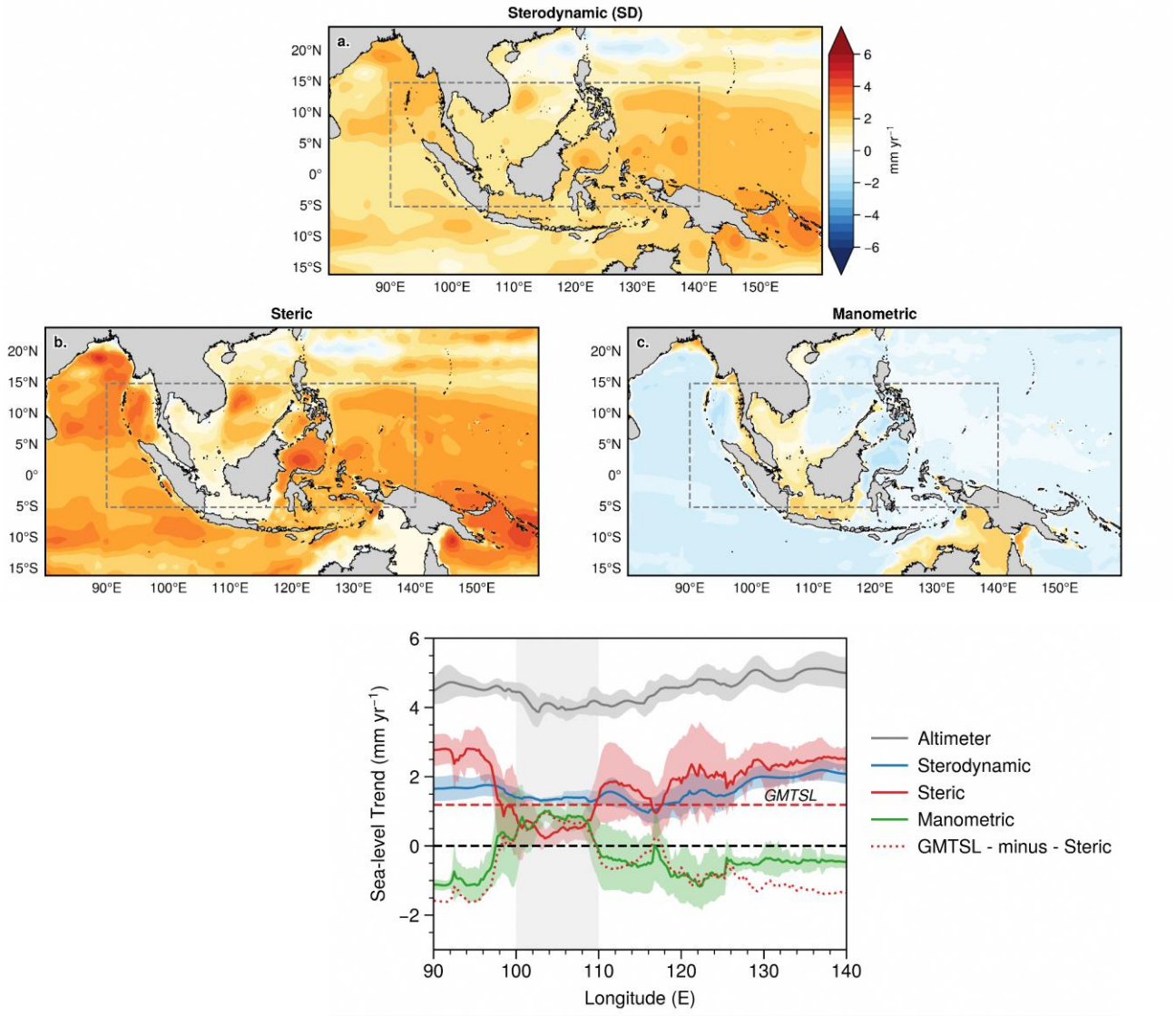

Figure 12.10: (a) Sterodynamic (SD) sea-level rise trend decomposed into, b) steric and c) manometric sea-level rise, estimated from high-resolution ocean reanalysis system (ORAS5). A sub-domain in the SEAS encompassing Sunda shelf, south China sea and the eastern Indian and western Pacific Oceans (gray-dashed rectangle) is shown to highlight the respective contribution of steric and manometric components to sterodynamic sea level change d) Different components of sterodynamic sea-level rise, latitudinally-averaged over the region highlighted by rectangle in panels a, b, and c. The correspondence between the trends of steric anomalies (with respect to global-mean thermosteric sea level - red-dotted curve) and the manometric solution (green) is also shown. The number of valid grid-points in the latitudinal averaging (panel d) is given in Appendix A3.

In principle, the sterodynamic sea-level change can be viewed as a combined response to two different physical processes: the sea-level change caused by local density (steric sea-level change) and the sea-level change due to sea-water (mass) redistribution (manometric sea-level change); i.e.

$$\frac{\vartheta\eta}{\vartheta t} = \frac{1}{g\rho_0}\frac{\vartheta(p_b - p_a)}{\vartheta t} - \frac{1}{\rho_0}\int_{-H}^{\eta}\frac{\vartheta\rho}{\vartheta t}dz \qquad (12.1)$$

The first term in the RHS represents the sea-level change due to ocean mass variations which can be estimated from ocean bottom pressure changes (Pb) corrected for atmospheric loading (Pa). Note that Pa is the local sea-level pressure (SLP) anomaly with respect to the instantaneous average of SLP over the global ocean (Gregory et al. 2019). This term has been known as the bottom pressure sea level in the past literature and renamed to manometric sea-level change in

Gregory et al. (2019). And, the second term in the RHS represents the steric sea-level change estimated as the time-derivative of seawater density. We estimated steric sea-level changes from ocean temperature and salinity from ORAS5, using the equation of state (Jacket and Mcdougal, 1995). The manometric sea-level is obtained by subtracting the steric sea level from the sterodynamic sea level (Eqn. 12.1).

Figure 12.10b and 12.10c show the steric and manometric sea-level rise in the SEAS respectively. Steric sea-level rise contributes the sterodynamic sea-level rise mainly over deep oceans (Figure 12.10b and c.f. Figure 12.1 showing the water depth) while manometric rise is more prominent over shallow shelf regions in the SEAS (Figure 12.10c). This “depth-dependent” contribution of steric and manometric sea-level change has been reported earlier (e.g. Landerer et al. 2007a).

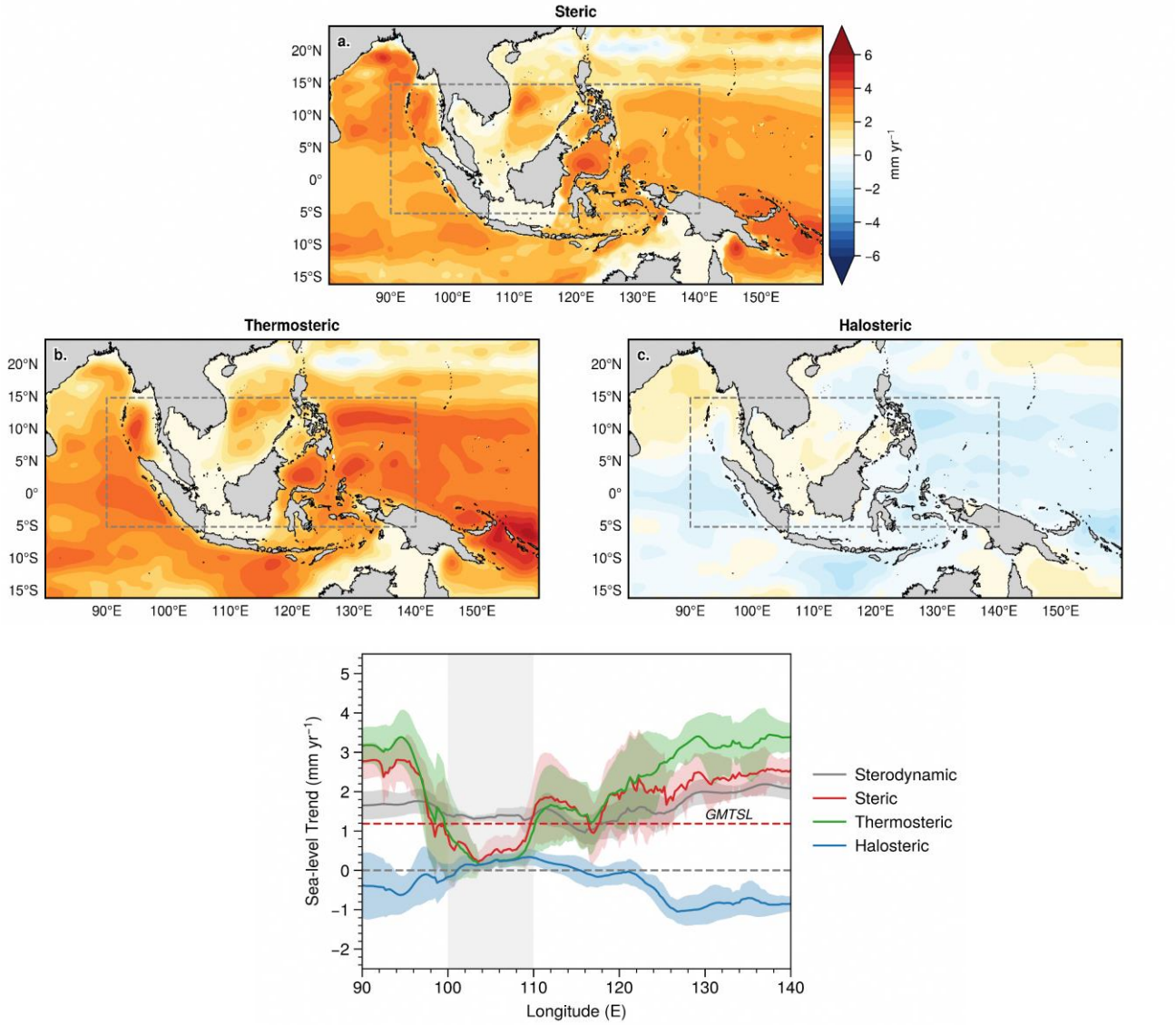

Figure 12.11: (a) Steric sea-level-rise trend decomposed into, b) thermosteric and c) halosteric sea-level rise in the SEAS estimated from high-resolution ocean reanalysis system (ORAS5). A sub-domain encompassing Sunda shelf, south China sea

and the western Indian and eastern Pacific Oceans (gray rectangle) is shown to highlight the contribution of respective components to steric sea-level rise d) Components of steric sea-level rise, latitudinally-averaged over the region highlighted by rectangle in panels a, b, and c. Red dashed line indicates the global-mean thermosteric sea-level trend for the period 1993 - 2021, estimated from ORAS5 ocean temperature and salinity (1.2 mm/yr).

As the deep ocean is more efficient in storing heat than shallow waters, the former experiences more thermosteric sea-level rise (Figure 12.11b) which leads to more steric sea-level rise over deep oceanic regions. At the same time, those enhanced deep ocean expansion would create a strong steric gradient (surface pressure gradient) between the deep and shallow regions leading to a redistribution of water to shelves, causing significant manometric sea-level rise over the shallow regions, as seen in Figure 12.10c. Readers may refer to Landerer et al. (2007b) to see more details of such mass redistribution process. Figure 12.11b indeed suggests that the steric sea-level rise in the SEAS is mostly driven by ocean thermal expansion and contribution from salinity changes (halosteric sea-level changes) is relatively weak (Figure 12.11c).

To understand the relative role of steric and manometric sea-level rise to sterodynamic sea-level change in our region better, let us focus over a small subdomain as highlighted by dashed rectangles on Figures 12.10 and 12.11. The selected region encompasses the shallow Sunda shelf (sea around Singapore) at its center and deep basins either side of it.

A meridionally-averaged distribution of sea-level trend, as shown in Figures 12.10d and Figure 12.11d, clearly shows how steric and manometric sea-level change contribute differently over deep and shallow regions in the SEAS. The steric sea-level trend drops significantly (falls close to zero) over the Sunda shelf and then rises at either side of the shelf where water depth increases sharply (off to the continental slope, c.f. Figure 12.1). The manometric sea-level trend appears to be a mirror of the steric sea-level trend (green and red curves in Figure 12.10d), supporting the notion that the ocean adjusts to the spatially non-uniform steric sea-level rise by redistributing the ocean mass from regions of larger steric sea-level rise to regions of smaller steric sea-level rise (Landerer et al. 2007b). Even though the exact physical mechanism through which this mass transfer occurs is rather complex and not understood fully (see Bingham and Hughes, 2012), it is interesting to note that the sterodynamic sea-level rise in the Sunda shelf and off Singapore is primarily associated with “ocean internal mass redistribution”. Figure 12.10d also suggests that the manometric sea-level rise could be driven by the gradient in steric sea-level anomalies with respect to global-mean thermosteric change (red-dotted curve in Figure 12.10d), rather than by the actual steric sea-level rise.

As mentioned above, the steric sea-level rise in the SEAS is mostly contributed by thermosteric changes as seen in Figures 12.11b and 12.11c. Even though the contribution of halosteric sea-level rise is weak compared to thermosteric changes, it is worth noting that the salinity contribution is positive in the SCS region and negative in the western Pacific and eastern Indian Ocean (Figures 12.11c and 12.11d). This spatial variability indicates the freshening of seawater in the SCS over the recent decades compared to the western Pacific for which the depth-integrated salinity seems increased. The physical processes that contribute to the halosteric sea-level rise in the SCS is not examined further for this report, but this will be an important perspective for CCRS research activities in future.

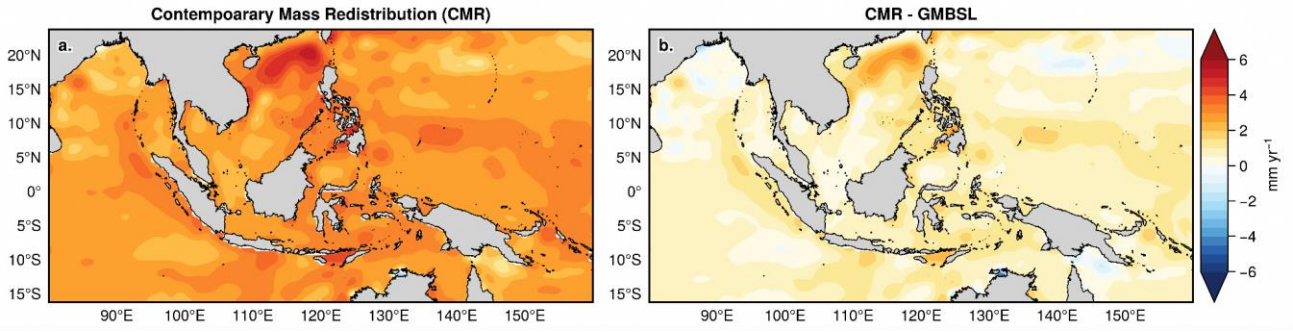

Figure 12.12: a) Sea-level rise trend from contemporary mass redistribution (CMR, as shown in Figure 12.9) estimated as the difference between altimeter and sterodynamic sea-level. Global-mean barystatic sea-level rise for the period 1993 - 2021 (2.1 mm/yr) is subtracted from CMR-driven sea-level rise (panel a) to highlight the GRD effects in the SEAS and shown in b.

We noted earlier that the CMR-driven sea-level rise (Figure 12.12a) includes the global-mean barystatic sea-level rise (GMBSL; ~2.1 mm/yr) and the regional deviations associated with the GRD effects. We have subtracted the GMBSL rate from the CMR sea-level trend to see if there are any notable deviations in the SEAS (Figure 12.12b). No significant deviations from GMBSL rate observed in the SEAS, except for a noticeable pattern in the northern SCS (Figure 12.12b). A few of the previous studies indicated that the GRD effects in the tropical regions are rather uniform (e.g. Frederikse et al. 2020; Wang et al. 2021), and hence, the anomalous CMR pattern seen in the northern SCS (Figure 12.12a) would probably be related to either any "uncaptured" sterodynamic signal in the ORAS5 or some other processes which may not be accounted for by the GRD effects. To investigate this further, we compared the dynamic sea-level (DSL) rise from other two reanalyses - GECCO3 (German contribution of the Estimating the Circulation and Climate of the Ocean; Köhl, A. 2020) and GLORYS 12V1 (Global Ocean Physics Reanalysis; Supplementary figure A12.4) over the same period, and found that the DSL rise in the northern SCS in those products conforms each other but differ to that from ORAS5. This indicates that the anomalous CMR signal in the northern SCS (Figure 12.5a) might be originating from uncertainties in SD sea-level change in this region as represented in reanalyses. We do not go into further details on it in this report. In general, Figure 12.12 suggests that the CMR related mean sea-level rise in the SEAS is predominantly driven by GMBSL rise and the GRD effects are negligible as suggested by earlier studies mentioned above.

As we have seen at the beginning of this section, the residual sea-level signal, i.e. signal obtained once the sterodynamic sea-level change is subtracted from GIA-corrected altimeter sea level, is considered an approximation to the contribution of CMR to sea-level rise over the satellite period in the SEAS (shown in Figure 12.12a). This approximated CMR contribution should be understood within the context of uncertainties associated with the sterodynamic sea-level changes, any other processes that contribute to the observed sea-level change, and the uncertainties in the altimeter measurements itself. Our sterodynamic sea-level estimate comes from a recently updated ocean reanalysis which encompasses the latest updates and advances in base ocean model and observational data assimilation for the post-altimetry era (see Zuo et al. 2019), and hence offer minimum uncertainties in the sea-level and other ocean state variables used in this report (ocean temperature and salinity). However, an exact assessment of the CMR driven sea-level rise should follow an independent estimate of GRD sea-level fingerprints using geodetic models (e.g. Harvey et al. 2021; Coulson et al. 2022). Such an exercise would also reveal the contribution of individual mass sources (e.g. Greenland ice sheet and mountain glaciers) to the observed sea-level rise in the SEAS. We are currently developing this analysis to include such independent CMR contributions using latest mass balance estimates from different sources (e.g. data from the Ice

Sheet Mass Balance Inter-comparison Exercise - IMBIE; Otosaka et al. 2023), which would complement the findings presented in this report in the near future.

12.4. Observed sea-level rise around Singapore

The vertical datum for all height measurements in Singapore (called Singapore Height Datum) is set to mean sea level at 0.0 m, which is taken as the average water level from the historical tide-gauge record at the Victoria Dock for the 1935 - 1937 period (Singapore Land Authority, Singapore). As we have seen in the introduction, a large portion of the Singapore mainland (especially the coastal zones) lies well below five meters of MSL. MSL changes, ranging from seasonal to long-term (over a period of 100 years), hence have great concern for the coastal regions of Singapore as it could adversely affect Singapore's coastal infrastructures.

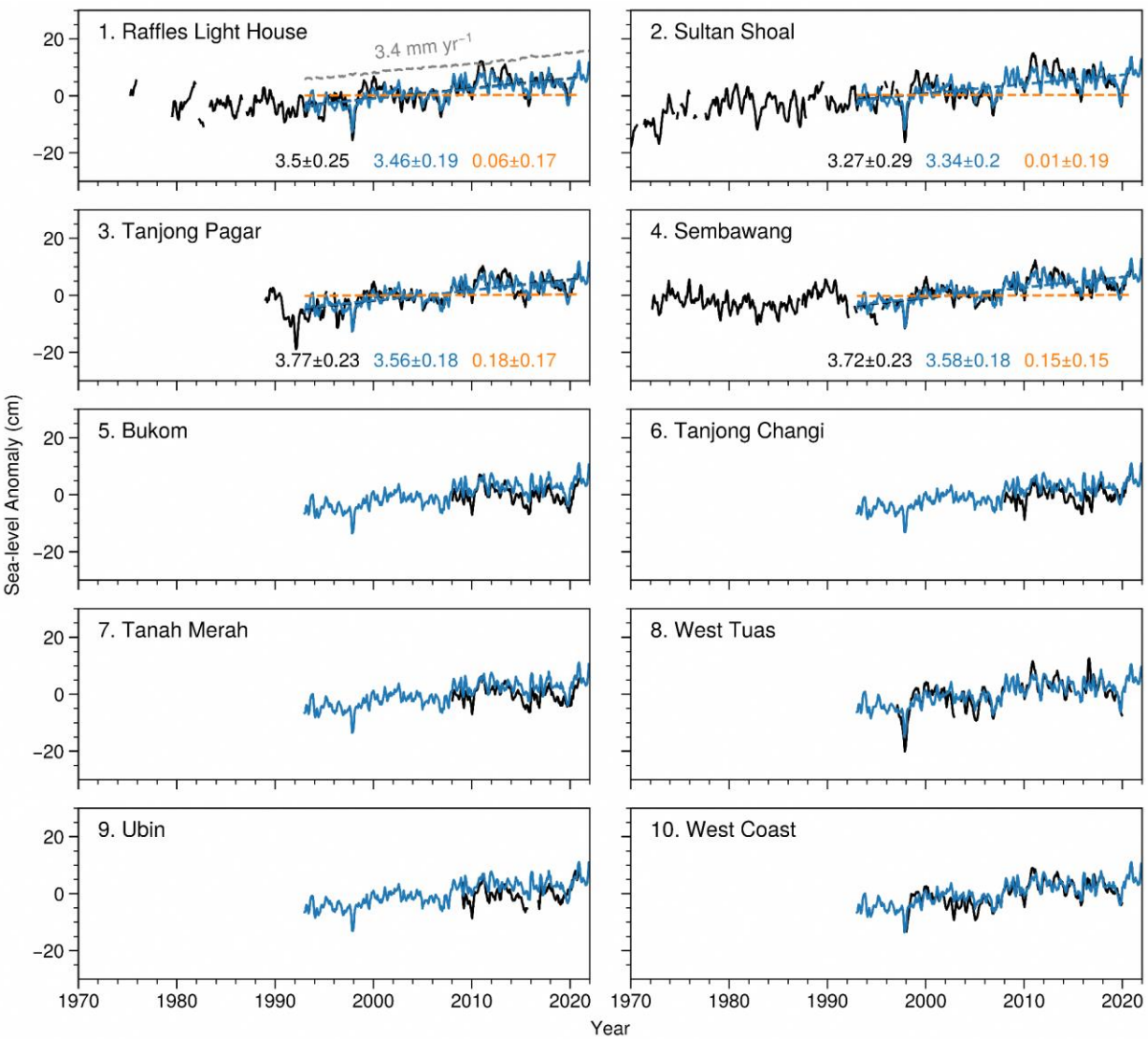

Figure 12.13: Time series of sea-level anomalies from tide gauges (black) and satellite altimetry (blue, averaged over 1 degree around each tide-gauge location). The difference between the tide-gauge and satellite time series is taken for the first four tide-

gauge records which have more than 90% of data during the satellite period (1993 - 2021). A linear trend based on the least-square method is also plotted as a dashed line over those four records (black - tide-gauge, blue - satellite, orange - difference. Units are mm/yr). The slope and standard error corresponding to each trend line are also given. The global-mean sea level from satellite altimetry (trend ~ 3.4 mm yr-1) is shown for a comparison in panel a (gray dashed curve), indicating that the mean sea-level rise off Singapore over the last three decades is consistent with the rate of global-mean sea-level rise.

Sea-level time series from ten tide-gauge records around Singapore are shown in Figure 12.13. Satellite sea-level data (¼ degree resolution) averaged at a 1-degree square domain around each tide-gauge record is also shown (blue curve). Note that, mean seasonal cycle (seasonal climatology) is removed from both satellite and tide-gauge data. There is a good level of agreement between tide gauge and altimeter time series at interannual periods (Figure 12.13), providing confidence on comparing their respective trends. Four out of ten records (Raffles Light House, Sultan Shoal, Tanjong Pagar and Sembawang) have more than 90% data over the altimeter period (1993 - 2021) and the trend estimates are given for those four records (Figure 12.13). As we have seen in section 12.3 and for Figure 12.8, difference in sea-level rise trend estimates between tide-gauge record and altimeter sea level could indicate rate of local VLM, which is shown for those four records.

Rate of sea-level rise around Singapore varies between 3.27 (Sultan Shoal) to 3.77 (Tanjong Pagar) with a mean rate (average rate for the four stations) of 3.56 mm/yr during 1993 - 2021. The mean rate from corresponding altimeter data (3.48 mm/yr) is close to tide-gauge measured sea-level rise. Figure 12.13 shows that the rates of sea-level rise from tide-gauge and satellite at the four tide-gauge stations agree well with each other. This agreement between tide-gauge and altimeter sea-level trends indicates that the rate of local VLM in Singapore might be weak (< 0.2 mm/yr) compared to other coastal locations in the southeast Asian region (see Figure 12.8). Local VLM consists of VLM caused by GIA and other processes (local subsidence, tectonics, etc). As shown in section 12.6 (Table 12.5), the GIA-induced land uplift rate is ~0.2 mm/yr. There is no consensus on the local subsidence or movements related to tectonics due to limited observations. See Section 12.6 for a detailed note on the VLM in Singapore.

Figure 12.13 also suggests that the rate of mean sea-level rise around Singapore is consistent with the rate of GMSL rise (~ 3.4 mm/yr) over the satellite period. However, it is worth noting a few points on the processes that drive sea-level changes around Singapore as discussed in section 12.3. Contemporary mass redistribution (CMR) turns out to be the main driver of observed sea level rise around Singapore (explains about 70% of the net observed rise). The CMR contribution mostly comes from the GMBSL rise over the 1993 - 2021 period which is about 2.1 mm/yr (Figure 12.12). On the other hand, manometric sea-level (ocean internal mass distribution) drives large part of the sterodynamic sea-level rise (~23% of the total rise) with a very weak contribution from steric sea-level rise (due to the fact that shallow shelf does not support large steric changes compared to deep ocean).

The combined contribution of both CMR and manometric sea-level suggests that nearly 90% of the observed sea-level rise off Singapore is “mass-driven”. The dominating contribution of CMR on sea-level rise around Singapore indicates how land ice melting from remote locations (mostly from mountain glaciers in mid-to-high latitudes) can impact low-lying countries in the equatorial regions. Also, the role of manometric sea level indicates that the dynamic sea-level changes off Singapore are essentially linked to ocean circulation, highlighting the importance of accurately resolving the circulation features in climate models to better predict the sterodynamic sea-level rise for the region. The coarse resolution of the current global climate models cannot resolve the narrow straits and coastal currents adequately, and our findings stress the need for high-resolution ocean modeling and dynamical downscaling of the ocean climate and sea level to obtain better future projections.

12.5 Sea-level projections

Sections 12.3 and 12.4 provide an overview of the historical sea-level change in Singapore and the Southeast Asian region, and important contextual

information on driving mechanisms that are also relevant to the spatio-temporal evolution of future sea-level rise in this region. In the following sections, we present future sea-level projections for both Singapore and Southeast Asia for several tide gauge locations. We also discuss the strengths and limitations of the projections in order to promote well-informed coastal protection planning measures.

The Intergovernmental Panel for Climate Change Sixth Assessment Report (IPCC AR6) (Fox-Kemper et al., 2021; Garner et al., 2021) published in 2021 produced global and local sea-level projections using state-of-the-art methodologies. Major advances in the sea-level projections in AR6 compared to previous IPCC reports (i.e., AR5 and SROCC) include: (i) the use of emulators to provide sea-level projections consistent with the AR6 assessment of equilibrium climate sensitivity and global surface temperature rise (Forster et al, 2021; Fox-Kemper et al, 2021; Slangen et al., 2022); (ii) the explicit consideration of accelerated sea-level associated with poorly-understood ice sheet instability mechanisms through high-end storylines (Fox-Kemper et al, 2021). One key difference is also the usage of historical tide gauge data in the AR6 methods of projecting vertical land movement, which contributes to RSL rise on a regional and local scale. This is the first time the non-climatic background component contributing to RSL rise has been included in the IPCC sea-level projections, using tide gauges. In this light, the following sections present sea-level projections from AR6 at the various tide gauges in Singapore and Southeast Asia.

We follow the calibrated uncertainty terminology used in the IPCC AR6 here, in which scientific confidence levels (low, medium, high) represent a qualitative assessment of the number of lines of evidence and level of agreement among studies, whereas the likelihood of any projected value of sea-level rise (e.g., *likely* range) is a quantitative measure of uncertainty, expressed as probabilities. Other sea level terminology used in this chapter follows that of Gregory et al. (2019). We focus on three Shared Socioeconomic Pathways (SSPs): SSP1-2.6, SSP2-4.5 and SSP5-8.5 for all the sea-level projections shown in the following sections, to be consistent with the climate projections presented in the other chapters of this report.

12.5.1 Data and methods

Here we outline the main methodology utilised in the IPCC AR6 projections and our V3 projections for sea level. But for more technical details, do refer to the detailed report (Chapter 9 of IPCC AR6 WGI).

AR6 methodology

Sea-level projections from the IPCC AR6 are produced using the Framework for Assessing Changes to Sea-level (FACTS; Kopp et al, 2023). FACTS employs a Monte Carlo approach across the various drivers of GMSL rise and includes localisation of these global projections using GRD patterns, information of sterodynamic sea-level change from CMIP6 models and vertical land motion (including the effect of GIA) based on Kopp et al (2014). In AR6, medium confidence sea-level projections are tabulated until 2150, whereas thereafter until 2300 are considered low confidence sea-level projections. The type and number of models used, combined with expert judgment assessments, vary largely across the individual drivers. No single method was used to derive the projected sea level change by the different drivers for a homogeneous time period (e.g., 2020 to 2150). Table 12.2 below summarises the methodology used to estimate each driver of the IPCC AR6 sea-level projections.

Table 12.2: Summarised methodologies respective to the sea level drivers according to 3 timelines: projections up till 2100, beyond 2100 till 2150 and till 2300. Heavily referenced from IPCC AR6 Chapter 9 and Table 1 from Slangen et al. (2022); refer to AR6 for full reference.

	Sea level driver	**Projection for 2014-2100 (*medium confidence*)**	**Projection for 2100-2150 (*medium confidence*)**	**Projections for 2150-2300 (*low confidence*)**

1	Thermal expansion	Two-layer emulator with climate sensitivity calibrated to the AR6 assessment and expansion coefficients calibrated to emulate CMIP6 models.	
2	Ocean dynamic sea level	Multivariate *t*-distribution fitted to ocean dynamic sea level produced from CMIP6 models. This distribution is derived from CMIP6 ensemble *zos* field after linear drift removal, then combined with the emulator-based global mean thermosteric projections.	
3	Glaciers	Gaussian process emulated glacier model: GlacierMIP (Marzeion et al., 2020; Edwards et al., 2021)	AR5 parametric model re-fit to GlacierMIP (Marzeion et al., 2020).
4	Greenland Ice Sheets	Medium confidence processes up to 2100: Emulated ISMIP6 simulations (Box 9.3) (Edwards et al., 2021)	Medium confidence processes: Parametric model fit to ISMIP6 simulations up to 2100 extrapolated based on either constant post-2100 rates or a quadratic interpolation to the multimodel assessed 2300 range. Assumption of constant rates of mass change after 2100. Low confidence processes: Structured expert judgement (Bamber et al., 2019)
5	Antarctic Ice Sheets	Medium confidence processes up to 2100: p-box including (1) Emulated ISMIP6 simulations (Edwards et al., 2021) and (2) LARMIP-2 simulations (Levermann et al., 2020) augmented by AR5 surface mass balance model. Processes considered are surface mass balance and ice dynamics, which includes marine ice sheet instability (MISI).	Medium confidence processes after 2100: p-box including (1) AR5 parametric AIS model and (2) LARMIP-2 simulations augmented by AR5 surface mass balance model, with both methods extrapolated based on either constant post-2100 rates or a quadratic interpolation to the multimodel assessed 2300 range. Low confidence processes: (1) Single ice-sheet-model ensemble simulations incorporating Marine Ice Cliff Instability (MICI) (DeConto et al., 2021) and (2) structured expert judgement (Bamber et al., 2019)
6	Land Water Storage	Statistical relationships between population and anthropogenic causes of changes in land water storage are determined: (1) Population and groundwater depletion relationship calibrated based on Konikow (2011), Wada et al., (2012) and Wada et al., (2016). (2) Population and dam impoundment relationship calibrated based on Chao et al., (2008), and adjusted to scenario-dependent based on the different SSP's population variations (Kopp et al., 2014).	

7	Vertical Land Motion	Using a Gaussian process spatiotemporal model based on tide-gauge data (updated from Kopp et al., (2014)) and GIA model, linear rates of VLM are derived.
8	Gravitational, rotational, and deformational (GRD) effects	Sea-level equation solver (Slangen et al., 2014a) driven by projections of ice sheet, glacier, and land water storage changes is used to compute annual sea-level fingerprints for each mass change contribution.

Deriving V3 sea-level projections for Singapore

The IPCC AR6 provided RSL projections for Singapore at 6 tide-gauges. These six tide-gauges are Sultan Shoal, Sembawang, Raffles Light House, Tanjong Pagar, West Coast and West Tuas. Although there are a total of 13 running tide gauges in Singapore that are managed by the Marine Port Authority (MPA), only the above-mentioned 6 tide gauges have records that span at least 15 years, which was the criteria for generating sea-level projections at tide gauges in AR6 (Kopp et al., 2014).

Annual tide-gauge data from the Permanent Service for Mean Sea-Level (PSMSL) play a crucial role in the AR6 sea-level projections for vertical land movement (VLM)—a component that distinguishes local sea level projections from regional and global projections. As part of the IPCC methodology, the tidal data is processed through a spatiotemporal Gaussian model developed by Kopp et al. (2014) to estimate VLM. This analysis generates a linear projected rate of VLM, along with a corresponding standard deviation (Kopp et al., 2014).

However, during quality checks on the Singapore tide-gauge data, errors in the Sembawang annual tide-gauge data were identified. Specifically, we worked with PSMSL and discovered that the data from the 1950s preceding a data gap was not referenced to the same benchmark as the rest of the dataset (Figure 12.14). The erroneous data associated with the Sembawang tide-gauge was subsequently revised and improved by Peter Hogarth from PSMSL. The improved dataset was reprocessed using the Kopp et al. (2014) model.

This step allowed us to generate revised VLM projections and update the AR6 sea level projections for the six tide gauges in Singapore. The AR6 projections without the VLM component were obtained from the IPCC authors (Garner et al., 2022). In accordance with the AR6 methodology, we added our revised VLM projections with the AR6 projections that do not contain the VLM component and generated the total projected RSL for all six locations in Singapore.

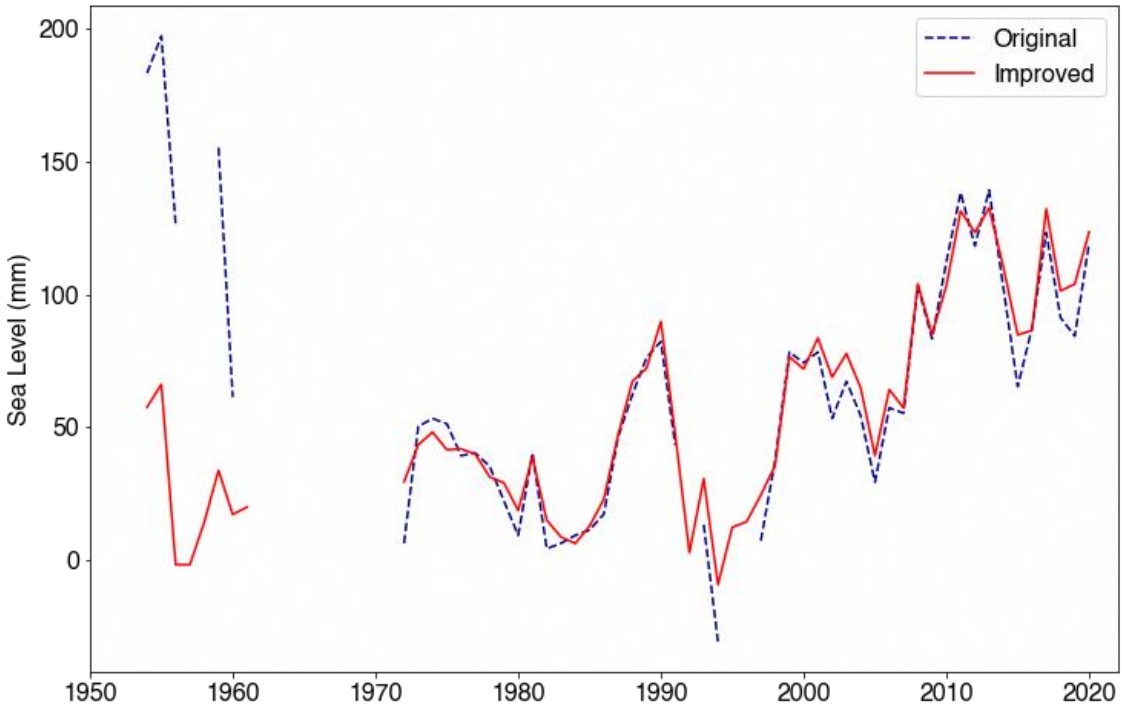

Figure 12.14: Annual tide-gauge data at Sembawang. Shown in dashed blue is the original data on PSMSL and red is the corrected data.

12.5.2 Global-mean sea level projections

According to the IPCC AR6 WGI Report, global-mean sea-level (GMSL) is projected to rise across all future climate scenarios. Until 2050, in accordance with the AR5 and Special Report on the Ocean and Cryosphere in a Changing Climate (SROCC) reports, the projected GMSL rise shows little variation depending on different scenarios. However, after 2050, the scenarios start to show more significant differences (Fox-Kemper et al., 2021).

There is medium confidence in these projections, with a *likely* GMSL rise of 0.19 (0.16–0.25) m under SSP1-2.6 and 0.23 (0.20–0.30) m under SSP5-8.5 by 2100 (Figure 12.15).

The IPCC AR6 suggests an alternative approach to addressing uncertainty in future GMSL rise by factoring in the uncertainty associated with the timing of specific sea-level rise thresholds. Focusing on projections that only incorporate processes with medium confidence, it is *likely* that GMSL will surpass 0.5 m sometime between 2080 and 2170 under SSP1-2.6 and between 2070 and 2090 under SSP5-8.5.

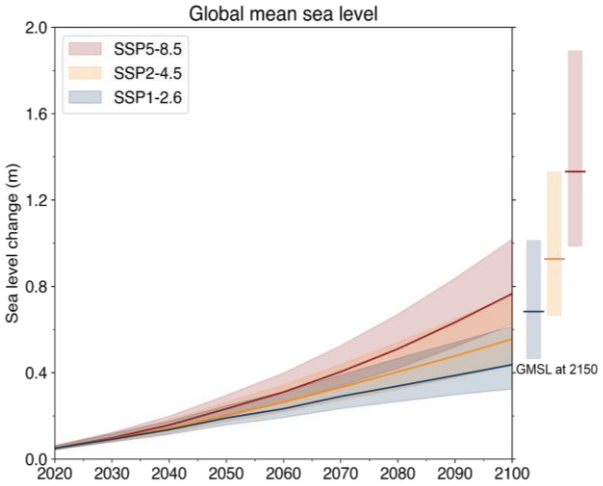

Figure 12.15: Projected rise in global-mean sea-level up to 2150, relative to IPCC AR6 baseline 1995 - 2014, under three emission scenarios (SSP1-2.6, SSP2-4.5 and SSP5-8.5). Solid curves represent the median

(50th percentile), whilst the shaded bands represent the *likely* range (17th to 83rd percentile).

It is *likely* that GMSL will exceed 1.0 m between 2150 and beyond 2300 under SSP1-2.6, and between 2100 and 2150 under SSP5-8.5. However, it is *unlikely* to surpass 2.0 m until after 2300 under SSP1-2.6, whereas it is *likely* to do so between 2160 and 2300 under SSP5-8.5 (Fox-Kemper et al., 2021).

12.5.3 Sea-level projections for Singapore

In the following subsections, we provide a comprehensive analysis of our sea-level projections. Our findings encompass both medium and low confidence projections, offering valuable insights for planning and decision-making. The medium confidence sea-level projections extend up to the year 2150 (Section 12.5.3.1). These projections serve as a robust basis for mitigation planning, providing stakeholders with a reliable framework for addressing potential sea-level rise impacts within a reasonable timeframe. Additionally, we present low confidence sea-level projections that extend beyond 2150, up until 2300 (Section 12.5.3.2). Despite their lower confidence level, these projections hold significance as they represent potential outcomes that cannot be entirely disregarded. By including these projections, we aim to equip stakeholders with a more comprehensive understanding of the range of possibilities, enabling them to make better-informed decisions.

12.5.3.1 Medium-confidence sea-level projections to 2150

Here we present sea-level projections at the six tide gauges in two ways: (i) continuous projections for the period 2014-2100; and (ii) projected ranges at 2150 (Figure 12.16 and 12.17). Figure 12.16 provides a timeseries visualisation of the projected change in mean sea level at the six locations, whilst Figure 12.17 summarises the projections by 2150 under the low, medium and high emission scenario on a map of Singapore.

A consistent methodology was used in the AR6 sea-level projections for the period 2014-2100, so we show these as continuous time series. For the period from 2100 to 2150, additional methodological assumptions were made that resulted in discontinuities in the time series. Therefore, we show only the projected ranges at 2150. All sea-level projections are expressed relative to the AR6 baseline period of 1995-2014.

Annual tide-gauge records of the change in RSL as recorded by these tide gauges prior to 2020 are also shown in Figure 12.17. See Table 12.3 for values of the median and *likely* range of sea-level projections at these gauges for three scenarios.

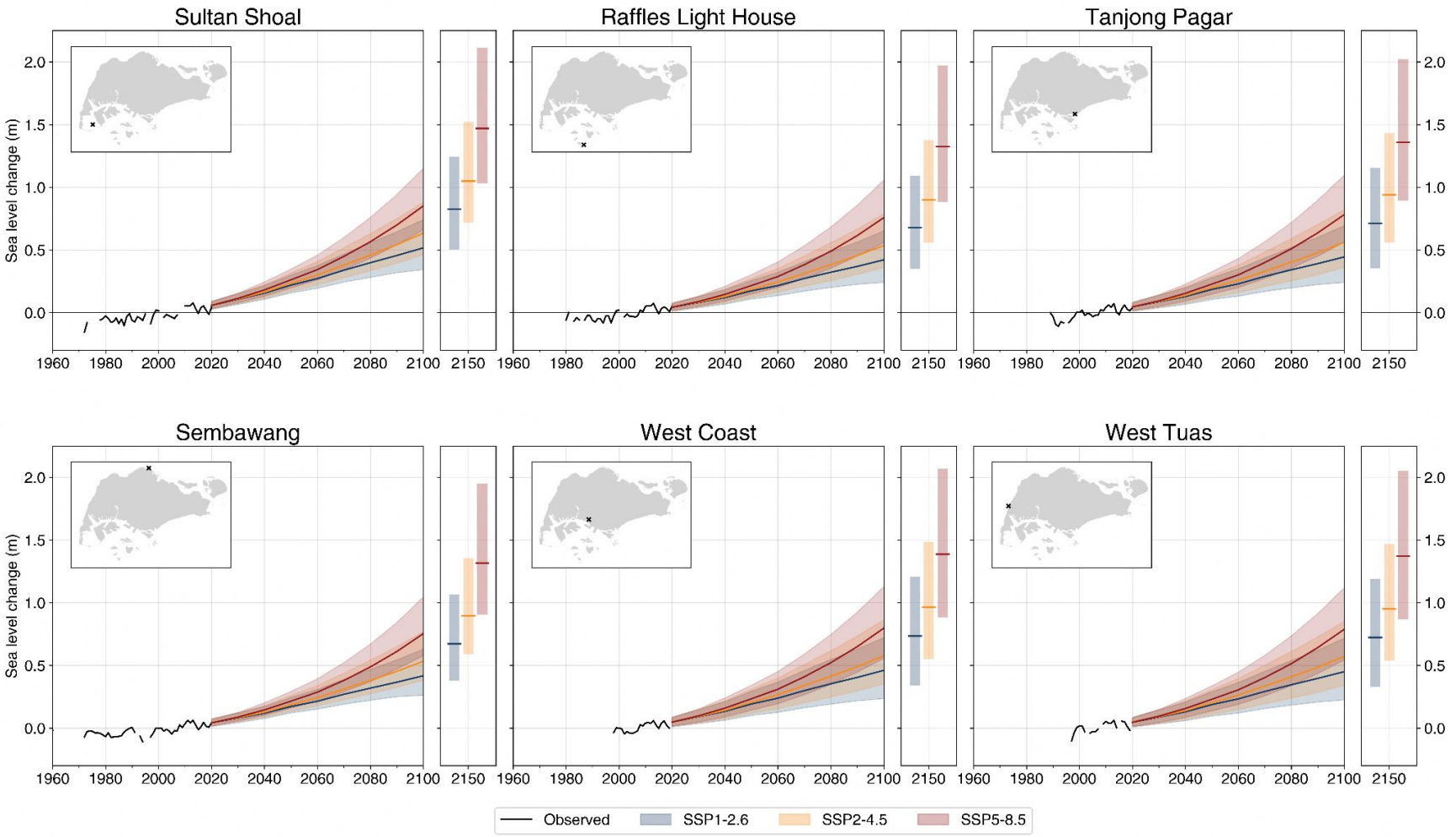

Figure 12.16: Time series of relative sea level change at the six primary Singapore tide gauges. Black solid line before 2020 shows observed relative sea level using annual tide gauge data taken from PSMSL. After 2020, continuous mean sea level projections up till 2100 and at 2150 for 3 SSPs (SSP1-2.6, SSP2-4.5, SSP5-8.5) are shown. Median (colored solid lines) and *likely* range (shaded regions) of the projections are shown. Projections at Sembawang have been adjusted with the new VLM projections taken into consideration. Both observed and projections are relative to the baseline 1995 – 2014. Individual locations of these tide gauges, indicated with a black cross, are shown on a map of Singapore on the top right corner.

Figure 12.17: Projected relative sea-level rise in Singapore at six tide-gauges (Sembawang, West Tuas, West Coast, Tanjong Pagar, Raffles Light House and Sultan Shoal) by 2150 under three emission scenarios (SSP1-2.6, SSP2-4.5 and SSP5-8.5). Values shown reflect the median (*likely* range) projected sea-level change by 2150 relative to the IPCC AR6 baseline 1995 - 2014.

Tide Gauges	SSP1-2.6		SSP2-4.5		SSP5-8.5	
	2100	**2150**	**2100**	**2150**	**2100**	**2150**
Sultan Shoal	0.51 (0.34 – 0.74)	0.82 (0.50 – 1.24)	0.63 (0.46 – 0.88)	1.05 (0.72 – 1.52)	0.85 (0.66 – 1.15)	1.47 (1.03 – 2.12)
Sembawang	0.42 (0.26 – 0.63)	0.67 (0.38 – 1.07)	0.53 (0.38 – 0.77)	0.9 (0.59 – 1.36)	0.75 (0.58 – 1.04)	1.32 (0.90 – 1.95)
Raffles Light House	0.42 (0.24 – 0.65)	0.68 (0.35 – 1.09)	0.54 (0.36 – 0.79)	0.9 (0.56 – 1.38)	0.76 (0.56 – 1.06)	1.32 (0.88 – 1.97)
Tanjong Pagar	0.44 (0.24 – 0.69)	0.71 (0.35 – 1.16)	0.56 (0.36 – 0.82)	0.94 (0.56 – 1.43)	0.78 (0.56 – 1.10)	1.36 (0.89 – 2.02)
West Coast	0.46 (0.24 – 0.72)	0.74 (0.34 – 1.21)	0.58 (0.35 – 0.86)	0.97 (0.55 – 1.49)	0.80 (0.55 – 1.13)	1.39 (0.88 – 2.07)
West Tuas	0.45 (0.23 – 0.72)	0.72 (0.33 – 1.19)	0.57 (0.34 – 0.85)	0.95 (0.54 – 1.47)	0.79 (0.54 – 1.12)	1.37 (0.87 – 2.05)
Local mean	0.45 ± 0.03	0.72 ± 0.05	0.57 ± 0.04	0.95 ± 0.06	0.79 ± 0.04	1.37 ± 0.06
Global mean	**0.44 (0.32 – 0.62)**	**0.68 (0.46 – 0.99)**	**0.56 (0.44 – 0.76)**	**0.92 (0.66 – 1.33)**	**0.77 (0.63 – 1.01)**	**1.32 (0.98 – 1.88)**

Table 12.3: Relative sea-level rise projections by 2100 in meters (relative to baseline 1995-2014) for 6 of Singapore's gauges and the global mean. Values at each tide-gauge correspond to the median projection (*likely* range). Local mean is the average of the median values across all six locations.

The spatial variability of projected RSL rise across the tide gauges in Singapore is found to be relatively small, with a variation of ± 3 - 6 cm by 2100 and 2150 (Table 12.3). Among these tide gauges, Sultan Shoal exhibits the highest projected RSL rise with 0.51 (0.34 - 0.74) m by 2100 under SSP1-2.6 and 0.85 (0.66 - 1.15) m under SSP5-8.5. By 2150, the projected rise at Sultan Shoal reaches 0.82 (0.50 - 1.24) m under SSP1-2.6 and 1.47 (1.03 - 2.12) m under SSP5-8.5. This information could be of relevance to stakeholders engaged in conservative mitigation planning for Singapore's shorelines. By referencing the estimates at Sultan Shoal, stakeholders can obtain a valuable indication for setting their mitigation strategies.

To gain a comprehensive understanding of the factors influencing sea-level change, the IPCC AR6 incorporates estimates from six key components: Antarctic Ice Sheet (AIS), Greenland Ice Sheet (GIS), Glaciers, Land Water Storage (LWS), Ocean Sterodynamic (OS) and Vertical Land Motion (VLM). The contribution of these processes to sea-level rise at Singapore's tide gauges at 2100 and 2150 are shown in Figures 12.18 and 12.19 (median and *likely* range). The methodology behind the derivation of these individual processes in the IPCC AR6 is described above in Section 12.5.1, Table 12.2.

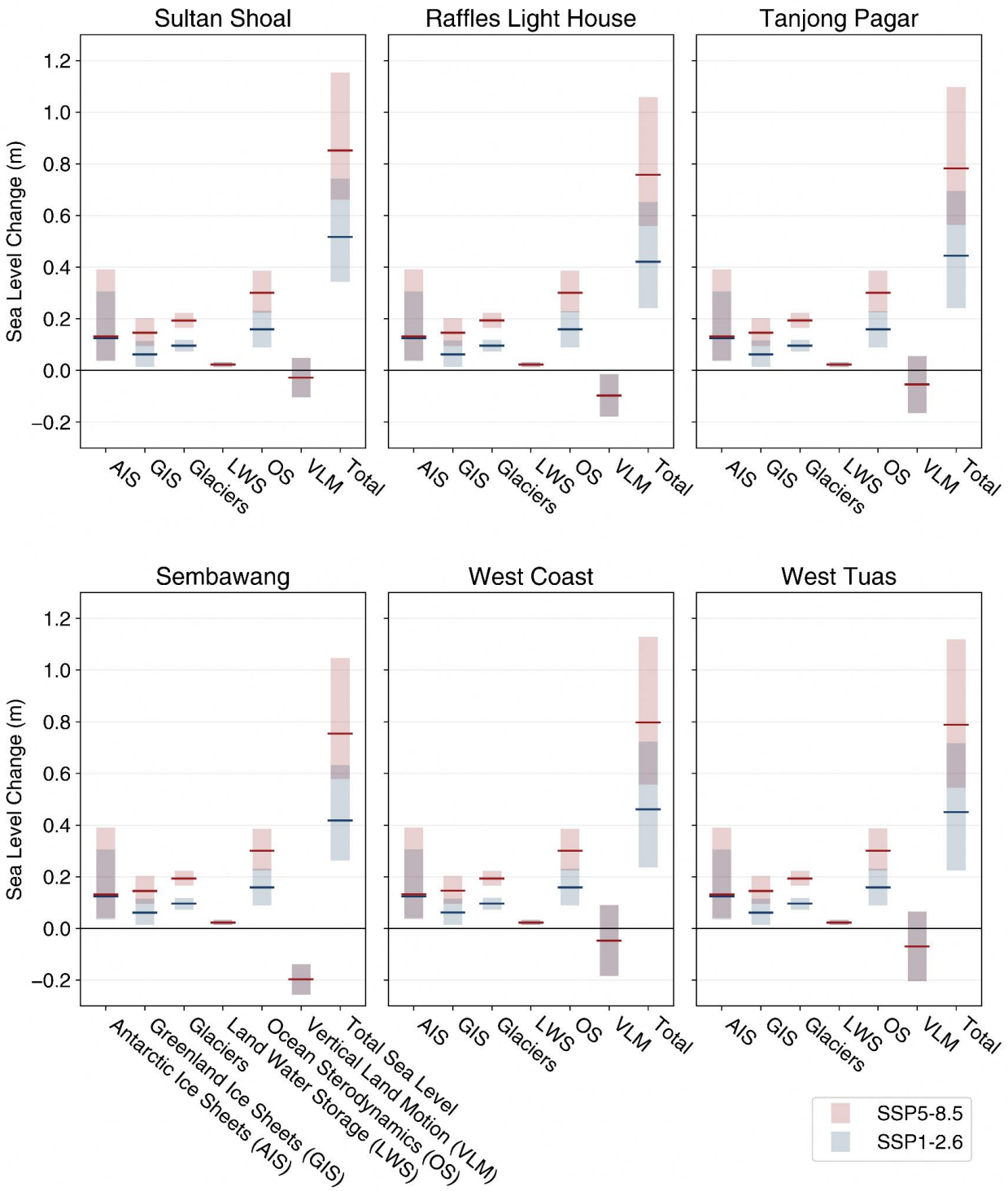

Figure 12.18: Antarctic Ice Sheet (AIS), Greenland Ice Sheet (GIS), Glaciers, Land Water Storage (LWS), Ocean Sterodynamics (OS) and Vertical Land Motion (VLM) contributions to the Total Sea Level rise in centimeters at 6 of Singapore's tide gauges by 2100 under SSP5-8.5 (red) and SSP1-2.6 (blue). *Likely* ranges (17th to 83rd percentile) are indicated with the shaded boxes. Bold, horizontal solid lines represent the median (50th percentile).

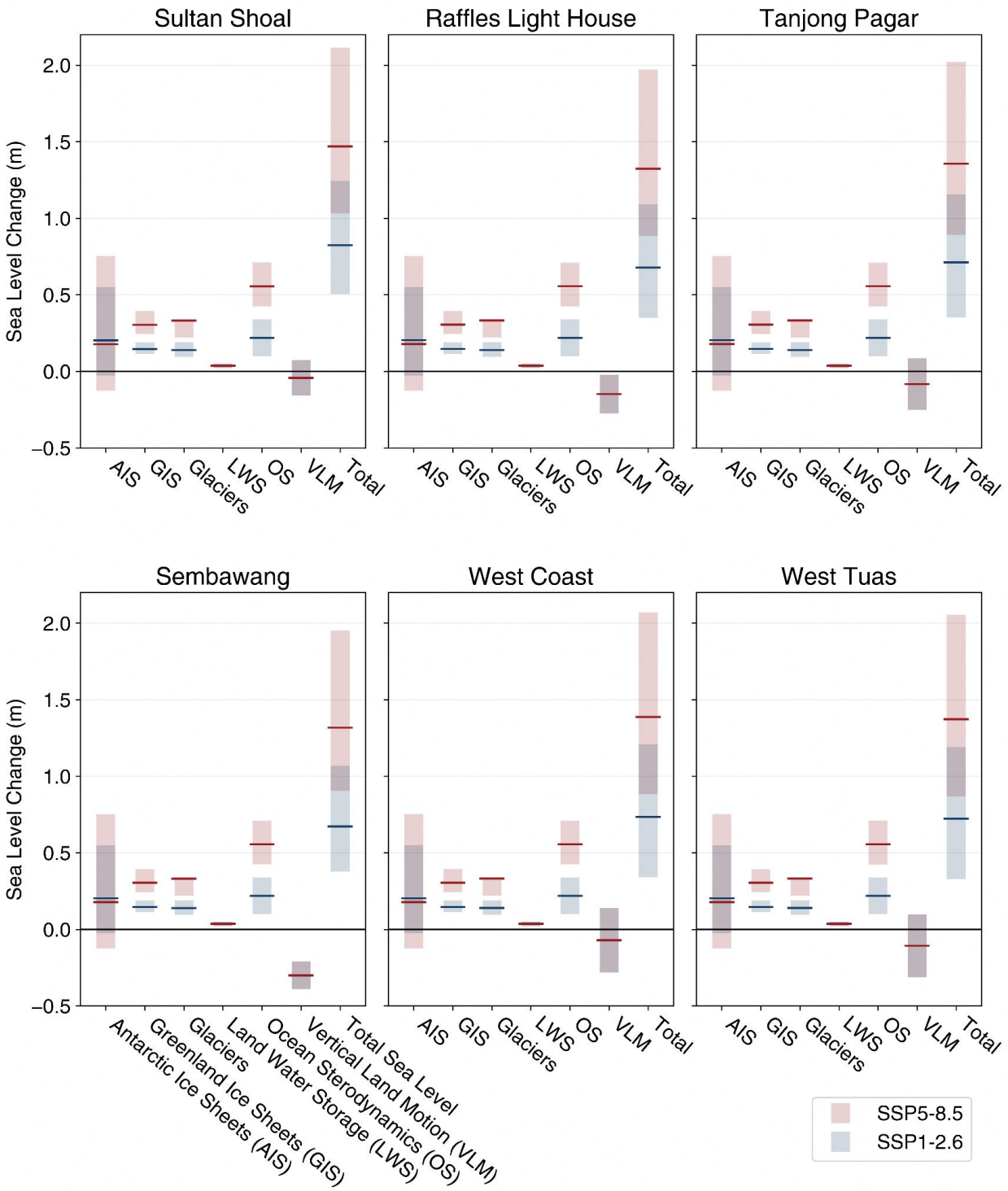

Figure 12.19: Antarctic Ice Sheet (AIS), Greenland Ice Sheet (GIS), Glaciers, Land Water Storage (LWS), Ocean Sterodynamics (OS) and Vertical Land Motion (VLM) contributions to the Total Sea Level rise in centimeters at 6 of Singapore's tide gauges by 2150 under SSP5-8.5 (red) and SSP1-2.6 (blue). *Likely* ranges (17th to 83rd percentile) are indicated with the shaded boxes. Bold, horizontal solid lines represent the median (50th percentile).

Contributor	SSP1-2.6	SSP2-4.5	SSP5-8.5	SSP5-8.5 (Global)
Ocean Sterodynamics	0.16 (0.09 – 0.23)	0.20 (0.15 – 0.26)	0.30 (0.22 – 0.39)	0.30 (0.24 – 0.36)
Greenland Ice	0.06 (0.01 – 0.12)	0.09 (0.05 – 0.15)	0.15 (0.10 – 0.20)	0.13 (0.09 – 0.18)
Antarctica Ice	0.12 (0.04 – 0.31)	0.13 (0.03 – 0.33)	0.13 (0.04 – 0.39)	0.12 (0.03 – 0.34)
Glaciers	0.10 (0.07 – 0.12)	0.13 (0.11 – 0.16)	0.19 (0.17 – 0.22)	0.18 (0.15 – 0.20)
Land Water Storage	0.02 (0.01 – 0.03)	0.02 (0.01 – 0.04)	0.02 (0.01 – 0.03)	0.03 (0.02 – 0.04)
Vertical Land Movement	0.03 (-0.04 – 0.10)	0.03 (-0.04 – 0.10)	0.03 (-0.07 – 0.10)	
Total	**0.51 (0.35 – 0.73)**	**0.63 (0.47 – 0.87)**	**0.85 (0.66 – 1.13)**	**0.77 (0.63 – 1.01)**

Table 12.4: Mean sea level projections under SSP1-2.6, SSP2-4.5 and SSP5-8.5 at Sultan Shoal, relative to baseline of 1995-2014, in meters by 2100. Individual contributions of the six components driving sea-level change and the total mean sea level are shown. Median values (*likely* range) are shown. Global mean sea level projections are shown on the far right column for the highest emission scenario SSP5-8.5.

Regardless of the emission scenario (SSP1-2.6 or SSP5-8.5), the AIS is projected to contribute the most to the uncertainty of total projected mean sea-level rise in Singapore by 2100 and 2150. Although the projected median values of sterodynamic sea-level change by 2100 and 2150 are larger than the projected median values of AIS, AIS could *likely* (83rd percentile) contribute more or just as much to the total mean sea level rise in Singapore (Table 12.4).

The changes in land water storage contributing to local sea-level rise in Singapore are almost negligible (median and *likely* range). In general, total sea-level rise (median) is projected to be higher for the worst-case scenario SSP5-8.5, with a larger *likely* range of uncertainties too. We see here that projected local sea-level rise in Singapore is largely scenario-dependent, with the exception of the contribution from the AIS and VLM, which was carefully explained in the IPCC AR6 Chapter 9 for projected global mean sea-level.

Unlike most of the other sea-level drivers, the *likely* range in the contribution of AIS to sea-level rise grows beyond 2100, as seen most significantly under SSP5-8.5. The IPCC AR6 emphasises that there is *low agreement* on the relationship between scenario-dependence and the net AIS contribution to sea level. The net changes in ice sheets are broadly driven by two processes: surface mass balance and ice dynamics. A possible reason behind a higher, albeit minimal, median sea-level rise driven by AIS under SSP1-2.6 as compared to SSP5-8.5 by 2150 (Figure 12.17) could be because of a negative contribution to sea-level rise from the Antarctic surface mass balance over the 21st century (Fox-Kemper et al., 2021). Warmer temperatures are associated with increased snowfall, and hence a fall in sea level. There is medium confidence that future contribution of the Antarctic surface mass balance to sea level will be negative under all emissions scenarios. However, it is *likely* that mass loss from the AIS from ice dynamic processes, which contributes positively to sea-level rise, will dominate in the longer term.

12.5.3.2 Low-confidence sea-level projections to 2300

In this subsection, we present a long-term perspective on sea-level rise in Singapore, focusing on one particular tide gauge: Sultan Shoal. In addition, we consider highly uncertain

ice sheet processes that could result in substantially larger sea-level rise than seen in the IPCC AR6 medium confidence projections. Sea-level projections beyond 2150 and/or that included uncertain ice-sheet feedback processes (e.g. Marine Ice Cliff Instability (MICI); DeConto and Pollard, 2016) were assessed by IPCC AR6 as having low confidence, i.e., there was low agreement and/or limited evidence to inform their assessment. However, the low confidence projections presented in this section provide important information for longer planning time-horizons and more fully represent the full range of potential future outcomes.

Essentially, there are two types of information on low confidence sea-level projections presented in IPCC AR6: (i) assessed ranges of GMSL rise at 2300 under the SSP1-2.6 and SSP5-8.5 emissions scenarios that do not include highly uncertain ice sheet feedback processes; (ii) low-likelihood high-impact storylines that include highly uncertain ice sheet feedback processes (such as MICI). Note that the storylines are presented as singular trajectories of sea-level rise that are available as local projections up to 2150. A qualitative description of the low-likelihood storylines presented in AR6 is presented in Box 9.4 (Fox-Kemper et al, 2021). The key storyline elements are: a strong warming scenario (e.g. linked to high real-world climate sensitivity); faster-than-projected disintegration of marine ice shelves and subsequent widespread onset of ice sheet instability processes in Antarctica; more frequent and severe melt events than expected for the Greenland ice sheet.

The main physical process considered in the LLHI storyline (low confidence) that is not included in the medium confidence projections presented in Sections 12.5.3.1 is the marine ice cliff instability (MICI). MICI is a process whereby ice cliffs at the edge of marine-terminating glaciers (such as in the Antarctic) become unstable and rapidly collapse. This process is a mechanism that could contribute to the potential collapse of the West Antarctic ice sheet, which could add to several meters of global sea-level rise by 2100 (e.g., DeConto and Pollard, 2016).

Figure 12.20 shows the single trajectories of LLHI storylines (83rd and 95 percentiles) at Sultan Shoal until 2300 and the low confidence projected GMSL by 2300 (17th to 83rd percentile, low confidence) that does not include the MICI processes.

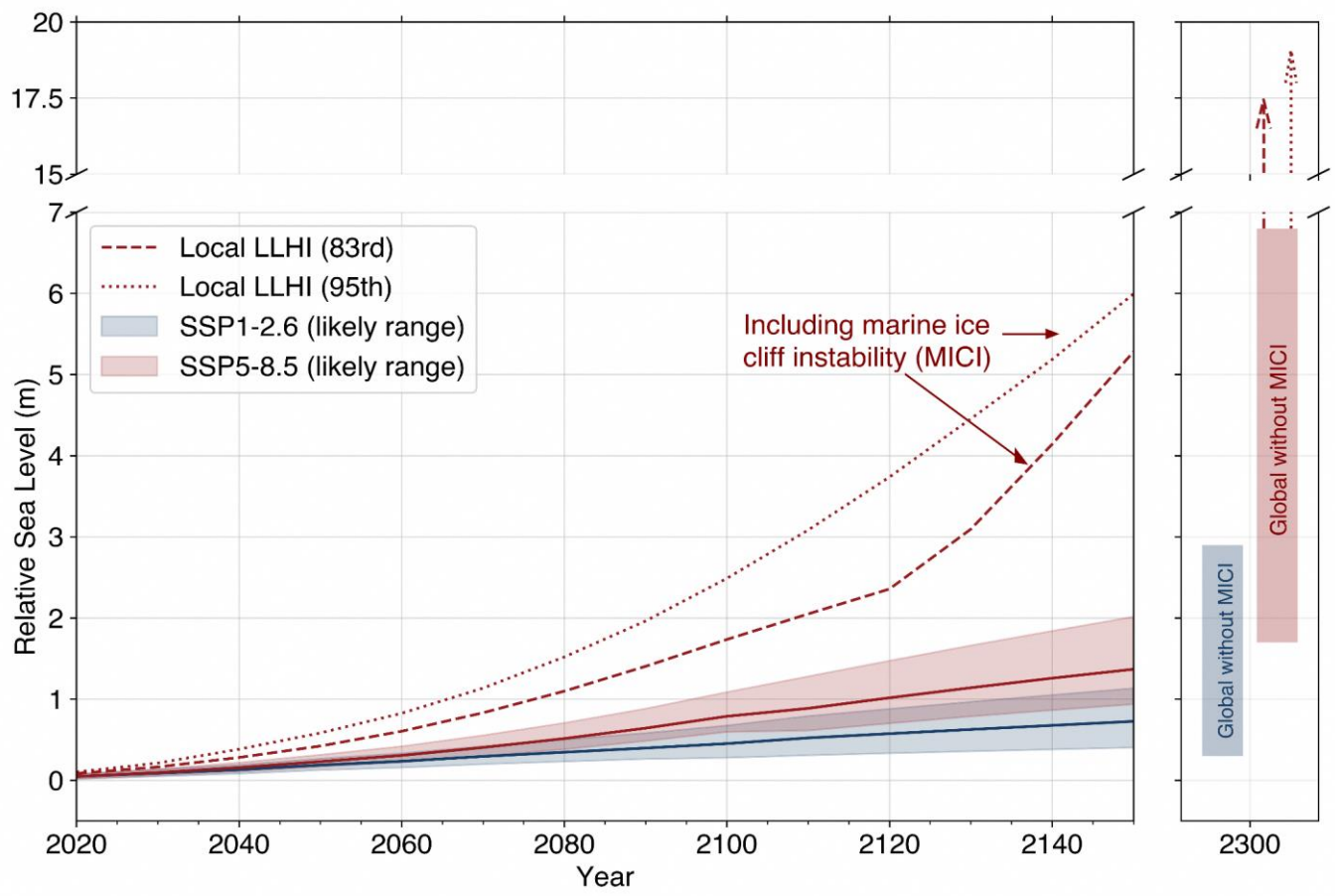

Figure 12.20: Low confidence total relative sea-level change at Sultan Shoal (Singapore) until 2300 (relative to 1995-2014 baseline) that include low-likelihood, high-impact (LLHI) ice sheet processes (i.e., MICI) that cannot be ruled out. Shaded regions before 2150 are medium confidence projections (median and *likely* range). Dashed (83rd percentile) and dotted (95th percentile) lines until 2150 and at 2300 (arrows) represent the low confidence LLHI storylines that include the unstable ice sheet processes. Low confidence projected global-mean sea-level change at 2300 that do not include MICI are shown with the shaded vertical bars. The future pathways shown are SSP1-2.6 (blue) and SSP5-8.5 (red).

The low confidence projected GMSL under SSP5-8.5 at 2300 could *likely* reach ~7 m (83rd percentile). However, if coupled with the highly uncertain ice sheet feedback processes such as MICI, 7 m of sea-level rise is projected to be obtained in Singapore just after 2150 under SSP5-8.5.

Based on the single trajectories of LLHI storylines for Singapore until 2300 (dashed and dotted lines in Figure 12.18), projected RSL rise could reach 6 m by 2150 and almost 20 m by 2300 under SSP5-8.5.

While it is not possible to provide robust likelihood information on any of the low confidence sea-level projections, we know that the assessed ranges at 2300 are much more *likely* to be reached than the LLHI storylines. Therefore, we recommend that decision makers treat the assessed ranges at 2300 as indicative of the committed sea-level rise under low and high emissions. The LLHI storylines represent much more severe outcomes that cannot be ruled out based on the current level of scientific knowledge. Choice and use of these storylines will depend on the risk appetite of adaptation planners depending on the sector and application. It is important to note that there is no single community-agreed definition of a plausible maximum sea-level rise scenario and stakeholders may wish to consider other estimates in the literature, such as Dayan et al (2021) and van de Wal et al (2022).

12.5.3.3 Differences in V3 compared to V2

Prior to the release of the AR6 sea level projections, mean sea level projections for Singapore are found in the Second National Climate Change Study for Singapore (V2) Chapter 8 'Changes in Time Mean Sea Level'. Released in 2015, this chapter was led by the UK Met Office. The V2 methods were based on the IPCC Fifth Assessment Report (AR5) sea-level projections, which represented the state-of-the-art at that time.

V2 provided only one set of medium confidence sea-level projections for Singapore based on moderate (RCP4.5) and high (RCP8.5) greenhouse gas emissions scenarios. V2 combined the *likely* range of global sea level rise from the IPCC AR5 with non-uniform spatial patterns of sea level change ("fingerprints") from Slangen et al. (2014) to derive a median and *likely* range of projected mean sea level rise for the same processes shown in V3 (i.e., ocean dynamics, Greenland and Antarctic ice sheets, glaciers and land water). Following AR5, V2 used the Representative Concentration Pathways (RCPs) climate change scenarios instead of the SSPs presented in AR6. RCP4.5 is comparable to SSP2-4.5 andRCP8.5 to SSP5-8.5. V2 provided medium confidence projections up until 2100.

The total mean sea-level rise shown in V2 under RCP4.5 was 0.53 (0.30 - 0.74) m and 0.73 (0.45 - 1.02) m under RCP8.5 at 2100. The median projected value under RCP4.5 is comparable to the average projected sea-level rise by 2100 under SSP2-4.5 in V3 (0.57 ± 0.04 m). Conversely, the median projected sea-level rise under RCP8.5 in V2 is slightly lower than the average projected sea-level rise by 2100 under SSSP5-8.5 in V3 (0.79 ± 0.04 m).

The V2 and V3 projections are relative to different baselines. The projections in V3 are relative to a different baseline 1995-2014 while the V2 projections are relative to 1986-2005. AR6 quantified the baseline adjustment as +0.03 m if adjusting the global-mean sea-level projections from AR5 to the AR6 baseline. As Singapore's rate of mean sea-level change is similar to the global mean (more in Section 12.4), we adopt this adjustment for the V2 sea-level projections as reflected in Figure 12.21.

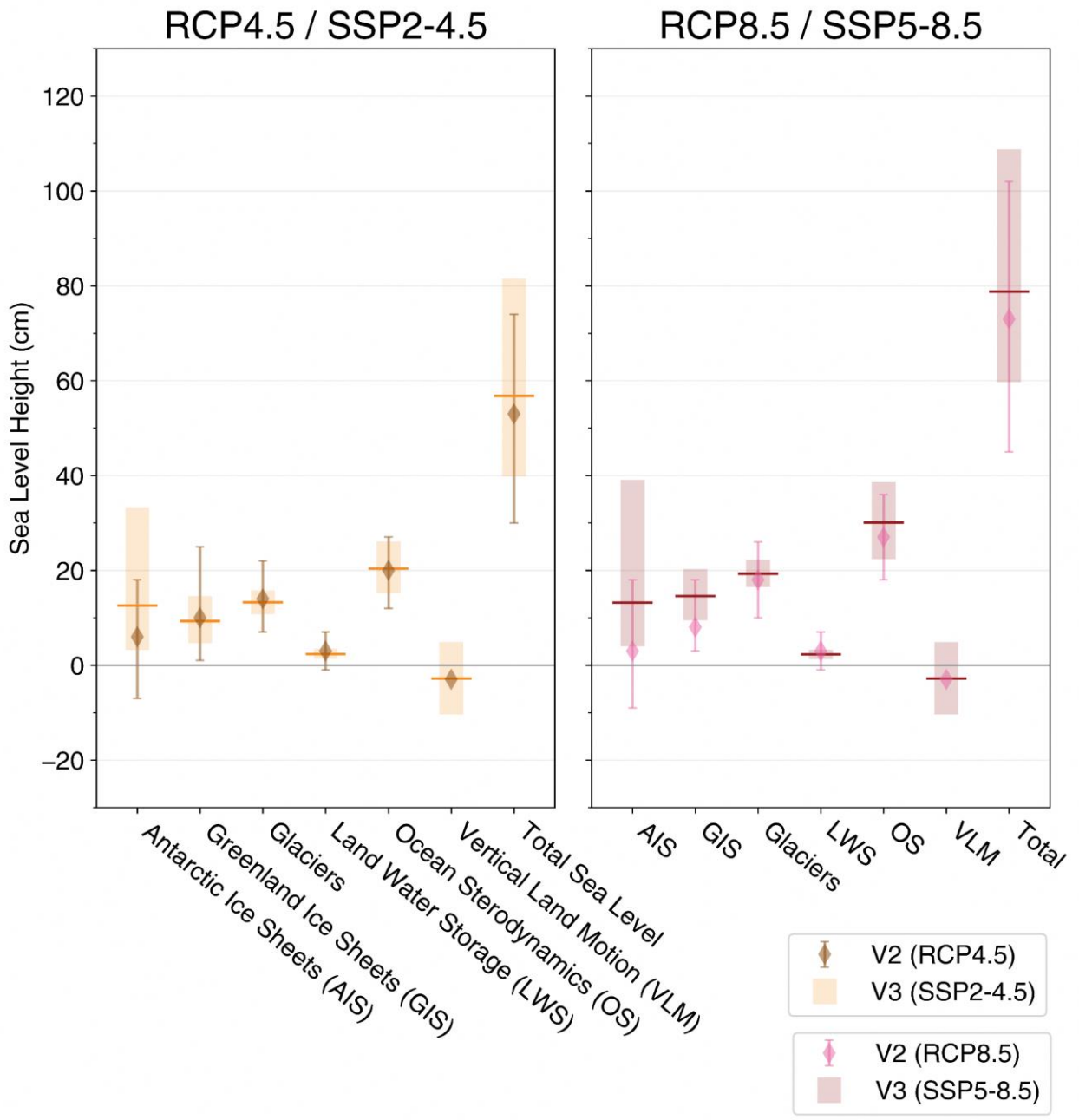

Figure 12.21: Summary of the sea-level projections given in V2 and V3 at 2100. Median (horizontal, bold lines for V3 and diamonds for V2) and *likely* range (shaded bars for V3 and error bars with caps for V2) shown from both V2 and V3. The projections from V3 shown here are at Sultan Shoal, whereas only one set of projections were given from V2.

The V2 projections show that sterodynamic sea-level change is arguably one of the largest, if not the largest (RCP8.5), component that contributes to the total projected sea-level rise. Both the median and *likely* range of the projected contribution of the AIS component had significantly increased in the V3 projections under both scenarios. Projected sea-level rise due to mass loss from glaciers and Greenland ice sheet and land water storage have reduced uncertainties in V3, stemming from improved modelling techniques and incorporation of more ice processes and feedback than the AR5 models which V2 projections were based on.

In the V3 projections, estimates of vertical land motion (VLM) contributing to RSL rise now consider more potential outcomes and non-climatic processes as compared to V2, where only one process—glacial isostatic adjustment—was considered (Kopp et al., 2014, Marzin et al., 2015). Therefore, this led to a larger range of uncertainties of RSL rise caused by VLM under all scenarios.

12.5.3.4 Coastal Vulnerability Analysis

Visualising and communicating coastal vulnerability is a crucial step in assessing the potential impacts of rising sea levels. One approach involves the use of digital elevation maps that depict specific elevations above a reference height, aligned with projected sea-level rise scenarios. These maps highlight areas that are at greater risk of inundation and can serve as valuable tools for decision-making and urban planning. However, it is important to note that this method represents just one way of assessing coastal vulnerability. Other approaches include assessing vulnerability based on socio-economic factors, ecological sensitivity, infrastructure exposure, and community resilience.

The Singapore Land Authority (SLA) provided digital elevation maps that visually depict elevations below 1 m, 2 m, and 5 m in Singapore, represented by dark blue shading (Figures 12.22, 12.23, and 12.24).

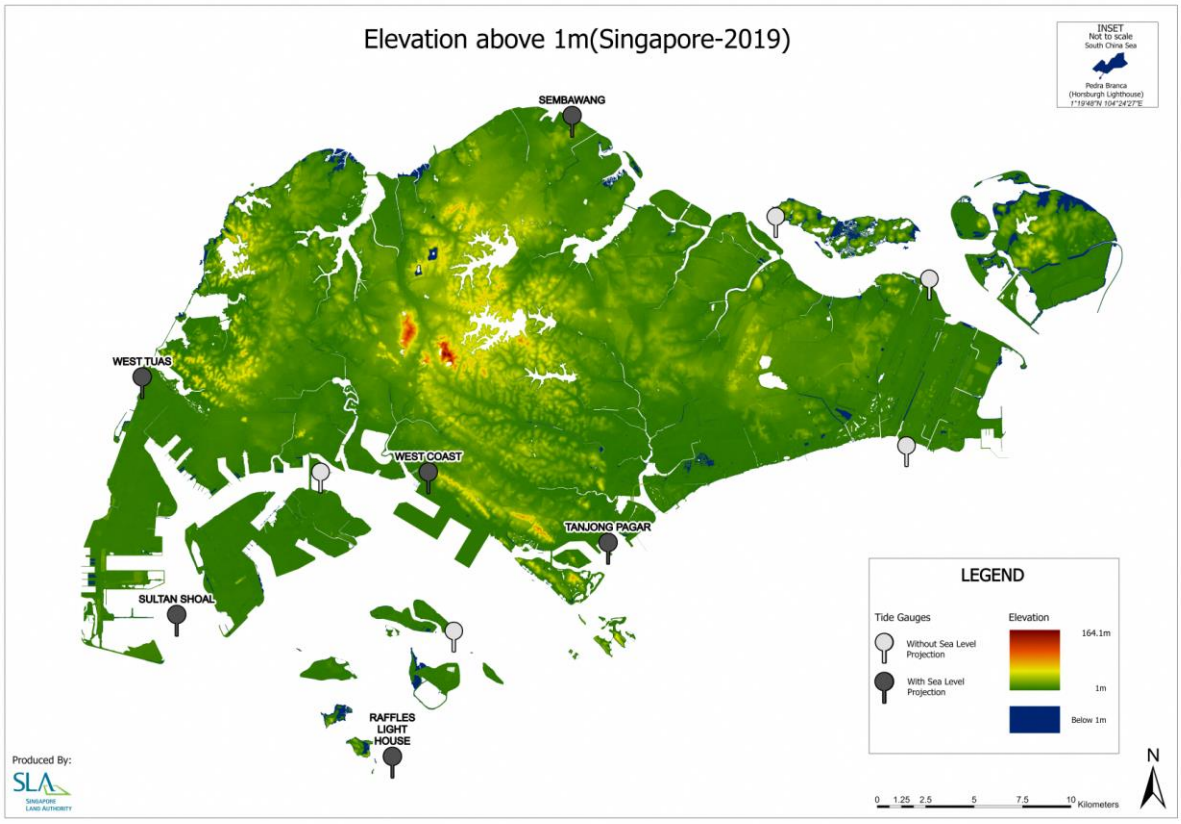

Figure 12.22: Digital Elevation Map of Singapore above mean sea level, with all elevations below 1 m indicated in dark blue.

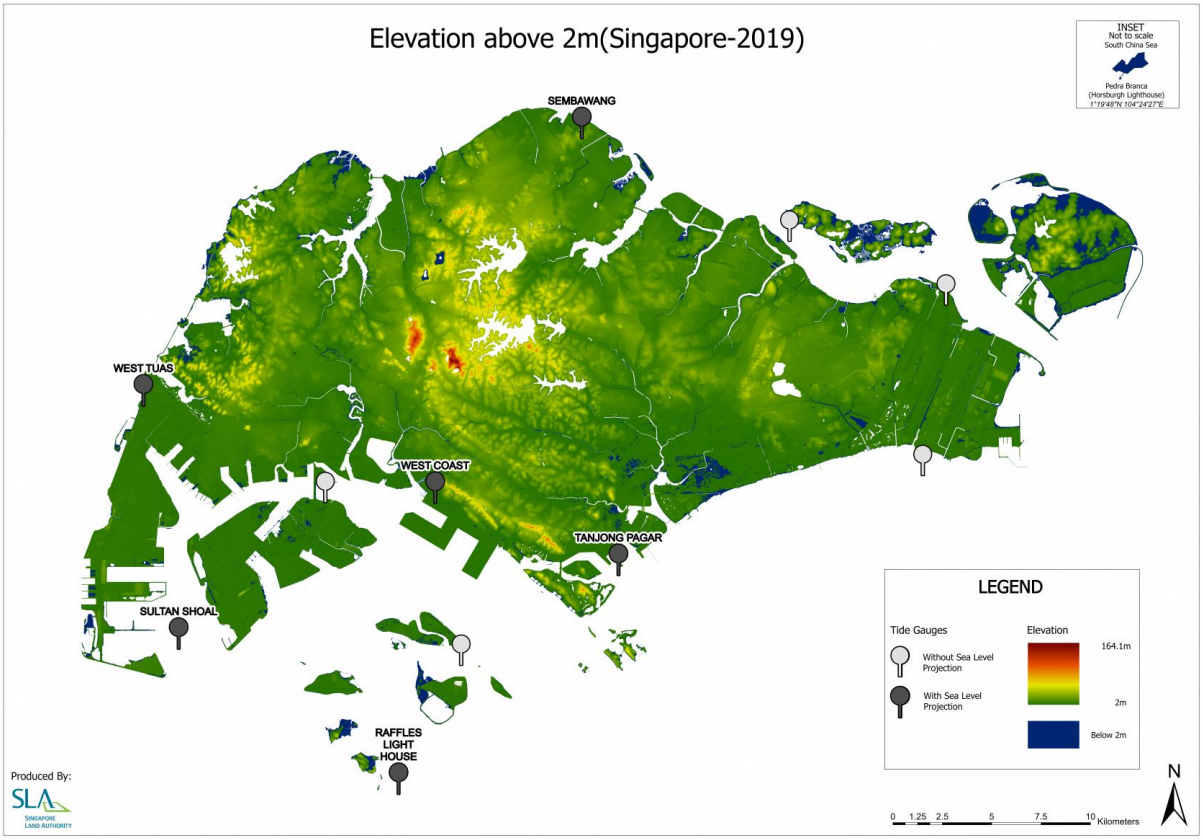

Figure 12.23: Digital Elevation Map of Singapore above mean sea level, with all elevations below 2 m indicated in dark blue.

These elevation thresholds correspond to key sea-level rise projections for specific time horizons. For instance, the 1-meter elevation represents the upper limit of the *likely* range projected for 2100 (medium confidence), while the 2-meter elevation corresponds to the upper limit of the *likely* range projected for 2150 (medium confidence). Additionally, the 5-meter elevation represents the upper limit of the *likely* range in a high-end scenario (low confidence) for 2150. All these projections are based on the worst-case future pathway SSP5-8.5. These digital elevation maps provide valuable insights into the potential impacts of sea-level rise in Singapore.

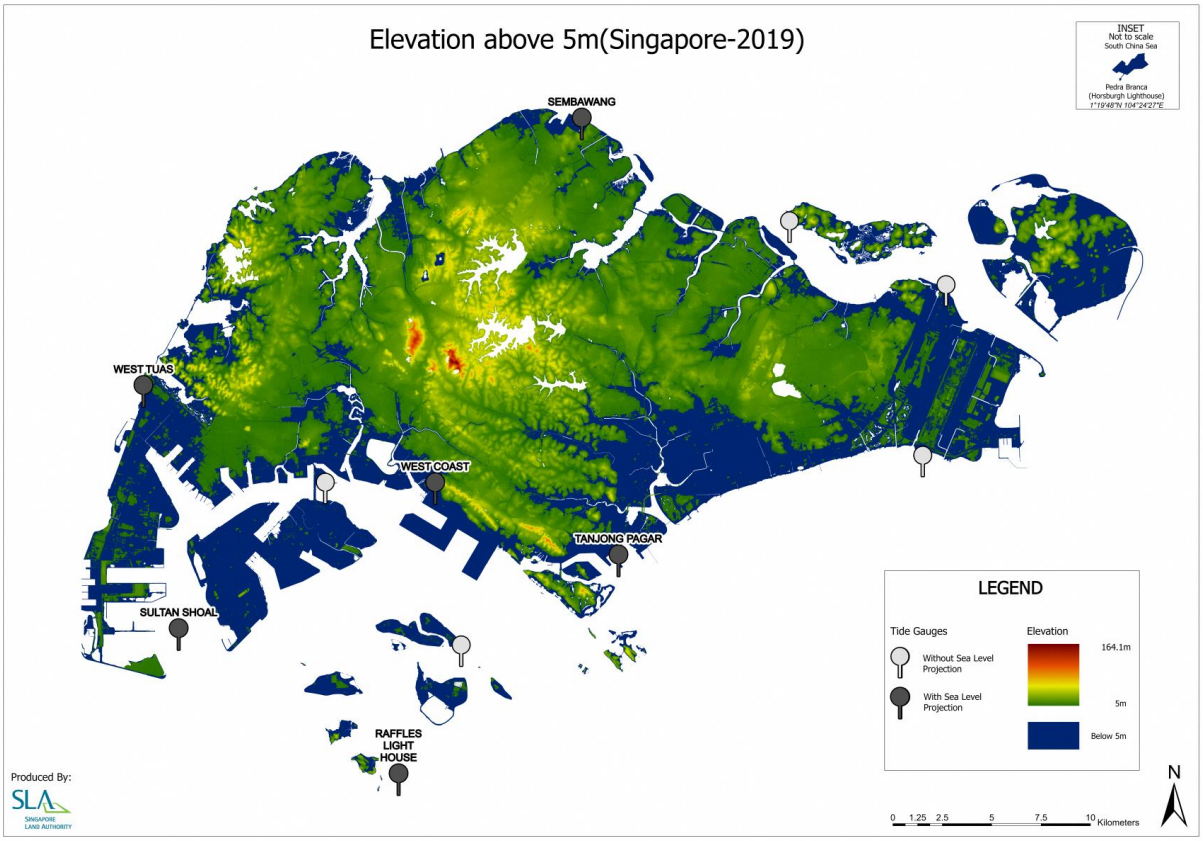

Figure 12.24: Digital Elevation Map of Singapore above mean sea level, with all elevations below 5 m indicated in dark blue.

Figure 12.24 presents a striking depiction of coastal vulnerability in Singapore, highlighting areas below 5 meters that could potentially be inundated. While this scenario is considered low-likelihood, it carries the potential for significant economic losses.

The vulnerable areas primarily encompass the southern shores of Singapore, including the Central Business District located near the southeastern coast. It is worth noting that further research is required to gain a more comprehensive understanding of this situation. Interestingly, the areas at risk of inundation, as indicated by the dark blue shading, appear to align with the reclaimed land in Singapore. This observation underscores the need for continued investigation and assessment of coastal vulnerability in relation to land reclamation efforts.

12.5.4 Sea-level projections in Southeast Asia

Here we present sea-level projections until 2150 (median and *likely* range) from the IPCC AR6 at some tide-gauge locations in Southeast Asia shown in Section 12.3. Time series of the projected RSL rise at a subset of the tide-gauges discussed in Section 12.3 are shown in Figure 12.25 in a bid to provide an evolution of sea level change. However, not all the tide-gauges shown in Section 12.3 passed the IPCC AR6 criteria to generate sea level projections.

Additional tide-gauge stations with sea-level projections are included here (i.e., additional cities in Southeast Asia; Table 12.5, Figure 12.26, Figure 12.27).

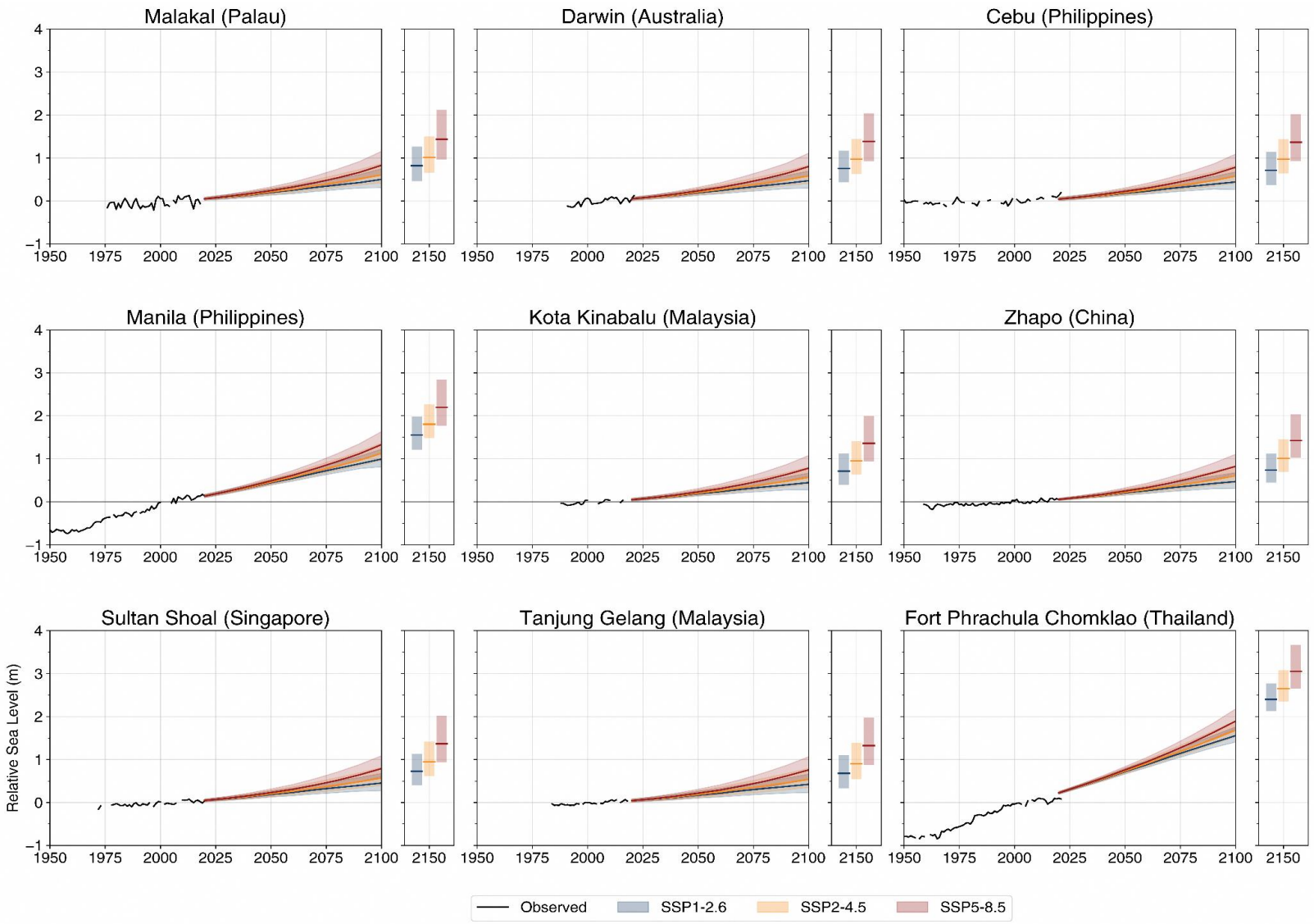

Figure 12.25: Time series plots of relative sea-level change in the past and projected future at a subset of tide gauges (country) discussed in Section 12.3. Shown in solid black are the annual tide gauge data taken from PSMSL at the respective tide gauges; shown in the other various colours with the shaded bands are the projected sea-level rise till 2100 under the different SSPs from the IPCC AR6. Observations and projections are relative to the baseline period 1995-2014.

	City/State (tide-gauge name)	SSP1-2.6		SSP2-4.5		SSP5-8.5	
		2100	2150	2100	2150	2100	2150
1	Cebu City (Cebu)	0.44 (0.26 - 0.68)	0.72 (0.37 - 1.15)	0.58 (0.41 - 0.83)	0.97 (0.64 - 1.44)	0.78 (0.58 - 1.09)	1.37 (0.92 - 2.02)
2	Manila (Manila, S. Harbour)	0.99 (0.81 - 1.22)	1.55 (1.21 - 1.98)	1.12 (0.96 - 1.37)	1.80 (1.49 - 2.26)	1.33 (1.13 - 1.63)	2.20 (1.77 - 2.85)
3	Phuket (Ko Taphao Noi)	0.50 (0.33 - 0.72)	0.80 (0.48 - 1.21)	0.60 (0.45 - 0.84)	1.00 (0.69 - 1.46)	0.82 (0.62 - 1.12)	1.42 (0.99 - 2.06)
4	Bangkok (Fort Phrachula Chomklao)	1.56 (1.41 - 1.76)	2.40 (2.13 - 2.77)	1.68 (1.54 - 1.91)	2.65 (2.35 - 3.09)	1.89 (1.71 - 2.18)	3.05 (2.65 - 3.67)
5	Johor Bahru (Johor Bahru)	0.43 (0.23 - 0.68)	0.70 (0.34 - 1.14)	0.55 (0.35 - 0.82)	0.93 (0.55 - 1.43)	0.77 (0.55 - 1.09)	1.34 (0.87 - 2.01)
6	Kuantan (Tanjung Gelang)	0.42 (0.23 - 0.66)	0.68 (0.33 - 1.1)	0.54 (0.35 - 0.8)	0.91 (0.55 - 1.39)	0.76 (0.55 - 1.06)	1.32 (0.87 - 1.98)
7	Kota Kinabalu (Kota Kinabalu)	0.44 (0.28 - 0.66)	0.71 (0.39 - 1.12)	0.56 (0.41 - 0.8)	0.95 (0.63 - 1.41)	0.78 (0.60 - 1.08)	1.36 (0.94 - 2.00)
8	Penang (Pulau Pinang)	0.39 (0.19 - 0.64)	0.64 (0.26 - 1.08)	0.5 (0.3 - 0.76)	0.85 (0.47 - 1.34)	0.71 (0.49 - 1.03)	1.25 (0.79 - 1.92)
9	Da Nang (Danang)	0.50 (0.32 - 0.74)	0.80 (0.45 - 1.22)	0.63 (0.44 - 0.89)	1.05 (0.69 - 1.52)	0.84 (0.64 - 1.14)	1.46 (1.02 - 2.09)
10	Yangon (Rangoon)	0.62 (0.43 - 0.84)	0.98 (0.64 - 1.40)	0.71 (0.53 - 0.96)	1.17 (0.83 - 1.62)	0.93 (0.72 - 1.23)	1.58 (1.14 - 2.21)
11	Palau (Malakal)	0.50 (0.31 - 0.75)	0.82 (0.46 - 1.27)	0.60 (0.42 - 0.87)	1.01 (0.65 - 1.51)	0.83 (0.61 - 1.16)	1.44 (0.96 - 2.12)
12	Darwin (Darwin)	0.47 (0.30 - 0.70)	0.76 (0.43 - 1.17)	0.58 (0.41 - 0.83)	0.97 (0.62 - 1.44)	0.80 (0.59 - 1.11)	1.38 (0.92 - 2.04)
13	Zhapo (Zhapo)	0.47 (0.31 - 0.68)	0.74 (0.44 - 1.12)	0.61 (0.45 - 0.84)	1.01 (0.70 - 1.46)	0.82 (0.64 - 1.11)	1.42 (1.02 - 2.03)
14	Singapore (Sultan Shoal)	0.51 (0.34 – 0.74)	0.82 (0.50 – 1.24)	0.63 (0.46 – 0.88)	1.05 (0.72 – 1.52)	0.85 (0.66 – 1.15)	1.47 (1.03 – 2.12)
	Global mean	**0.44 (0.32 – 0.62)**	**0.68 (0.46 – 0.99)**	**0.56 (0.44 – 0.76)**	**0.92 (0.66 – 1.33)**	**0.77 (0.63 – 1.01)**	**1.32 (0.98 – 1.88)**

Table 12.5: Projected relative sea level rise by 2100 and 2150 under SSP1-2.6, SSP2-4.5 and SSP5-8.5 at various locations in Southeast Asia and some peripheral locations (i.e., Zhapo, Darwin and Palau; Figure 12.26). The values shown are meters of sea-level change relative to baseline 1995-2014. Median (*likely* range) are presented. Projections of global mean sea level rise are also shown here, relative to the same baseline.

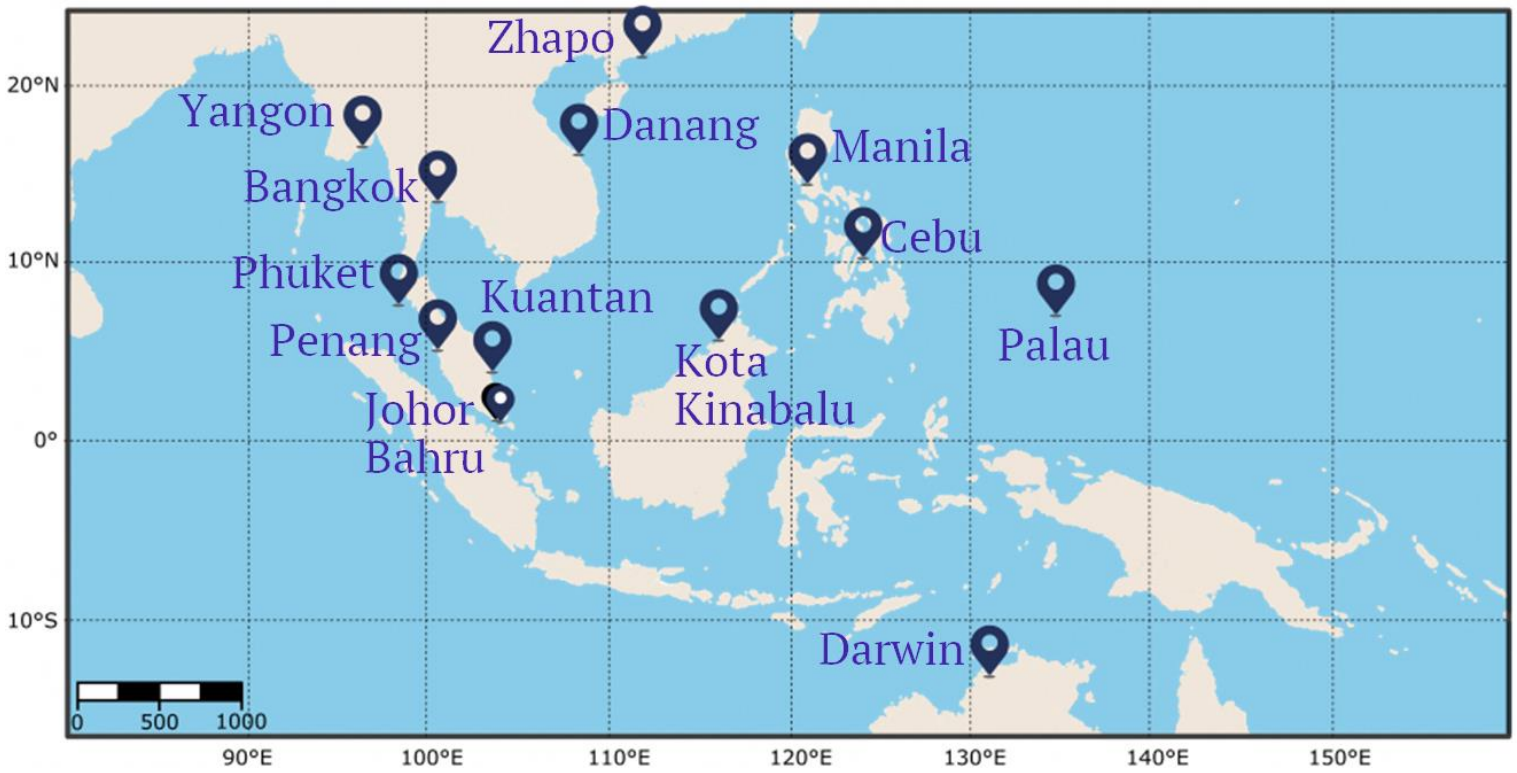

Figure 12.26: Location of the 13 tide-gauges in the various Southeast Asian cities and countries listed in Table 12.5. Labels on the map indicate the city names.

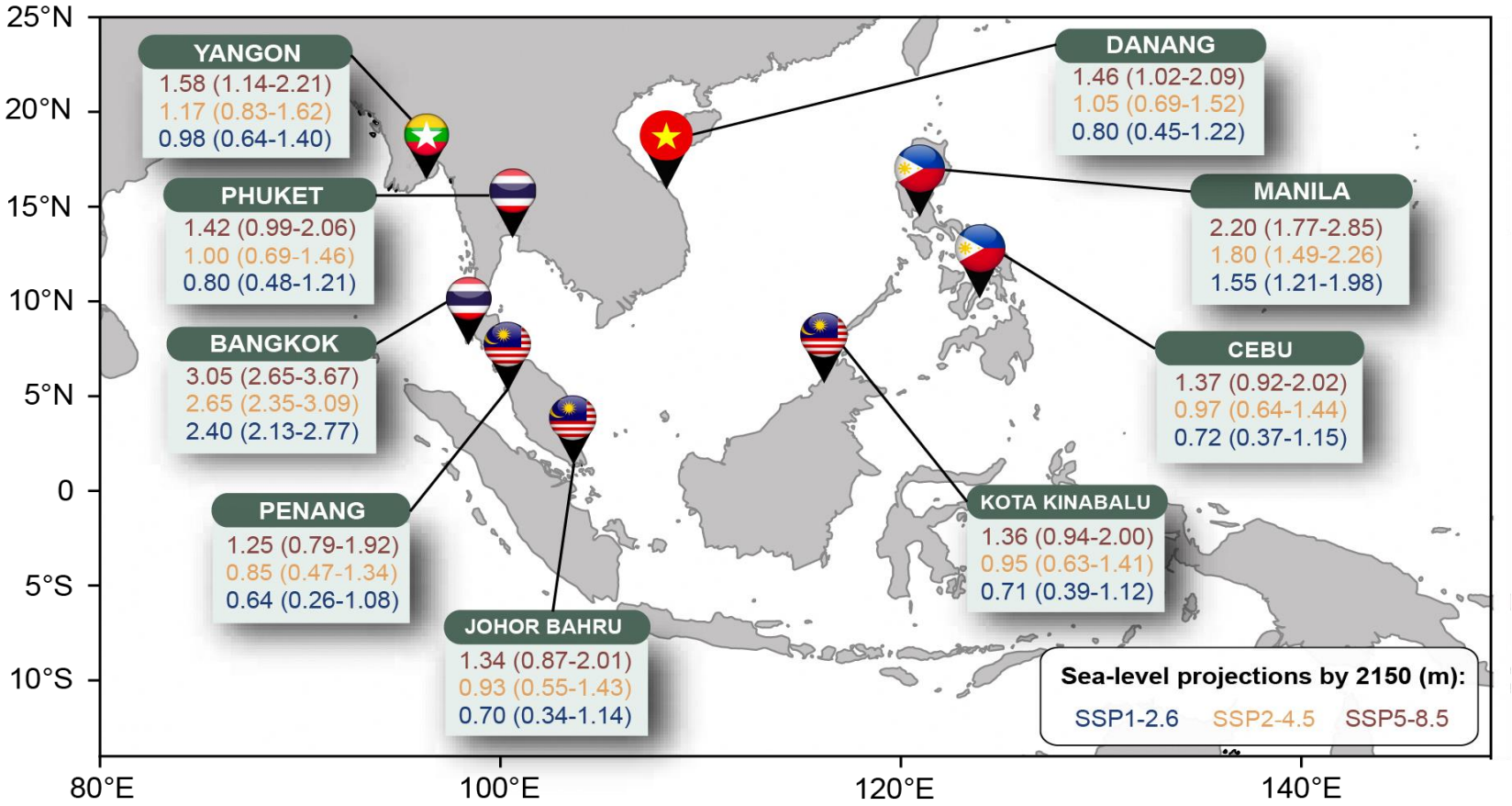

Figure 12.27: Projected relative sea-level rise at some of the most densely populated Southeast Asian cities by 2150 under all emission scenarios considered in V3. Projections are relative to the baseline period 1995–2014.

Over this century, RSL is projected to rise at all the tide gauges listed in Table 12.5 regardless of the future emissions scenarios by 2100 and 2150 (Figure 12.27). Similar to Singapore, RSL rise at most of these locations is *likely* to reach ~1 m by 2100 under the high greenhouse gas emissions scenario (SSP5-8.5).

However, this is with the exception of Manila and Fort Phrachula Chomklao, which will be addressed as 'Bangkok' from hereon as the tide gauge is located less than 10 km away from the populated city. By the end of the century (i.e., 2100), Manila and Bangkok are *likely* to experience RSL rise of more than 1.5 m and 2 m respectively under SSP5-8.5. Under the low emissions scenario, RSL rise could *likely* reach up to 1 m in most of these cities and up to 2 to 3 m in Manila and Bangkok by 2150 (Figure 12.27). Under the high emissions scenario RSL rise could *likely* reach up to 2 m in most cities and exceed 3m in Bangkok by 2150 (Figure 12.27).

Land subsidence due to excessive groundwater withdrawal has been a well-established factor causing RSL rise since the 1970s (e.g., Ahmed et al., 2020; Siringan et al., 2019, Niesters et al., 2021). In Bangkok, groundwater withdrawal has been attributed with land subsidence, with rates reaching up to 120 mm/yr in some areas (Aobpaet et al., 2013).

Several studies have also reported subsidence rates up to centimeters per year in some coastal areas around Manila due to groundwater extraction (Rodolfo et al., 2020; Kim et al., 2019). In both cases of Manila and Bangkok, the extraction of groundwater has outpaced the natural recharge rate of the aquifers. As water is pumped out, the pressure in the aquifer decreases, causing the soil and rock layers above it to compact and settle. Over time, this causes the land surface to sink, leading to subsidence (Galloway et al., 2011).

12.6 Vertical Land Movement

While global sea-level rise is driven primarily by the thermal expansion of oceans and the melting of land ice, the RSL changes experienced at specific locations are influenced by a range of additional factors (IPCC, 2021). One of the most significant factors is vertical land movement, or vertical land motion (VLM, which can cause the land to sink or rise relative to sea level (Church et al., 2013). This motion can result from a variety of natural and anthropogenic processes, including tectonic activity, sediment compaction, groundwater withdrawal, and human-made structures (Kench et al., 2018).

VLM is particularly important in regions such as Southeast Asia, where it can cause significant variations in local sea levels and exacerbate the impacts of global sea-level rise on coastal communities and infrastructure (Koh et al., 2021). In this section, we explore the factors of VLM and its importance for understanding RSL changes in the region. We use the term 'vertical land movement' in this section as referenced to Gregory et al. (2019), and the term 'vertical land motion' used in Section 12.5 is in accordance with the IPCC AR6 Chapter 9 terminology. The terms are often used interchangeably in publications, and do not have different physical meanings.

VLM describes the change in the height of the sea floor or land surface (Gregory et al., 2019) and it affects RSL change. The need for understanding and quantifying VLM is crucial for producing robust sea-level projections. Vertical displacements of the ground could either cause a fall or rise in mean sea level relative to the occupants on land, given that the mean geocentric sea level remains constant.

12.6.1 Factors causing vertical land movement

The rate of VLM and the extent to which it affects RSL change varies temporally and spatially. These factors can be natural and/or human-induced, and are able to have an impact on the land for up to millions of years (Figure 12.28).

One factor causing VLM arises due to changes in mass redistributions within the atmosphere, ocean and continents caused by natural or anthropogenic mechanisms (Pfeffer et al., 2017). The solid Earth is still in a state of isostatic disequilibrium and continues to respond to the loss of ice sheets during the Last Glacial Maximum about 21 thousand years ago (e.g., King et al., 2010). This ongoing GIA results in varied rates of vertical displacements across the globe.

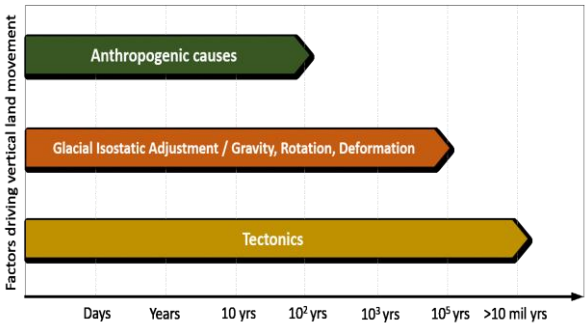

Figure 12.28: Significant factors driving vertical land movement (VLM) in Southeast Asia that are explained in Section 12.6.1. The temporal extent to which these factors affect VLM vary from days to millions of years (tectonics). Graphic and information is referenced to Pfeffer et la. (2017).

Similarly, ongoing contemporary changes in land-based ice sheets (e.g., melting Antarctic and Greenland ice sheets) and land water storage results in instantaneous changes in the geoid and VLM that must be considered. Together, these effects affect the rate of VLM and contribute to RSL change.

Other natural factors that can also cause VLM include seismic activity such as earthquakes (Wöppelmann et al., 2016). Earthquakes occur when tectonic plates in the earth's crust shift, causing a sudden release of energy that creates seismic waves. This movement can result in uplift or subsidence of the land, which can affect local RSL rise (Wöppelmann et al., 2016; Shirzaei et al., 2021). At different stages of the earthquake cycle, which includes interseismic, coseismic, and postseismic periods, there are different rates and spatio-temporal extent of land movement (Pollitz et al., 2018). The extent of subsidence or uplift in the land near the fault depends on several factors, including the magnitude and duration of the earthquake, the location of the fault, and the properties of the surrounding geology (Pollitz et al., 2018).

There are also anthropogenic factors such as groundwater withdrawal that can have significant impacts on VLM. Groundwater withdrawal causes the water table to drop, leading to a reduction in pore water pressure and compaction of sediment layers, which can cause subsidence (Galloway et al., 2019). Some of the cities that are most severely-affected by groundwater withdrawal-induced land subsidence include Mexico City, Bangkok and Jakarta (Galloway et al., 2019; Wassmann et al., 2016; Firman et al., 2019). In addition to groundwater extraction, there are other anthropogenic factors such as oil and gas extraction, mining, and the construction of large dams that can result in land subsidence (Zhang et al., 2018).

12.6.2 Observed vertical land movement in Singapore

Understanding the past and present state of VLM in Singapore is crucial for accurately assessing and predicting future sea-level rise impacts on low-lying coastal areas. In this section, we examine the current knowledge of observed VLM in Singapore from published sources and some existing global positioning system (GPS) and/or global navigation satellite system (GNSS) data.

VLM is often measured either using radar sensors or in situ GPS/GNSS stations. Studies such as Catalao and Fernandes (2013) and Catalao et al. (2020) had previously presented VLM rates in Singapore using the former technique. Both studies found greatest subsidence rates near the southeastern coasts of Singapore (-2 to -13 mm/yr, from 2011 to 2016, Catalao et al., 2020). Catalao et al. (2020) suggested that a correlation between the geological setting of Singapore and subsidence rates exists, due to lower subsidence rates observed for unconsolidated material as compared to higher subsidence rates for consolidated sand. However, this relationship is still understudied, and the period over which VLM rates were presented in Catalao et al. (2020) (i.e., 6 years) may be insufficient to robustly conclude the associated correlation with varied bedrock.

Another way of examining VLM is using GPS data. Figure 12.26 shows the time series of recorded land movement at two of Singapore's GPS/GNSS stations, named SIN1 and SING (Figure 12.26), taken from Nevada Geodetic Lab (Blewitt et al., 2018). Linear trends of the measurements were taken over different segments of time (i.e., before/after a data gap or shift) to approximately quantify the rate of VLM in Singapore over the last decade or so. SIN1 shows negligible VLM, with arguably little subsidence of -0.4 to -0.5 mm/yr

over the past ~10 years. On the other hand, a vertical downward shift was recorded at SING on 5 November 2015, with missing data the day before.

According to the Singapore Land Authority (SLA), the recorded subsidence of ~5 cm was likely caused by the earthquake that occurred in Indonesia on 4 November 2015 ("GPS Station at Bukit Timah Base Recorded Subsidence", 2015). Due to Singapore's close proximity to the Sunda megathrust fault that borders the Indonesian archipelago, land subsidence in Singapore due to any significant future seismic activity is yet again plausible (Gee et al., 2010; Hermawan et al., 2020). Such a phenomenon is not uncommon around the world. For instance, the 2011 Tohoku earthquake in Japan caused significant subsidence in coastal areas, while the 2010 earthquake in Haiti caused up to 20 cm of subsidence in some areas ("Earthquake-Induced Land Subsidence," 2018).

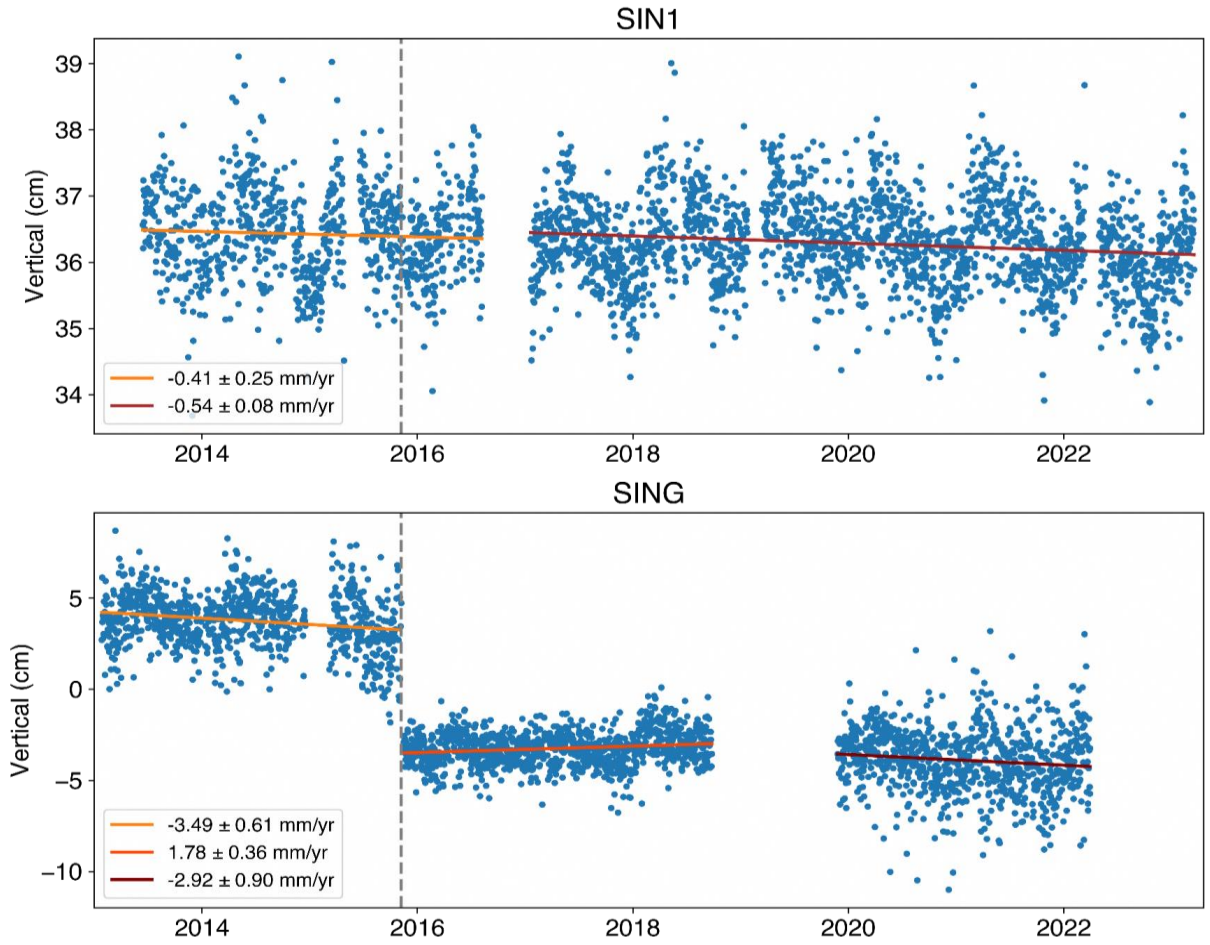

Figure 12.29: GNSS stations in Singapore (SIN1 and SING) showing the processed vertical component in centimeters (blue points). Linear trends were also plotted (in shades of orange and red) over different time periods in an attempt to show the rate of VLM observed in Singapore at these stations. Vertical dashed line represents an earthquake occurrence that most likely explains the vertical shift in measurements at SING. Data taken from the Nevada Geodetic Lab (Blewitt et al., 2018).

However, subsidence was not observed at the other station, SIN1. A number of factors could have explained this discrepancy, given that Singapore is a comparatively small island-state. GPS stations are designed to detect changes in the position of the ground, which can be caused by a variety of factors, including tectonic movement, subsidence, and even human activity (Bock et al., 2016).

The accuracy and sensitivity of GPS measurements can vary depending on factors

such as the location of the station, the type of equipment used, and the surrounding geology (Hashimoto et al., 2011; Ozawa et al., 2008). In the case of the November 4 2015 earthquake, it is possible that the other GPS station in Singapore was located further away from the epicenter of the earthquake, or was situated in an area where the ground was less susceptible to subsidence (Dragert et al., 2001). Additionally, variations in local geological conditions, such as soil composition and depth, can also influence the magnitude of subsidence recorded at different GPS stations (Hu and Wang, 2019).

It is also important to note that subsidence is not always a uniform phenomenon and can vary in magnitude and location depending on the specific conditions of the area affected by the earthquake (Bock et al., 2016). Therefore, it is possible that the lack of subsidence recorded at the other GPS station in Singapore may be due to a combination of factors related to the site, the earthquake, and the measurement equipment used (Ozawa et al., 2008).

While GPS measurements can be a powerful tool for monitoring VLM, earthquakes can introduce a level of uncertainty into these measurements due to a range of factors. For example, the magnitude and type of earthquake can influence the magnitude and distribution of vertical land movement, while the sensitivity and accuracy of GPS equipment can vary depending on the specific site conditions. As a result, it can be challenging to accurately quantify vertical land movement and associated uncertainties in the aftermath of an earthquake.

12.6.3 Future vertical land movement and its associated uncertainties to relative sea-level rise in Singapore

As shown above, the GPS data suggests that different parts of Singapore experience different rates of VLM over the past few years. Although more detailed study needs to be done for accurate conclusions, we could nonetheless hypothesize that land is subsiding in some parts of Singapore over the past few years (Tay et al., 2022). This has important implications for research on past and future sea-level studies, as stakeholders should be ultimately concerned about the relative rise in sea-level with VLM taken into account.

Tide Gauge	Rate of vertical land movement due to GIA (VLM in mm/yr)	Rate of sea-level change due to GIA (mm/yr)
Sultan Shoal	0.21	-0.38
Sembawang	0.19	-0.35
Raffles Light House	0.20	-0.37
Tanjong Pagar	0.19	-0.36
West Coast	0.20	-0.37
West Tuas	0.21	-0.38

Table 12.6: Rates of vertical land movement due to GIA and sea-level change due to GIA component of VLM. Results taken from ICE6G_C (Peltier et al., 2015).

As of 2022, the IPCC AR6 projections of VLM at tide gauges are the only set of projections that consider more than vertical deformation due to GIA. The projections are derived using a Gaussian process model that sums the global, regional and local fields, whereby the local component is generated based on a GIA model and historical tide-gauge data, in a bid to include non-climatic background factors (Kopp, 2013). Tide-gauges record changes in RSL and hence,

the measurements are inclusive of any net changes in VLM.

VLM is projected to cause a fall in sea level in Singapore by 2150 (median) at almost all the tide gauges (Section 12.5.3.1, Figure 12.17). This could be largely dominated by the effects of GIA, which are causing multi-millennium rates of land uplift (Table 12.6). However, the range of uncertainties in the VLM projections (Figure 12.16 and 12.17; Table 12.4) include the possibility of VLM adding to sea-level rise in Singapore (upper bound of *likely* range), instead of a fall (median). Additionally, tectonic activity is another factor that was not accounted for in the AR6 VLM projections, which increases the quantitative and qualitative uncertainties associated with future VLM in Singapore. The prediction of earthquakes alone with any degree of accuracy, for example, remains elusive and a challenging task for scientists (e.g., Jordan, 2011; McGuire, 2014).

Site-specific analyses of VLM for Singapore play a crucial role in strengthening the knowledge base for informed coastal decision making. Comprehensively understanding the local sea-level budget at coastal locations in terms of the driving processes is a high scientific priority for addressing the challenges posed by RSL rise.

Acknowledgements

We thank the Permanent Service for Mean Sea Level (PMSL) and the National Oceanographic Centre (NOC), UK for maintaining the platform for continuous usage of monthly and annual tide-gauge data. Specifically, we want to thank Peter Hogarth from PSMSL/NOC for putting in great effort in correcting the erroneous tide-gauge data.

We would also like to extend our gratitude to Robert Kopp and Gregory Garner from the IPCC AR6 team for their assistance in deriving the sea-level projections shown in this report. Additionally, we also want to acknowledge and thank Benjamin P. Horton and Jennifer Weeks for their constructive feedback and comments along the way whilst this chapter was taking shape.

We acknowledge the Copernicus Marine Service (CMS) for redistributing the gridded sea surface height data from satellite altimetry and also for providing Global Ocean Physics Reanalysis data (GLORYS12V1). We dually acknowledge ocean reanalysis groups (ORAS5, GECCO3) for making their ocean state estimates publicly available.

Finally we thank all the external reviewers for their suggestions and comments which helped to improve this chapter significantly.

Appendix

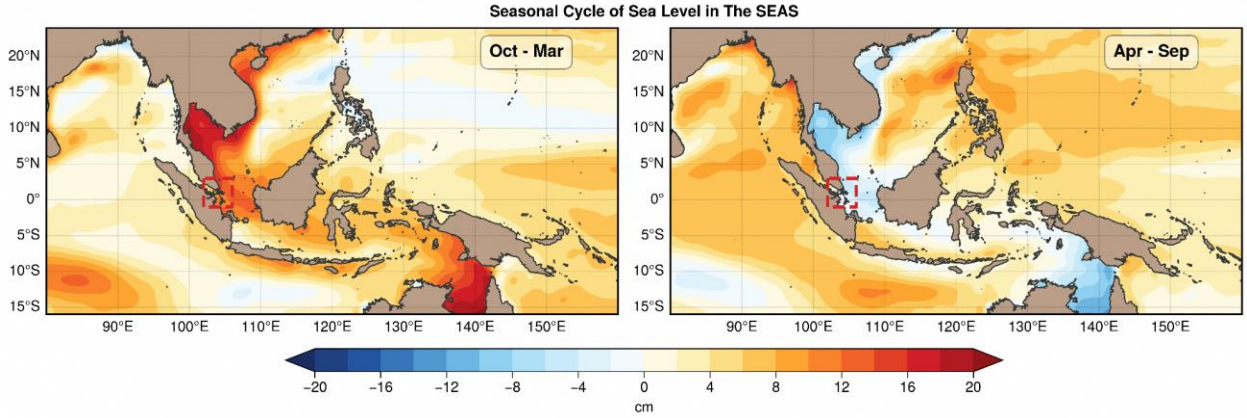

Figure A12.1: Seasonal cycle of sea level in the southeast Asian seas computed from satellite data for the period 1993 - 2021.

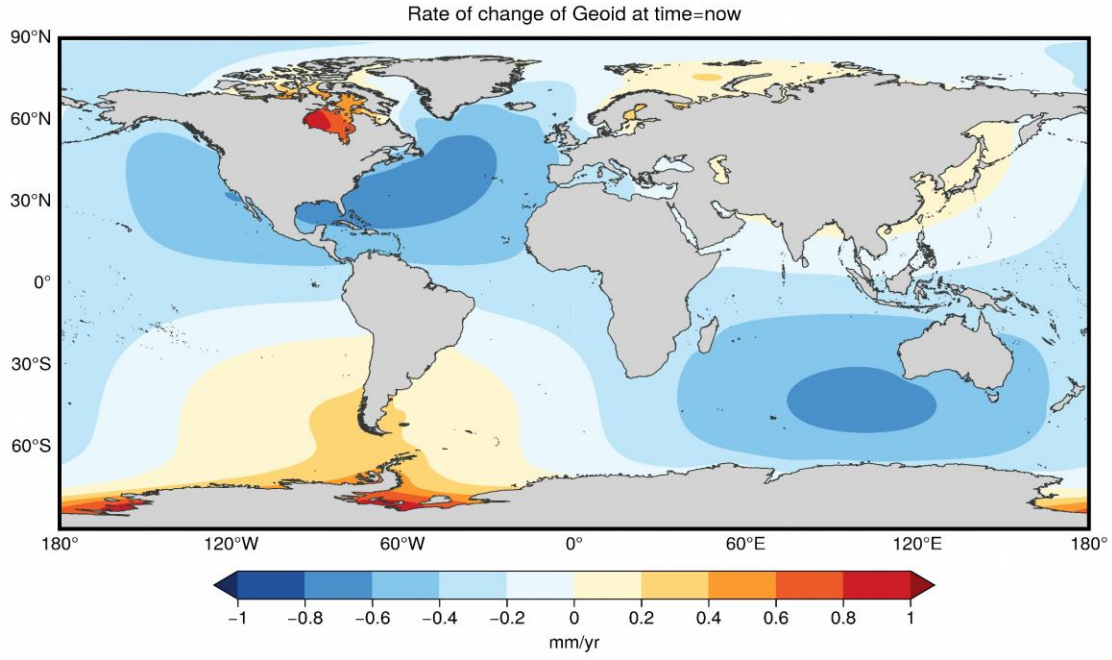

Figure A12.2: Sea surface height change due to changes in gravity (Geoid) associated with GIA from ICE-5G (Peltier et al. 2004).

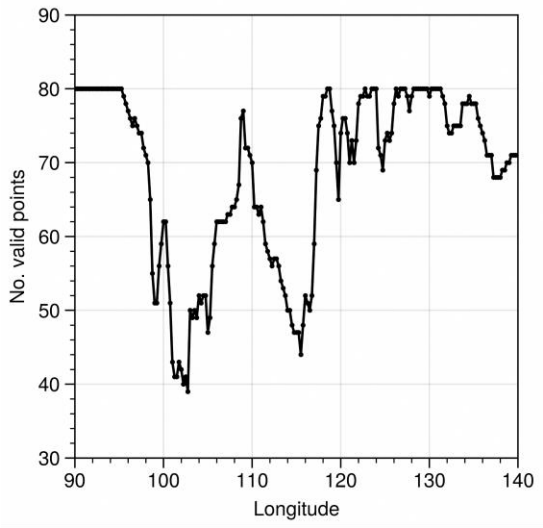

Figure A12.3: Number of valid grid-points (i.e. ocean grid points) used in the latitudinal averaging of sea-level trends shown in Figures 12.7 and 8.

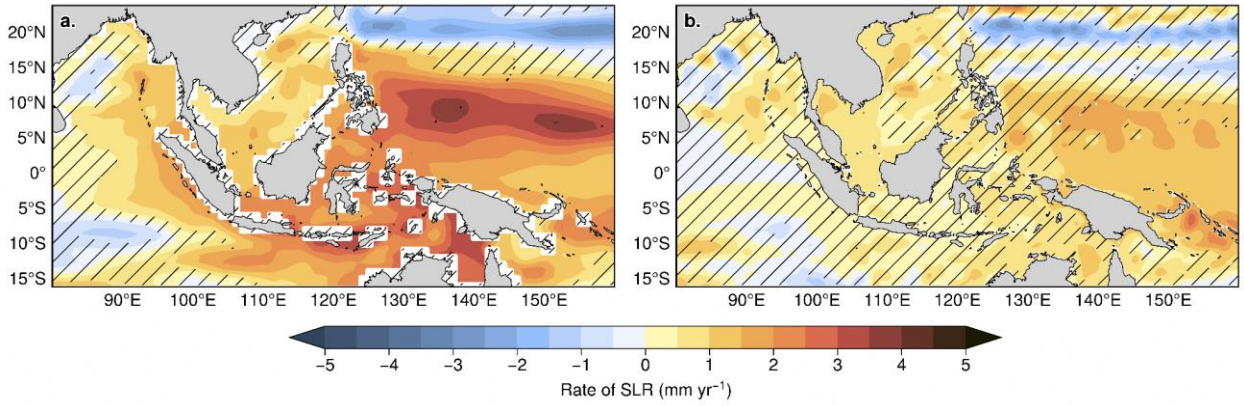

Figure A12.4: Dynamic sea-level rise trend from GECCO3 (German contribution of the Estimating the Circulation and Climate of the Ocean) and GLORYS 12V1 (Global Ocean Physics Reanalysis; https://doi.org/10.48670/moi-00021). For GECCO (GLORYS), the trend estimation covers the period 1993 - 2018 (1993 - 2020). The patches on each panel indicate the trends which are not significant at 95% confidence level.

References

ABC News. (2015, November 4). Magnitude 6.3 earthquake strikes eastern Indonesia. https://abcnews.go.com/International/wireStory/magnitude-63-earthquake-strikes-eastern-indonesia-34915559

Ahmed, A., Khan, M. S., Abdullah, S. A., & Shoaib, M. (2020). Land subsidence and sea level rise impact on Jakarta coastal areas. Environmental Science and Pollution Research, 27(22), 27955-27968.

Albert *et al.* (2016) Interactions between sea-level rise and wave exposure on reef island dynamics in the Solomon Islands. *Environ. Res. Lett.* **11** 054011, https://doi:10.1088/1748-9326/11/5/054011

Alley, R. B., & Alley, K. E. (2018). The rise and fall of ice sheets. Scientific American, 319(5), 54-61. (This article provides a general introduction to ice sheet dynamics and the role of marine ice cliff instability in the collapse of the West Antarctic ice sheet.)

Allison, L.C., Palmer, M.D., Haigh, I.D., (2022), Projections of 21st century sea level rise for the coast of South Africa, *Environ. Res. Commun.* **4** 025001, 10.1088/2515-7620/ac4a90

Aobpaet, Anuphao & Caro Cuenca, Miguel & Hooper, Andy & Trisirisatayawong, Itthi. (2013). InSAR time-series analysis of land subsidence in Bangkok, Thailand. International Journal of Remote Sensing. 34. 2969-2982. 10.1080/01431161.2012.756596.

Argus, D. F., Peltier, W. R., Drummond, R. and Moore, A..W., (2014) The Antarctica component of postglacial rebound model ICE-6G_C (VM5a) based upon GPS positioning, exposure age dating of ice thicknesses, and relative sea level histories. Geophys. J. Int., 198(1), 537-563, doi:10.1093/gji/ggu140.

Asian Development Bank. (2018). Addressing Climate Change and Migration in Asia and the Pacific. Retrieved from https://www.adb.org/sites/default/files/publication/446576/addressing-climate-change-migration-asia-pacific.pdf

Bamber, J.L., M. Oppenheimer, R.E. Kopp, W.P. Aspinall, and R.M. Cooke (2019) Ice sheet contributions to future sea-level rise from structured expert judgment. Proceedings of the National Academy of Sciences, 116(23), 11195–11200, doi:10.1073/pnas.1817205116

Barnard, P.L., Erikson, L.H., Foxgrover, A.C. *et al.* (2019) Dynamic flood modeling essential to assess the coastal impacts of climate change. *Sci Rep* **9**, 4309. https://doi.org/10.1038/s41598-019-40742-z

Blewitt, G., W.C. Hammond, C. Kreemer (2018), Harnessing the GPS Data Explosion for Interdisciplinary Science, Eos, 99, https://doi.org/10.1029/2018EO104623 (link).

Bingham, R. J., and Hughes, C. W. (2012), Local diagnostics to estimate density-induced sea level variations over topography and along coastlines, *J. Geophys. Res.*, 117, C01013, doi:10.1029/2011JC007276.

Bock, Y., Melgar, D., Crowell, B. W., & Haase, J. S. (2016). Real-time seismology and earthquake damage mitigation. Annals of Geophysics, 59(1), S0101. https://doi.org/10.4401/ag-7102.

Bott L.-M., Schöne T., Illigner J., Haghshenas Haghighi M., Gisevius K., Braun B. (2021) Land subsidence in Jakarta and Semarang Bay – The relationship between physical processes, risk perception, and household adaptation Ocean Coast Manag. 211 pp 105775.

Cannaby, H., Palmer, M. D., Howard, T., Bricheno, L., Calvert, D., Krijnen, J., Wood, R., Tinker, J., Bunney, C., Harle, J., Saulter, A., O'Neill, C., Bellingham, C., and Lowe, J. (2016) Projected sea level rise and changes in extreme storm surge and wave events during the 21st century in the region of Singapore, Ocean Sci., 12, 613–632, https://doi.org/10.5194/os-12-613-2016.

Catalao, J., D. Raju, and R. Fernandes (2013) Mapping vertical land movement in Singapore using INSAR and GPS.

Catalao, J., D. Raju, and G. Nico. (2020) INSAR maps of land subsidence and sea level scenarios to quantify the flood inundation risk in coastal cities: The case of Singapore. Remote Sensing, 12(2):296.

Chao, B.F., Y.H. Wu, and Y.S. Li (2008) Impact of artificial reservoir water impoundment on global sea level.. Science (New York, N.Y.), 320(5873), 212–4, doi:10.1126/science.1154580.

Church, J. A. and White, N. J. (2011) Sea-level rise from the late 19th to the early 21st century, Surv. Geophys., 32, 585–602, https://doi.org/10.1007/s10712-011-9119-1.

Church, J. A., Clark, P. U., Cazenave, A., Gregory, J. M., Jevrejeva, S., Levermann, A., ... & Unnikrishnan, A. S. (2013). Sea level change. In Climate Change 2013: The Physical Science Basis. Contribution of Working

Group I to the Fifth Assessment Report of the Intergovernmental Panel on Climate Change (pp. 1137-1216). Cambridge University Press.

Church, J. A., Clark, P. U., Cazenave, A., Gregory, J. M., Jevrejeva, S., Levermann, A., Merrifield, M. A., Milne, G. A., Nerem, R. S., Nunn, P. D., Payne, A. J., Pfeffer, W. T., Stammer, D., and Unnikrishnan, A. S.: Sea-level change, in: Climate Change 2013: The Physical Science Basis, Contribution of Working Group I to the Fifth Assessment Report of the Intergovernmental Panel on Climate Change, edited by: Stocker, T. F., Qin, D. D., Plattner, G. K., Tignor, M., Allen, S. K., Boschung, J., Nauels, A., Xia, Y., Bex, V., and Midgley, P. M., Cambridge University Press, https://doi.org/10.1017/CBO9781107415324.

DeConto, R.M. et al., (2021) The Paris Climate Agreement and future sea-level rise from Antarctica. Nature, in press.

Coulson, S. et al. (2022) A detection of the sea level fingerprint of Greenland Ice Sheet melt. *Science* **377**, 1550-1554. DOI:10.1126/science.abo0926

Dangendorf, S., Hay, C., Calafat, F. M., Marcos, M., Piecuch, C. G., Berk, K., & Jensen, J. (2019). Persistent acceleration in global sea-level rise since the 1960s. *Nature Climate Change*, 9, 705– 710.

Dayan, Hugo & Le Cozannet, Goneri & Sabrina, Speich & Thieblemont, Remi. (2021). High-End Scenarios of Sea-Level Rise for Coastal Risk-Averse Stakeholders. Frontiers in Marine Science. 8. 10.3389/fmars.2021.569992.

DeConto, R. M., & Pollard, D. (2016). Contribution of Antarctica to past and future sea-level rise. Nature, 531(7596), 591-597.

Dieng, H. B., Delcroix, T., Arnault, S., & Cazenave, A. (2021). Revisiting global sea level budget since 1961: importance of vertical land motion. Scientific reports, 11(1), 1-11.

Douglas, B., (2001) Chapter 3 Sea level change in the era of the recording tide gauge, Sea Level Rise - History and Consequences, 10.1016/S0074-6142(01)80006-1, (37-64).

Dragert, H., Wang, K., & James, T. S. (2001). A silent slip event on the deeper Cascadia subduction interface. Science, 292(5521), 1525-1528. https://doi.org/10.1126/science.1058715

Earthquake-Induced Land Subsidence. (2018, May 2). USGS. https://www.usgs.gov/natural-hazards/earthquake-hazards/science/earthquake-induced-land-subsidence

Edwards, T.T.L. et al., (2021) Projecting the land ice contribution to sea level rise this century. Nature, in press.

England M et al. (2014) Recent intensification of wind-driven circulation in the Pacific and the ongoing warming hiatus. Nat Clim Chang 4:222–227

Farrell , W.E., Clark, J.A. (1976) On Postglacial Sea Level, *Geophysical Journal International*, Volume 46, Issue 3, 647–667, https://doi.org/10.1111/j.1365-246X.1976.tb01252.x

Feng M, Li Y, Meyers G (2004) Multi-decadal variations of Fremantle sea level: footprint of climate variability in the tropical Pacific. Geophys Res Lett 31:L16302.

Firman, T., Sofyan, H., & Novirman, J. (2019). The Challenge of Groundwater Overexploitation and Land Subsidence in Jakarta. Journal of Urban Affairs, 41(4), 451-463.

Forster, P., Storelvmo, T., Armour, K., Collins, W., Dufresne, J.-L., Frame, D., Lunt, D. J., Mauritsen, T., Palmer, M. D., Watanabe, M., Wild, M., and Zhang, H.: The Earth's Energy Budget, Climate Feedbacks, and Climate Sensitivity, in: Climate Change 2021: The Physical Science Basis. Contribution of Working Group I to the Sixth Assessment Report of the Intergovernmental Panel on Climate Change, edited by: Masson-Delmotte, V., Zhai, P., Pirani, A., Connors, S. L., Péan, C., Berger, S., Caud, N., Chen, Y., Goldfarb, L., Gomis, M. I., Huang, M., Leitzell, K., Lonnoy, E., Matthews, J. B. R., Maycock, T. K., Waterfield, T., Yelekçi, O., Yu, R., and Zhou, B., Cambridge University Press, Cambridge, United Kingdom and New York, NY, USA, Cambridge, United Kingdom and New York, NY, USA, 923–1054, https://doi.org/10.1017/9781009157896.009.

Fox-Kemper, B., H.T. Hewitt, C. Xiao, G. Aðalgeirsdóttir, S.S. Drijfhout, T.L. Edwards, N.R. Golledge, M. Hemer, R.E. Kopp, G. Krinner, A. Mix, D. Notz, S. Nowicki, I.S. Nurhati, L. Ruiz, J.-B. Sallée, A.B.A. Slangen, and Y. Yu, (2021): Ocean, Cryosphere and Sea Level Change. In Climate Change 2021: The Physical Science Basis. Contribution of Working Group I to the Sixth Assessment Report of the Intergovernmental Panel on Climate Change [Masson-Delmotte, V., P. Zhai, A. Pirani, S.L. Connors, C. Péan, S. Berger, N. Caud, Y. Chen, L. Goldfarb, M.I. Gomis, M. Huang, K. Leitzell, E. Lonnoy, J.B.R. Matthews, T.K. Maycock, T. Waterfield, O. Yelekçi, R. Yu, and B. Zhou (eds.)]. Cambridge University Press, Cambridge, United Kingdom and New York, NY, USA, pp. 1211–1362, doi:10.1017/9781009157896.011.

Frederikse, T., Landerer, F., Caron, L. et al. (2020) The causes of sea-level rise since 1900. *Nature* **584**, 393–397. https://doi.org/10.1038/s41586-020-2591-3

Freymueller, J. T., Haeussler, P. J., & Elliott, J. (2018). Active tectonics of Alaska. University of Alaska Press.

Galloway, D. L., Jones, D. R., & Ingebritsen, S. E. (2019). Land subsidence in the United States. US Geological Survey.

Galloway, D. L., et al. (2011). Land subsidence: natural causes, human-induced, and an evolving legacy. Environmental and Engineering Geoscience, 17(2), 227-251.

Gangadharan, N., Goosse, H., Parkes, D., Goelzer, H., Maussion, F., and Marzeion, B. (2022) Process-based estimate of global-mean sea-level changes in the Common Era, Earth Syst. Dynam., 13, 1417–1435, https://doi.org/10.5194/esd-13-1417-2022.

Garner, G. G., T. Hermans, R. E. Kopp, A. B. A. Slangen, T. L. Edwards, A. Levermann, S. Nowikci, M. D. Palmer, C. Smith, B. Fox-Kemper, H. T. Hewitt, C. Xiao, G. Aðalgeirsdóttir, S. S. Drijfhout, T. L. Edwards, N. R. Golledge, M. Hemer, G. Krinner, A. Mix, D. Notz, S. Nowicki, I. S. Nurhati, L. Ruiz, J-B. Sallée, Y. Yu, L. Hua, T. Palmer, B. Pearson, (2021). IPCC AR6 Global Mean Sea-Level Rise Projections. Version 20210809. Dataset accessed [YYYY-MM-DD] at https://doi.org/10.5281/zenodo.5914709.

GEBCO Bathymetric Compilation Group 2022 (2022) The GEBCO_2022 Grid - a continuous terrain model of the global oceans and land. NERC EDS British Oceanographic Data Centre NOC. doi:10.5285/e0f0bb80-ab44-2739-e053-6c86abc0289c

Gee, M. J. R., et al. (2010) The 2004 Indian Ocean tsunami in Indonesia: Observations on the northern limit in the Indian Ocean and Andaman Sea. Earth and Planetary Science Letters, 297(3-4), 634-642.

Gomez, N., & Warner, R. C. (2018) Marine ice cliff instability: Recent progress and future prospects. Earth-Science Reviews, 177, 709-720. (This review article provides a more detailed examination of marine ice cliff instability and its implications for sea level rise.)

Gregory, J.M., Griffies, S.M., Hughes, C.W. et al. (2019) Concepts and Terminology for Sea Level: Mean, Variability and Change, Both Local and Global. Surv Geophys 40, 1251–1289. https://doi.org/10.1007/s10712-019-09525-z

Gregory, J. M., and Coauthors (2013) Twentieth-Century Global-Mean Sea Level Rise: Is the Whole Greater than the Sum of the Parts?. *J. Climate*, **26**, 4476–4499, https://doi.org/10.1175/JCLI-D-12-00319.1.

Hashimoto, M., Fukuda, J., & Matsu'ura, M. (2011). Why do some GPS stations detect non-tectonic velocity transients?—Comparison of GPS observation and geologic information. Earth and Planetary Science Letters, 312(1-2), 171-182. https://doi.org/10.1016/j.epsl.2011.10.018

Hay, C. C., Morrow, E., Kopp, R. E. & Mitrovica, J. X. (2015) Probabilistic reanalysis of twentieth-century sea-level rise. *Nature* **517**, 481–484; erratum **552**, 278 (2017).

Harvey, T.C., Hamlington, B.D., Frederikse, T. et al. (2021) Ocean mass, sterodynamic effects, and vertical land motion largely explain US coast relative sea level rise. *Commun Earth Environ* **2**, 233. https://doi.org/10.1038/s43247-021-00300-w

Hermawan, I., et al. (2020). Megathrust Earthquakes along the Indonesian Sunda Megathrust Fault: A Review on Seismic Hazard Assessment. Geosciences, 10(8), 287.

Holgate, S.J.; Matthews, A.; Woodworth, P.L.; Rickards, L.J.; Tamisiea, M.E.; Bradshaw, E. (2013) Foden, P.R.; Gordon, K.M.; Jevrejeva, S., and Pugh, J., New data systems and products at the Permanent Service for Mean Sea Level. *Journal of Coastal Research*, 29 (3): 493–504.

Hu, J. C., & Wang, Y. (2019). Dynamic Characteristics of GPS Monitoring Sites and Its Influence on Seismic Deformation Observations. Journal of Earth Science, 30(2), 424-433. https://doi.org/10.1007/s12583-018-0843-2

IPCC. (2021). Climate change 2021: The physical science basis. Contribution of Working Group I to the Sixth Assessment Report of the Intergovernmental Panel on Climate Change. Cambridge University Press.

Jackett DR, McDougall TJ (1995) Minimal adjustment of hydrographic profiles to achieve static stability. J Atmos Ocean Technol 12(4):381–389

Jevrejeva, S., Moore, J. C., Grinsted, A., and Woodworth, P. L. (2008), Recent global sea level acceleration started over 200 years ago? *Geophys. Res. Lett.*, 35, L08715, doi:10.1029/2008GL033611.

Jordan, T. H. (2011). Earthquake predictability, brick by brick. Seismological Research Letters, 82(2), 181-186. https://doi.org/10.1785/gssrl.82.2.181

Kench, P. S., McLean, R. F., Brander, R. W., Nichol, S. L., Smithers, S. G., Ford, M. R., ... & Aslam, M. (2018). Geological effects of tsunami on reef islands result in

coral cover decline and volume and shoreline changes. Earth Surface Processes and Landforms, 43(3), 648-663.

Koh, H. L., Teo, S. C., Caballero-Anthony, M., & Esteban, M. (2021). Southeast Asia's coastal challenge: Managing seas in the era of climate change. Springer Nature.

Konikow, L.F. (2011) Contribution of global groundwater depletion since 1900 to sea-level rise. Geophysical Research Letters, 38(17), doi:10.1029/2011gl048604

Kopp, R.E. et al. (2014) Probabilistic 21st and 22nd century sea-level projections at a global network of tide gauge sites. Earth's Future, 2, 383–406, doi:10.1002/2014ef000239.

Kopp, R.E. et al. (2017) Evolving Understanding of Antarctic Ice-Sheet Physics and Ambiguity in Probabilistic Sea-Level Projections. Earth's Future, 5(12), 1217–1233, doi:10.1002/2017ef000663

Kopp, R. (2013). Does the mid-Atlantic United States sea level acceleration hot spot reflect ocean dynamic variability?. Geophysical Research Letters. 40. 10.1002/grl.50781.

Kopp, R., Garner, G., Hermans, T., Jha, S., Kumar, P., Slangen, A., Turilli, M., Edwards, T., Gregory, J., Koubbe, G., Levermann, A., Merzky, A. Nowicki, S. Palmer, M., and C. Smith (2023). The Framework for Assessing Changes To Sea-level (FACTS) v1.0-rc: A platform for characterizing parametric and structural uncertainty in future global, relative, and extreme sea-level change. 10.5194/egusphere-2023-14.

King, Matt & Altamimi, Zuheir & Boehm, Johannes & Bos, Machiel & Dach, Rolf & Elosegui, Pedro & Fund, F. & Pajares, Manuel & Lavallée, David & Cerveira, Paulo & Penna, Nigel & Riva, Riccardo & Steigenberger, Peter & Van Dam, Tonie & Vittuari, L. & Williams, Simon & Willis, Pascal. (2010). Improved Constraints on Models of Glacial Isostatic Adjustment: A Review of the Contribution of Ground-Based Geodetic Observations. Surveys in Geophysics. 31. 465-507. 10.1007/s10712-010-9100-4.

Landerer, F. W., J. H. Jungclaus, and J. Marotzke (2007a), Regional dynamic and steric sea level change in response to the IPCC-A1B scenario, *J. Phys. Oceanogr.*, 37(2), 296– 312.

Landerer, F., J. H. Jungclaus, and J. Marotzke (2007b), Ocean bottom pressure changes lead to a decreasing length-of-day in a warming climate, *Geophys. Res. Lett.*, 34, L06307, doi:10.1029/2006GL029106

Landerer, F. W., Jevrejeva, S., & Riva, R. E. M. (2015). Coastal sea level rise with warming above 2 °C. Proceedings of the National Academy of Sciences, 112(45), 14239-14244.

Levermann, A. et al. (2020) Projecting Antarctica's contribution to future sea level rise from basal ice shelf melt using linear response functions of ice sheet models (LARMIP-2). Earth System Dynamics, 11(1), 35–76, doi:10.5194/esd-11-35-2020

Martinez-Asensio, A., Wöppelmann, G., Ballu, V., Becker, M., Testut, L., Magnan, A.K. et al. (2019) Relative Sea-level rise and the influence of vertical land motion at tropical Pacific Islands. *Global and Planetary Change*, 176, 132– 143.

Marzeion, B. et al. (2020) Partitioning the Uncertainty of Ensemble Projections of Global Glacier Mass Change. Earth's Future, 8(7), doi:10.1029/2019ef001470

Marzin, C., R. Rahmat, D. Bernie, L. Bricheno, E. Buonomo, D. Calvert, H. Cannaby, S. Chan, M. Chattopadhyay, W. K. Cheong, M. E. Hassim, L. Gohar, N. Golding, C. Gordon, J. Gregory, D. Hein, A. Hines, T. Howard, T. Janes, R. Jones, E. Kendon, J. Krijnen, S. Y. Lee, S. Y. Lim, C. F. Lo, J. Lowe, G. Martin, K. McBeath, K. McInness, C. McSweeney, M. Mizielinski, J. Murphy, C. O'Neill, M. Palmer, G. Redmond, C. Roberts, S. Sahany, M. Sanderson, C. Scannell, D. Sexton, F. Shaw, J. Slingo, X. Sun, J. Tinker, S. Tucker, C. Wang, S. Webster, S. Wilson, R. Wood, S. Zhang (2015) Singapore's Second National Climate Change Study – Phase 1. [Web link: http://ccrs.weather.gov.sg/publications-second-National-Climate-Change-Study-Science-Reports]

McGuire, R. K. (2014). The tragedy of earthquake prediction in the United States: A historical examination. Seismological Research Letters, 85(6), 1163-1172. https://doi.org/10.1785/0220140071

Merrifield, M. A. (2011). A Shift in Western Tropical Pacific Sea Level Trends during the 1990s. *Journal of Climate*, 24(15), 4126– 4138. https://doi.org/10.1175/2011jcli3932.1

Meyssignac, B., Boyer, T., Zhao, Z., Hakuba, M. Z., Landerer, F. W., Stammer, D., Köhl, A., Kato, S., L'Ecuyer, T., Ablain, M., Abraham, J. P., Blazquez, A., Cazenave, A., Church, J. A., Cowley, R., Cheng, L., Domingues, C. M., Giglio, D., Gouretski, V., Ishii, M., Johnson, G. C., Killick, R. E., Legler, D., Llovel, W., Lyman, J., Palmer, M. D., Piotrowicz, S., Purkey, S. G., Roemmich, D., Roca, R., Savita, A., Schuckmann, K., Speich, S., Stephens, G., Wang, G., Wijffels, S. E., and Zilberman, N. (2019) Measuring Global Ocean Heat Content to Estimate the Earth Energy Imbalance,

Front. Mar. Sci., 6, 432, https://doi.org/10.3389/fmars.2019.00432, 2019.

Ministry of Sustainability and the Environment. (2021) Climate Change in Singapore. Retrieved from https://www.mse.gov.sg/climate-change/climate-change-in-singapore

Mitchum, G.T., & Wyrtki, K. (1988) Overview of Pacific sea level variability, Marine Geodesy, 12:4, 235-245, DOI: 10.1080/15210608809379595

Nerem, R. S., Beckley, B. D., Fasullo, J. T., Hamlington, B. D., Masters, D., & Mitchum, G. T. (2018). Climate-change–driven accelerated sea-level rise detected in the altimeter era. *Proceedings of the National Academy of Sciences*, 115(9), 2022– 2025.

Niesters, Lisa-Michéle & Schöne, Tilo & Illigner, Julia & Haghshenas Haghighi, Mahmud & Gisevius, Konstantin & Braun, Boris. (2021). Land subsidence in Jakarta and Semarang Bay -The relationship between physical processes, risk perception, and household adaptation. Ocean & Coastal Management. 211. 105775. 10.1016/j.ocecoaman.2021.105775.

Nicholls, R.J., Lincke, D., Hinkel, J. et al. A global analysis of subsidence, relative sea-level change and coastal flood exposure. Nat. Clim. Chang. 11, 338–342 (2021). https://doi.org/10.1038/s41558-021-00993-z

Nicholls, Robert & Cazenave, Anny. (2010). Sea-Level Rise and Its Impact on Coastal Zones. Science (New York, N.Y.). 328. 1517-20. 10.1126/science.1185782.

Nidheesh, A. G., Lengaigne, M., Vialard, J., Unnikrishnan, A. S. and Dayan, H. (2013) Decadal and long-term sea level variability in the tropical Indo-Pacific Ocean. Climate Dyn., 41(2), 381–402.

Okem, A., J. Petzold, B. Rama, and N. Weyer (eds.)]. In Press, pp. 321–445, www.ipcc.ch/srocc/chapter/chapter-4-sea-level-rise-and-implications-for-low-lying-islands-coasts-and-communities/.

Oppenheimer, M. et al. (2019) Sea Level Rise and Implications for Low Lying Islands, Coasts and Communities. In: IPCC Special Report on the Ocean and Cryosphere in a Changing Climate [Pörtner, H.-O., D.C. Roberts, V. Masson-Delmotte, P. Zhai, M. Tignor, E. Poloczanska, K. Mintenbeck, M. Nicolai,

Otosaka, I. N., Shepherd, A., Ivins, E. R., Schlegel, N.-J., Amory, C., van den Broeke, M. R., Horwath, M., Joughin, I., King, M. D., Krinner, G., Nowicki, S., Payne, A. J., Rignot, E., Scambos, T., Simon, K. M., Smith, B. E., Sørensen, L. S., Velicogna, I., Whitehouse, P. L., A, G., Agosta, C., Ahlstrøm, A. P., Blazquez, A., Colgan, W., Engdahl, M. E., Fettweis, X., Forsberg, R., Gallée, H., Gardner, A., Gilbert, L., Gourmelen, N., Groh, A., Gunter, B. C., Harig, C., Helm, V., Khan, S. A., Kittel, C., Konrad, H., Langen, P. L., Lecavalier, B. S., Liang, C.-C., Loomis, B. D., McMillan, M., Melini, D., Mernild, S. H., Mottram, R., Mouginot, J., Nilsson, J., Noël, B., Pattle, M. E., Peltier, W. R., Pie, N., Roca, M., Sasgen, I., Save, H. V., Seo, K.-W., Scheuchl, B., Schrama, E. J. O., Schröder, L., Simonsen, S. B., Slater, T., Spada, G., Sutterley, T. C., Vishwakarma, B. D., van Wessem, J. M., Wiese, D., van der Wal, W., and Wouters, B. (2023) Mass balance of the Greenland and Antarctic ice sheets from 1992 to 2020, Earth Syst. Sci. Data, 15, 1597–1616, https://doi.org/10.5194/essd-15-1597-2023.

Ozawa, S., Murakami, M., Kaidzu, M., Tada, T., & Sagiya, T. (2008). Anomalously large crustal deformation before the Niigata-Ken Chuetsu earthquake in 2007 detected by GEONET. Geophysical Research Letters, 35(22), L22303. https://doi.org/10.1029/2008gl035596

Peltier, W.R, Argus, D.F. and Drummond, R. (2015) Space geodesy constraints ice-age terminal deglaciation: The global ICE-6G_C (VM5a) model. J. Geophys. Res. Solid Earth, 120, 450-487, doi:10.1002/2014JB011176.

Peltier, W.R., (2004). Global Glacial Isostasy and the Surface of the Ice-Age Earth: The ICE-5G (VM2) Model and GRACE, Ann. Rev. Earth and Planet. Sci., 32, 111-149. https://doi.org/10.1146/annurev.earth.32.082503.144359

Peltier, W. R., and Tushingham, A. M. (1991), Influence of glacial isostatic adjustment on tide gauge measurements of secular sea level change, *J. Geophys. Res.*, 96(B4), 6779– 6796, doi:10.1029/90JB02067.

Permanent Service for Mean Sea Level (PSMSL), (2023) "Tide Gauge Data", Retrieved Aug 2022 from http://www.psmsl.org/data/obtaining/.

Pfeffer, J., Spada, G., A. Mémin, J.-P. Boy, P. Allemand, Decoding the origins of vertical land motions observed today at coasts, Geophysical Journal International, Volume 210, Issue 1, July 2017, Pages 148–165, https://doi.org/10.1093/gji/ggx142

Pollitz, F. F., Bürgmann, R., Banerjee, P., & Nagarajan, B. (2018). Earthquake cycle deformation, transient detection, and geodetic slip rates in subduction zones. Journal of Geophysical Research: Solid Earth, 123(3), 1893-1909.

Rodolfo, Kelvin & Eco, Rodrigo & Sulapas, Joyce & Morales, Anieri & Lagmay, Alfredo Mahar & Amelung, Falk. (2020). Disaster in Slow Motion: Widespread Land Subsidence in and Around Metro Manila,

Philippines Quantified By Insar Time-Series Analysis. 1068.

Royston, S. et al. (2018) Sea-Level Trend Uncertainty With Pacific Climatic Variability and Temporally-Correlated Noise. Journal of Geophysical Research: Oceans, 123(3), 1978–1993, doi:10.1002/2017jc013655.

Royston, S., Bingham, R. J., and Bamber, J. L. (2022) Attributing decadal climate variability in coastal sea-level trends, Ocean Sci., 18, 1093–1107, https://doi.org/10.5194/os-18-1093-2022.

Slangen A. B. A., Palmer M. D., Camargo C. M. L., Church J. A., Edwards T. L., Hermans T. H. J., Hewitt H. T., Garner G. G., Gregory J. M., Kopp R. E., Santos V. M. and van de Wal R. S. W. (2023). The evolution of 21st century sea-level projections from IPCC AR5 to AR6 and beyond. Cambridge Prisms: Coastal Futures, 1, E7. doi:10.1017/cft.2022.8.

Slangen, A.B.A., J.A. Church, X. Zhang, and D. Monselesan, (2014) Detection and attribution of global mean thermosteric sea-level change. Geophysical Research Letters, 41(16), 5951–5959, doi:10.1002/2014gl061356.

Shirzaei, M., Freymueller, J., Törnqvist, T.E. et al. Measuring, modelling and projecting coastal land subsidence. Nat Rev Earth Environ 2, 40–58 (2021). https://doi.org/10.1038/s43017-020-00115-x

Smith, C.J. et al. (2018) FAIR v1. 3: A simple emissions-based impulse response and carbon cycle model. Geoscientific Model Development, 11(6), 2273–2297.

Siringan, F. P., Taniguchi, M., Shimada, J., & Lapus, M. R. (2019). Land subsidence, aquifer system compaction and sea-level rise in the coastal aquifers of Manila Bay and Bangkok. Science of the Total Environment, 655, 843-856.

Swapna, P., J. Jyoti, R. Krishnan, N. Sandeep, and S.M. Griffies (2017) Multidecadal Weakening of Indian Summer Monsoon Circulation Induces an Increasing Northern Indian Ocean Sea Level. Geophysical Research Letters, 44(20), 10560–10572, doi:10.1002/2017gl074706.

Tamisiea, M.E., and J.X. Mitrovica (2011) The moving boundaries of sea level change: Understanding the origins of geographic variability. Oceanography 24(2):24–39, doi:10.5670/oceanog.2011.25.

Tay, C., Lindsey, E.O., Chin, S.T. et al. Sea-level rise from land subsidence in major coastal cities. Nat Sustain 5, 1049–1057 (2022). https://doi.org/10.1038/s41893-022-00947-z

Tkalich, P., Vethamony, P., Babu, M. T., and Pokratath, R. (2009) Seasonal sea level variability and anomalies in the Singapore Strait, Proceedings of International Conference in Ocean Eng., ICOE 2009 IIT Madras, Chennai, India.

Tkalich, P., Vethamony, P., Luu, Q.-H., and Babu, M. T. (2013) Sea level trend and variability in the Singapore Strait, Ocean Sci., 9, 293–300, https://doi.org/10.5194/os-9-293-2013.

Unnikrishnan A., Nidheesh G., Lengaigne M. (2015) Sea-level-rise trends off the Indian coasts during the last two decades. Curr Sci 108:966–971.

Wal, R.S.W. & Nicholls, R. & Behar, David & McInnes, K. & Stammer, D. & Lowe, Jason & Church, J. & DeConto, R. & Fettweis, Xavier & Goelzer, Heiko & Haasnoot, M. & Haigh, I. & Hinkel, Jochen & Horton, B. & James, T. & Jenkins, Adrian & LeCozannet, G. & Levermann, Anders & Lipscomb, W. & White, K.. (2022). A High-End Estimate of Sea Level Rise for Practitioners. Earth's Future. 10. 10.1029/2022EF002751.

Vinogradov, S. V., and Ponte, R. M. (2011), Low-frequency variability in coastal sea level from tide gauges and altimetry, *J. Geophys. Res.*, 116, C07006, doi:10.1029/2011JC007034.

von Schuckmann, K., Cheng, L., Palmer, M. D., Hansen, J., Tassone, C., Aich, V., Adusumilli, S., Beltrami, H., Boyer, T., Cuesta-Valero, F. J., Desbruyères, D., Domingues, C., García-García, A., Gentine, P., Gilson, J., Gorfer, M., Haimberger, L., Ishii, M., Johnson, G. C., Killick, R., King, B. A., Kirchengast, G., Kolodziejczyk, N., Lyman, J., Marzeion, B., Mayer, M., Monier, M., Monselesan, D. P., Purkey, S., Roemmich, D., Schweiger, A., Seneviratne, S. I., Shepherd, A., Slater, D. A., Steiner, A. K., Straneo, F., Timmermans, M.-L., and Wijffels, S. E. (2020) Heat stored in the Earth system: where does the energy go?, Earth Syst. Sci. Data, 12, 2013–2041, https://doi.org/10.5194/essd-12-2013-2020.

von Schuckmann, K., Minière, A., Gues, F., Cuesta-Valero, F. J., Kirchengast, G., Adusumilli, S., Straneo, F., Ablain, M., Allan, R. P., Barker, P. M., Beltrami, H., Blazquez, A., Boyer, T., Cheng, L., Church, J., Desbruyeres, D., Dolman, H., Domingues, C. M., García-García, A., Giglio, D., Gilson, J. E., Gorfer, M., Haimberger, L., Hakuba, M. Z., Hendricks, S., Hosoda, S., Johnson, G. C., Killick, R., King, B., Kolodziejczyk, N., Korosov, A., Krinner, G., Kuusela, M., Landerer, F. W., Langer, M., Lavergne, T., Lawrence, I., Li, Y., Lyman, J., Marti, F., Marzeion, B., Mayer, M., MacDougall, A. H., McDougall, T., Monselesan, D. P., Nitzbon, J., Otosaka, I., Peng, J., Purkey, S., Roemmich, D., Sato, K., Sato, K., Savita, A.,

Schweiger, A., Shepherd, A., Seneviratne, S. I., Simons, L., Slater, D. A., Slater, T., Steiner, A. K., Suga, T., Szekely, T., Thiery, W., Timmermans, M.-L., Vanderkelen, I., Wjiffels, S. E., Wu, T., and Zemp, M. (2023) Heat stored in the Earth system 1960–2020: where does the energy go?, Earth Syst. Sci. Data, 15, 1675–1709, https://doi.org/10.5194/essd-15-1675-2023.

von Schuckmann, K., Palmer, M.D., Trenberth, K.E., Cazenave, A., Chambers, D., Champollion, N., Hansen, J., Josey, S.A., Loeb, N., Mathieu, P-P., Meyssignac, B., and Wild, M. (2016) An imperative to monitor Earth's energy imbalance, Nat. Clim. Change, 6, 138–144, https://doi.org/10.1038/nclimate2876.

Wada, Y. et al. (2016) Fate of water pumped from underground and contributions to sea-level rise. Nature Climate Change, doi:10.1038/nclimate3001.

Wada, Y. et al. (2012) Past and future contribution of global groundwater depletion to sea-level rise. Geophysical Research Letters, 39(9), doi:10.1029/2012gl051230.

Wang, J., Church, J. A., Zhang, X., Gregory, J. M., Zanna, L., & Chen, X. (2021). Evaluation of the local sea-level budget at tide gauges since 1958. *Geophysical Research Letters*, 48, e2021GL094502. https://doi.org/10.1029/2021GL094502

Wassmann, R., Thevs, N., & Bandholtz, T. (2016). Bangkok's sinking realities: impacts and adaptations. Climate and Development, 8(4), 328-337.

WCRP Global Sea Level Budget Group: Global sea-level budget 1993–present (2018) Earth Syst. Sci. Data, 10, 1551–1590, https://doi.org/10.5194/essd-10-1551-2018.

Woodworth, P. L., Melet, A., Marcos, M., Ray, R. D., Wöppelmann, G., Sasaki, Y. N., Cirano, M., Hibbert, A., Huthnance, J. M., Monserrat, S., and Merrifield, M. A.(2019) Forcing Factors Affecting Sea Level Changes at the Coast, Surv. Geophys., 40, 1351–1397, https://doi.org/10.1007/s10712-019-09531-1.

Woppelmann, Guy & Marcos, Marta. (2015). Vertical land motion as a key to understanding sea level change and variability. Reviews of Geophysics. 54. n/a-n/a. 10.1002/2015RG000502.

Wyrtki, K. (1987), Indonesian through flow and the associated pressure gradient, *J. Geophys. Res.*, 92(C12), 12941– 12946, doi:10.1029/JC092iC12p12941.

Zanna, L., S. Khatiwala, J.M. Gregory, J. Ison, and P. Heimbach (2019) Global reconstruction of historical ocean heat storage and transport. Proceedings of the National Academy of Sciences, 116(4), 1126–1131, doi:10.1073/pnas.1808838115.

Zhang, P., Liu, J., Zhang, Z., Xu, Z., Zhao, W., & Wang, H. (2018) The effects of human activities on vertical land motion in the Beijing plain, China. Environmental Earth Sciences, 77(8), 310.

Zuo, H., Balmaseda, M. A., Tietsche, S., Mogensen, K., and Mayer, M. (2019) The ECMWF operational ensemble reanalysis–analysis system for ocean and sea ice: a description of the system and assessment, Ocean Sci., 15, 779–808, https://doi.org/10.5194/os-15-779-2019.